Shock Waves in Bubbly Cavitating Flows

Part I. Shock Waves in Cloud Cavitation

Part II. Bubbly Cavitating Flows Through a Converging-diverging Nozzle

Thesis by
Yi-Chun Wang

In Partial Fulfillment of the Requirements
for the Degree of
Doctor of Philosophy

California Institute of Technology
Pasadena, California

1996

(Defended May 22, 1996)

Acknowledgements

"The Lord is my shepherd, I shall not be in want." I thank God for the incomparable riches of his grace. I have received from him everything I need and even more.

I am immensely grateful to my advisor, Professor Christopher Brennen, for his outstanding supervision, encouragement, and patience. His superior research vision has guided me through some very interesting aspects of cavitating flows. Sincere appreciation goes to Professor Theodore Wu who led me to Caltech and has been very generous to me. My indebtedness is due to Professor Allan Acosta. He is always willing to help. I also want to thank Professor Tim Colonius for some valuable discussions regarding the numerical computation of the nozzle flow. Special thanks to Dr. Andrew Lewis for his help in preparing this thesis which is produced by LaTeX packages he wrote.

The thesis is dedicated to my parents who explored in me the spirit of persistence and inspired me to do my best in any situation. My deepest love and appreciation go to my wife, Esther, a unique and precious gift from God. We share and support each other all the time. Without her, this thesis would have been impossible.

Shock Waves in Bubbly Cavitating Flows

Part I. Shock Waves in Cloud Cavitation

Part II. Bubbly Cavitating Flows Through a Converging-diverging Nozzle

by

Yi-Chun Wang

In Partial Fulfillment of the
Requirements for the Degree of
Doctor of Philosophy

Abstract

Two problems are considered in this thesis: the nonlinear dynamics of a cloud of cavitation bubbles, and bubbly cavitating flows in a converging-diverging nozzle. The focus of the first problem is to explore the characteristics of the growth and collapse of a spherical cloud of bubbles. The prototypical problem solved considers a finite cloud of nuclei that is exposed to a decrease in the ambient pressure which causes the cloud to cavitate. A subsequent pressure recovery then causes the cloud to collapse. This is typical of the transient behaviour exhibited by a bubble cloud as it passes a body or the blade of a ship propeller. The simulations employ the fully nonlinear, non-barotropic, homogeneous two-phase flow equations coupled with the Rayleigh-Plesset equation

for the dynamics of individual bubbles. A Lagrangian integral method is developed to solve this set of equations. The computational results confirm the idea put forward by Mørch and his co-workers (Mørch [1980], [1981], [1982]; Hanson *et al.* [1981]) who speculated that the collapse of the cloud involved the formation of a shock wave on the surface of the cloud and that inward propagation and geometric focusing of this shock would lead to very large localized pressure pulses. The effects of varying the bubble population density, the cavitation number, and the ratio of the cloud size to the bubble size are examined. The theoretical results are shown to provide a satisfactory explanation for dynamic structures and acoustic signature observed in recently conducted experiments of cloud cavitation at California Institute of Technology (Reisman and Brennen [1996]; Brennen *et al.* [1996]). It is concluded that the formation and focusing of bubbly shock waves are responsible for the severe noise and damage potential in cloud cavitation.

The second problem investigates the nonlinear behavior of a bubbly cavitating flow, both steady and unsteady, through a converging-diverging nozzle. Two different flow regimes are found from steady state solutions: quasi-steady and quasi-unsteady. The former is characterized by the large spatial fluctuations in the downstream of the flow. Bifurcation occurs as the flow transitions from one regime to the other. An analytical expression for the critical bubble size at bifurcation is obtained. Finally, unsteady solutions in a period of consecutive times are presented. These solutions are characterized by the downstream spatial fluctuations coupled with large pressure pulses changing in both magnitude and location with time. The characteristics of these pulses are similar to the shock pulses of Part I and are produced by the local violent collapse of the bubbles in the flow.

Contents

List of Figures

Figures for Part I

Figures for Part II

Nomenclature

a	Diagonal element of the coefficient matrix in the discretized pressure equation
A	Dimensionless radius of bubble cloud, dimensionless cross-sectional area of duct
A_0	Dimensionless initial cloud radius, dimensionless cross-sectional area of duct at which a Lagrangian particle located at $t = 0$
A^*	Cross-sectional area of duct
A_s^*	Upstream cross-sectional area of duct
b	Off-diagonal element of the coefficient matrix in the discretized pressure equation
c^*	Sonic speed in bubbly mixture
C_P	Pressure coefficient
C_{Pc}	Critical pressure coefficient at which bifurcation occurs
$C_{P\infty}$	Pressure coefficient at infinity from the cloud, $(p_\infty^* - p_0^*)/\frac{1}{2}\rho_L^* U^{*2}$

C_{PMIN} Minimum pressure coefficient at infinity, minimum pressure coefficient at throat for pure liquid nozzle flow

D Dimensionless length scale of the low pressure perturbation

D^* Length scale of the low pressure perturbation

f Dimensionless frequency, a term in the integral pressure equation

g Inhomogeneous term in the pressure equation

I Dimensionless acoustic impulse

j Indice

J Jacobian of the transformation from Lagrangian coordinates to Eulerian coordinates

k Polytropic index for the gas inside the bubbles

K Coefficient in the Poisson pressure equation

L Dimensionless length of the nozzle

M Coefficient in the Poisson pressure equation

N Total number of Lagrangian nodes, coefficient in the Poisson pressure equation

p_a Dimensionless far-field acoustic pressure radiated by the cloud

p^*_∞ Pressure at infinity from the cloud

p^* Fluid pressure

p^*_0 Fluid pressure at undisturbed reference condition

p^*_a Far-field acoustic pressure radiated by the cloud

p_s^*	Upstream pressure in duct flow
p_V^*	Vapor pressure
Q	Coefficient matrix of the discretized pressure equation
r	Dimensionless Eulerian radial coordinate measured from the center of cloud, r^*/R_0^*
r_0	Dimensionless Lagrangian radial coordinate measured from the center of cloud and equal to r at the undisturbed reference condition
r^*	Eulerian radial coordinate measured from the center of cloud
R	Dimensionless bubble radius
R_0	Dimensionless initial bubble radius
R_c	Dimensionless critical bubble radius at which bifurcation occurs
R_0^*	Initial bubble radius at undisturbed reference condition
R_s^*	Upstream bubble radius in duct flow
Re	Reynolds number
S^*	Surface tension of the liquid
t	Dimensionless time
t_G	Dimensionless duration of the low pressure perturbation
t^*	Time
T	Integral operator in the pressure equation
T_B^*	Natural period of bubble pulsation
T_C^*	Time scale of acoustic wave propagation through the cloud

u	Dimensionless fluid velocity
u^*	Fluid velocity
u_s^*	Upstream velocity in duct flow
U^*	Reference velocity
V^*	Volume of the cloud
V_{BMAX}	Dimensionless maximum total volume of bubbles in the cloud
w	Dimensionless bubble wall velocity in Lagrangian coordinates
We	Weber number
x	Dimensionless Eulerian coordinate in duct flow, x^*/R_s^*
x_0	Dimensionless Lagrangian coordinate in duct flow, equal to x at $t = 0$
x_e	Dimensionless end point of the computational domain in duct flow
x_n	Dimensionless location of the nozzle inlet
x^*	Eulerian Coordinate in duct flow
α	Void fraction
α_0	Initial void fraction
α_s	Upstream void fraction
β	Bubble/cloud interation parameter, $\alpha_0(1-\alpha_0)A_0^2/R_0^2$
ϵ	Numerical residual at each iteration stage in solving the integral pressure equation
η	Dimensionless bubble population per unit liquid volume, $\eta^* R_0^{*3}$
η^*	Bubble population per unit liquid volume

γ	Residual weighting factor in the iterative algorithms for solving the integral pressure equation
μ_E^*	Effective dynamic viscosity of the liquid
ω	Relaxation factor in the iterative algorithms for solving the integral pressure equation
ω_B^*	Natural frequency of bubble pulsation
ρ	Dimensionless mixture density
ρ_0	Dimensionless mixture density at $t = 0$
ρ_g	Dimensionless gas density inside a bubble, ρ_g^*/ρ_L^*
ρ_g^*	Gas density inside a bubble
ρ_s^*	Upstream mixture density
ρ_L^*	Liquid Density
σ	Cavitation number
ξ	Dummy variable
ζ	Dummy variable
$\triangle t$	Time step

General Introduction

Bubbly cavitating flows belong to a special category of the gas-liquid two-phase flows. In cavitating flows bubble/flow interactions and bubble/bubble interactions are important physical phenomena which strongly modify the flow dynamics and acoustics compared to non-cavitating flows. In a cavitating flow the nuclei are convected into a region of low pressure, grow explosively to macroscopic size, and collapse violently when they are convected back to a high pressure region. The bubble/flow interactions are highly nonlinear in such a flow. Theoretically, an approximate model for individual traveling bubble cavitation is the Rayleigh-Plesset equation (Plesset [1948]), which relates the dynamics of a single bubble to the far-field pressure perturbation experienced by the bubble. However, when the frequency of cavitation events increases in space or time such that they begin to interact with one another, a whole new set of phenomena may be manifest. The bubble/bubble interaction through the hydrodynamics of the surrounding liquid may significantly influence the whole flow field. This can result in more deleterious cavitation effects, namely

an increase in the cavitation erosion and noise.

The first part of this thesis is focused on a particularly violent type of cavitation called "cloud cavitation," a structure which consists of numerous cavitating bubbles in close proximity. Most previous theoretical studies of the dynamics of cavitating clouds have been linear or weakly nonlinear analyses which have identified the natural frequencies and modes of cloud oscillation (see, for example, d'Agostino and Brennen [1983], [1989]; Kumar and Brennen [1991], [1992], [1993]) but have not, as yet, shown how a cloud would behave during the massively nonlinear response in a cavitating flow. Experiments have demonstrated that the coherent collapse of bubble clouds can result in greater noise generation and greater damage potential than would be expected from the cumulative effect of the collapse of the individual bubbles which make up the cloud. However, the basic dynamics and acoustics of cloud cavitation are still poorly understood.

To model the bubbly mixture, concepts from continuum mechanics was adopted by many previous investigators. Two basic assumptions are integral to this approach: 1) The size of bubbles are much larger than the kinetic dimensions of molecules, such as distances between the molecules, mean free path of molecules, etc. Thus in the dimension of the non-homogeneties (the bubbles), large number of molecules are contained. 2) The bubbles are characterized by a lengthscale many times smaller than characteristic lengths over

which the mixture properties vary. The first assumption enables us to employ the conservation equations for classical fluid dynamics for each phase. The second assumption makes it possible to use the method of ensemble averaging of the conservation equations for each phase over an intermediate length scale in which a large number of bubbles are included in any infinitesimal volume. Biesheuvel and van Wijngaarden [1984] derived a continuum mixture model which included the effects of bubble dynamics, liquid compressibility and relative motion between two phases by volumetric averaging. This model has been successfully applied to describe the phenomena of both small amplitude and large amplitude wave propagation through liquids containing small gas bubbles (see, for example, van Wijngaarden [1972]; Noordzij [1973]; Noordzij and van Wijngaarden [1974]; Kameda and Matsumoto [1995]). The same mathematical model is used in this thesis except that the effects of liquid compressiblity and relative motion between the phases are neglected. Note that d'Agostino and Brennen [1989] examined the validity of both approximations and found that they have very little effect on the basic dynamics of the flow such as its natural frequencies. The main contribution of these effects is the damping that they cause at the bubble resonant frequency. This can be incorporated by taking an appropriate value of the effective viscosity in place of liquid viscosity used in the Rayleigh-Plesset equation (Chapman and Plesset [1971]). Furthermore, present model is only valid for

a dilute bubbly mixture with small bubble void fraction. This is the case for many engineering cavitating flows where the population density of upstream nuclei is very small.

In bubbly cavitating flows, the inertia effects caused by the explosive expansion and collapse of bubbles can dominate all other effects. The pressure changes in the surrounding liquid generate rapid bubble volume changes which result in global accelerating velocity fields. Associated with the mixture acceleration is a global pressure gradient which in turn effects the pressure encountered by each individual bubble in the mixture. These bubble/flow and bubble/bubble interactions can only be accurately described when the dynamics of the bubbles in the flow are modeled appropriately. The Rayleigh-Plesset equation for the bubble radial pulsation is used in the present model. It will be shown that the consequences of Rayleigh-Plesset dynamics cause many difficulties in the numerical computation.

Another issue in the modeling of the bubbly cavitating flow is that the incorporation of the Rayleigh-Plesset equation induces a different dynamic scale (time or distance) to the flow. It is well known that the resonant period of individual bubbles has a significant effect on the propagation of acoustic waves as long as the period of the wave is close to or higher than the resonant period of the bubbles. It is found in this thesis that for a mixture with finite dimension, such as a bubble cloud, the ratio of the global dynamic scale (for example, the

time for an acoustic wave to travel across the cloud) to the microscale of the bubble plays a critical role in determining the mixture dynamics both in the linear and in the nonlinear regimes.

The first problem in this thesis investigates the characteristics of the collapse dynamics of a cavitating cloud which has no acceleration with respect to an inertial frame. However, many engineering cavitating flows are associated with the flow acceleration, such as the cavitating flow on a hydrofoil. Inertia effects of the mean flow must be included to properly model these types of flow. The second model problem explored in this thesis concerns nonlinear bubbly cavitating flows through one-dimensional converging-diverging nozzles. This is an important problem by itself in many engineering applications, but has not, previously, been studied in the context of bubble/bubble interactions. The nozzle flow is also a useful model of any cavitating flow in which a low pressure region causes the flow to accelerate, e.g., the cavitating flow on the suction surface of a hydrofoil. Therefore, study of the 1-D accelerating flow with bubble cavitation effects may have value in building up fully nonlinear solutions for the practical higher dimensional flows. Note that Kubota *et al.* [1992] proposed a numerical modeling for unsteady cavitating flows on a two dimensional hydrofoil using the Navier-Stokes equations of the mixture coupled with Rayleigh-Plesset bubble dynamics. Although their model can exhibit the shedding of cavitation clouds and the generation of

vortex cavitation, the results showed very small pressure peaks on the suction surface of the foil. Many experiments all registered very large positive pressure pulses in this kind of flow (see, for example, Wade and Acosta [1966]; Le *et al.* [1993]; Brennen *et al.* [1996]). One possible reason of this inconsistency is that they employed some artificial diffusivities in both the mixture momentum equation and the Rayleigh-Plesset equation to eliminate the instability caused by the nonlinear convective terms in these equations. This may suppress the large local acceleration caused by the violent collapse of the bubbles in the flow and therefore eliminate the production of these pulses. Parenthetically, it is shown in this thesis that very large pressure pulses can occur due to the violent bubble collapse. Futhermore, it is these pulses that cause the computational difficulties.

The same mathematical model as employed in the first problem is applied for the accelerating nozzle flow. Both steady and unsteady solutions are investigated to explore the characteristics of this kind of flow. The Bernoulli effect caused by the growing and collapsing bubbles in the nozzle generates important interaction effects. In contrast to the spherical cloud, the internal flow configuration causes the dynamics of the bubbles to have a much more dramatic influence on the mean flow through the mass and momentum conservation equations of the confined mixture.

Part I

Shock Waves in Cloud Cavitation

Chapter 1

Introduction

In many flows of practical interest one observes the periodic formation and collapse of a "cloud" of cavitation bubbles. Such a structure, which has a foamy appearance and consists of numerous cavitating bubbles, is termed "cloud cavitation." The temporal periodicity may occur naturally as a result of the shedding of cavitating vortices or it may be the response to a periodic disturbance imposed on the flow. Common examples of imposed fluctuations are the interaction between rotor and stator blades in a pump or turbine and the interaction between a ship's propeller and the inhomogeneous wake created by the hull.

Experimental studies have shown that intensive noise and damage potential are associated with the collapse of a cavitating cloud of bubbles (see, for example, Bark and Berlekom [1978]; Shen and Peterson [1978], [1980]; Bark [1985]; Franc and Michel [1988]; Kubota *et al.* [1989]; Le *et al.* [1993];

Reisman *et al.* [1994]). Moreover, it is demonstrated that when clouds of cavitation bubbles collapse coherently, they result in greater material damage (see, for example, Soyama *et al.* [1992]) and greater noise generation (see, for example, Reisman *et al.* [1994]) than would be expected from the cumulative effect of the collapse of the individual bubbles which make up the cloud. However, the precise physical phenomena involved in cloud cavitation have not, as yet, been properly understood and the basic explanation of the enhanced noise and damage potential is still not clear. In the first part of this thesis the nonlinear growth and collapse of a spherical cloud of cavitation bubbles and the thereby generated pressure and momentum pulses responsible for noise and erosion are examined. A continuum mixture model coupled with the Rayleigh-Plesset equation is solved numerically by a Lagrangian integral method. The results show that the collapse of the cloud may be accompanied by the formation of an inward propagating bubbly shock wave. As the shock passes the bubbles in the cloud, very large pressure pulses are produced due to the violent collapse of the bubbles. This in turn accelerates the mixture velocity and increases the pressure gradient in the mixture. Due to these coupled effects and the spherically geometric focusing, the shock speeds up and rapidly gains strength as it approaches the center of the cloud. Very complicated bubble-bubble interactions are observed when the shock propagates to the center of the cloud, produces very high pressure, which then causes a rebound of the cloud. The

first collapse and rebound, which induce a large volumetric acceleration of the cloud, can cause a large peak in the far-field acoustic noise. The magnitudes of the subsequent peaks in each collapse and rebound cycle decay continuously due to the bubble damping mechanisms. After several cycles, the cloud begins to oscillate at its natural frequency. Understanding such bubbly flow and shock wave processes is important because these flow structures propagate the noise and produce the impulsive loads on nearby solid surfaces in a cavitating flow. The results of this thesis suggest that the formation and focusing of the bubbly shock wave is one of the major mechanisms for the enhanced noise and damage potential associated with cloud cavitation.

1.1 Theoretical Developments for the Dynamics of Cavitation Clouds

Analytical studies of the dynamics of cavitation clouds can be traced to the work of van Wijngaarden [1964] who first attempted to model the behavior of a collapsing layer of bubbly fluid next to a flat wall and found higher average pressures at the wall as result of the interactive effects of bubble dynamics. The work of van Wijngaarden represents the earliest use of continuum mixture models in the study of cloud dynamics. Later investigators employed several different but equivalent mixture models to investigate shock wave propaga-

tion in liquids containing small gas bubbles (see, for example, Noordzij [1973]; Noordzij and van Wijngaarden [1974]; Kameda and Matsumoto [1995]). The oscillating structure of the bubbly shock waves and how some of the important relaxation processes such as the bubble-liquid relative motions and the heat transfer between phases affect the structural evolution of the shocks were extensively studied by these work.

Continuing on the dynamics of cavity clouds, Chahine [1982b], [1982a] explored numerical methods which incorporate the individual bubbles using matched asymptotic expansions. His model assumes instantaneous transmission of ambient conditions to the individual bubble and thus neglects the compressibility of the cloud. Later, d'Agostino and Brennen [1983] investigated the linearized dynamics of a spherical cloud of bubbles using a continuum mixture model coupled with the Rayleigh-Plesset equation and showed that the interaction between bubbles leads to a coherent dynamics of the cloud, including natural frequencies that can be much smaller than the natural frequencies of individual bubbles. Omta [1987] linearized the Biesheuvel-van Wijngaarden homogeneous flow equations for bubbly mixtures (Biesheuvel and van Wijngaarden [1984]) and obtained solutions to the flow in a spherical bubble cloud under a number of simplified assumptions. Several conclusions he reached are similar to those of d'Agostino and Brennen (d'Agostino and Brennen [1983]). Indeed the literature on the linearized

dynamics of clouds of bubbles is growing rapidly (see also, for example, d'Agostino *et al.* [1988], d'Agostino and Brennen [1989]; Prosperetti [1988]). However, bubble clouds in engineering cavitating flows always experience large amplitudes of pressure perturbations and it is well known that the dynamics of a bubble can be highly nonlinear (see, for example, Prosperetti [1975]). The nonlinear convective effects in pratical flows may also produce significant nonlinear effects in the dynamics and acoustics of real bubble clouds. An attempt to understand these nonlinear effects was undertaken in the work of Kumar and Brennen [1991], [1992], [1993]. Using Fourier expansion theory, they found weakly nonlinear solutions to a number of cloud problems by retaining only the terms that are quadratic in the amplitude. One interesting phenomenon that emerges from this nonlinear analysis involves the interactions between the bubbles of different size that would commonly occur in any real cloud. The phenomenon, called "harmonic cascading" (Kumar and Brennen [1992]), occurs when a relatively small number of larger bubbles begins to respond nonlinearly to external excitation. Then the higher harmonics produced by the nonlinearity will excite the much larger number of smaller bubbles at their natural frequency. The process can then be repeated to even smaller bubbles. In essence, this nonlinear effect causes a cascading of fluctuation energy to smaller bubbles and higher frequencies.

Another approach to the modeling of the interaction dy-

namics of cavities was developed by Chahine and his coworkers (Chahine and Duraiswami [1992]; Chahine *et al.* [1992]). Three dimensional Boundary Element Methods have been employed to simulate the deformations of the individual bubbles within collapsing clouds in inhomogeneous flow fields or close to solid boundaries. It has been shown that the bubbles on the periphery of the cloud develop inwardly directed reentrant jets. However, most clouds contain many thousands of bubbles, impossible to be handled by any high speed computer at this time. It therefore is advantageous to examine the nonlinear behavior of cavitation clouds using continuum mixture models. The recent numerical modeling of unsteady cavitating flows on a hydrofoil by Kubota *et al.* [1992] is an important step in the direction of engineering application using continuum bubbly mixture models. However, the artificial diffusivities they used for the reason of numerical stability may suppress the collapse of the bubbles so that to eliminate some highly nonlinear phenomena such as the formation of shock waves.

Another perspective on the subject of collapsing clouds was that introduced by Mørch, Hanson and Kedrinskii (Mørch [1980], [1981], [1982]; Hanson *et al.* [1981]). They speculated that the collapse of a cloud of bubbles involves the formation and inward propagation of a shock wave and that the geometric focusing of this shock at the center of a cloud creates the en-

hancement of the noise and damage potential associated with cloud collapse. However, they assumed that the bubbles are completely annihilated after the shock passing. This implies that all the bubbles are filled with pure vapor. But this implies no real sonic speed for the bubbly mixture and hence makes the shock wave solutions inappropriate. Fully nonlinear solutions for spherical cloud dynamics were first obtained by Wang and Brennen [1994], [1995b], [1995a]. Their computational results show that the continuum models of the cloud indeed manifest the shock wave phenomena and thus confirm the idea put forward by Mørch and his coworkers.

1.2 Topics of Present Research

This thesis presents studies of the basic dynamics and the consequent acoustics of a bubble cloud in a massively nonlinear cavitating flow. The model of the spherical cloud problem is described in Chapter 2. Sections 2.1 and 2.2 describe the non-dimensional quantities to be used and the basic problem to be solved. Governing equations, initial conditions and boundary conditions are given in Section 2.3. Section 2.4 describes the far-field pressure perturbation to be experienced by the cloud. The typical response of a single bubble to this pressure perturbation is also shown.

The numerical method for solving these equations is discussed in Chapter 3. The derivation of the Lagrangian integral equations is given in Section 3.1.

Section 3.2 describes the iteration algorithms used to find the mixture pressure coefficient and points out the inherent numerical difficulties of the problem.

Computational results and discussion are presented in Chapter 4. The characteristics of the nonlinear dynamics of the cloud are described in Section 4.1. The development of a bubbly shock wave as well as the structure of the shock during the collapse of the cloud are also described. Furthermore, a typical strength of the pressure pulse produced by shock-induced local bubble collapse is illustrated. Section 4.2 describes the inherent numerical difficulty by showing a typical rate of convergence for solving the integral equation of mixture pressure coefficient. The number of iterations at each time step is directly affected by the strength of the shock pulse and grows very fast as the shock moves into the cloud and accumulates its strength. Typical rates of convergence for different iteration algorithms are also compared. Section 4.3 describes an important parameter in cloud dynamics. This parameter is termed as the "bubble/cloud interaction parameter." Physical meaning of this parameter is discussed. It is shown that different values of the bubble/cloud interaction parameter will result in different collapse scenarios of the cloud. Three cloud collapse modes are identified and described in Section 4.4. The phenomena of the formation and focusing of the shocks are different in each mode. The characteristics of the far-field acoustic pulses produced by the cloud dynamics are presented in Section 4.5. Power spectral density of the

pulses shows several important features of the acoustic noise produced by the nonlinear dynamics of the cloud. Some of these characteristics have been observed in experiments. The far-field impulse generated by the cloud collapse is examined in Section 4.6. The impulses generated during different collapse modes are compared. Correlation of the acoustic impulses with various flow parameters are also included. It is found that the impulse is strongly correlated with the normalized maximum total volume of bubbles in the cloud. The rapid increase of the speed of the shock as it propagates into the cloud is described in Section 4.7. Results from three different initial void fractions are presented. In Section 4.8, the present analytical results are compared with the recent experimental results obtained here, at Caltech (Reisman and Brennen [1996]; Brennen *et al.* [1996]). Correlation of the measured pressure signals with high speed movies of cloud cavitation associated with cavitating hydrofoil clearly showed that the formation and subsequent collapse of large scale bubble clouds produce very large pressure pulses which can be explained by the present theory.

Chapter 2

The Model Problem and Governing Equations

A prototypical problem is constructed to explore the basic dynamics of the nonlinear growth and collapse of a spherical cloud of bubbles. The spherical symmetry makes the problem tractable without losing the fundamental dynamics.

2.1 Dimensionless Quantities

The variables in all the following figures and equations are non-dimensionalized using the initial bubble radius, R_0^*, and a reference flow velocity, U^*. All quantities with superscript * represent dimensional values; without this superscript the quantities are non-dimensional. For example, the non-dimensional bubble radius $R = R^*/R_0^*$, the non-dimensional bubble population per unit liquid

volume $\eta = \eta^*(R_0^*)^3$, the non-dimensional mixture velocity $u = u^*/U^*$, the non-dimensional radial coordinate $r = r^*/R_0^*$, and the non-dimensional time $t = t^*U^*/R_0^*$. The Reynolds number Re, Weber number We, pressure coefficient of the mixture C_P, and cavitation number σ are defined as follows:

$$
\begin{aligned}
Re &= \rho_L^* U^* R_0^* / \mu_E^* \\
We &= \rho_L^* U^{*^2} R_0^* / S^* \\
C_P &= (p^* - p_0^*)/(\frac{1}{2}\rho_L^* U^{*^2}) \\
\sigma &= (p_0^* - p_V^*)/(\frac{1}{2}\rho_L^* U^{*^2})
\end{aligned}
$$

where ρ_L^* is the liquid density, μ_E^* is the effective viscosity of liquid which incorporates the various bubble-damping mechanisms, namely acoustic, thermal, and viscous damping, described by Chapman and Plesset [1971], S^* is the surface tension of the liquid, p_V^* is the vapor pressure inside the bubble, p_0^* is the initial equilibrium pressure in the mixture, and p^* is the mixture pressure. From the definition of cavitation number, σ, we know that small values of σ indicate that the initial equilibrium pressure is close to the vapor pressure and the bubbles therefore cavitate more readily.

2.2 The Model Problem

Consider a spherical cloud of bubbles surrounded by an unbounded pure liquid as shown in Figure 2.1. The liquid is at rest infinitly far from the cloud. Compared to the large compressibility of the cloud, the pure liquid is assumed incompressible. It is assumed that the population of bubbles per unit volume of liquid, η, within the cloud, is piecewise uniform initially and that there is no coalescence or break-up of bubbles. Since relative motion between the two phases and the mass of liquid vaporized or condensed are both neglected, it follows that η remains both constant and piecewise uniform within the cloud. The radius of the cloud is represented by $A(t)$, a function of time t. The bubble radius in the cloud is $R(r,t)$, a function of radial coordinate r and time. The bubbles are assumed to be spherical and to contain uniform water vapor and residual permanent gas. The problem to be solved is as follows. The cloud and the whole domain of liquid are initially in equilibrium. Starting at $t = 0$, a far-field driving pressure, $C_{P\infty}(t)$, is imposed on the pure liquid at infinity and the response of the cloud to this pressure perturbation is to be studied.

2.3 Basic Equations

The basic equations used are those of d'Agostino and Brennen [1983], [1988], [1989] except that all the nonlinear convective terms are retained since these

are important in the context of the highly nonlinear growth and collapse of the cloud. The dimensionless forms of the continuity and momentum equations for the spherical bubbly flow are:

$$\frac{1}{r^2}\frac{\partial(r^2u)}{\partial r} = \frac{12\pi\eta R^2}{3+4\pi\eta R^3}\frac{DR}{Dt} \quad ; \quad r \le A(t) \tag{2.1}$$

$$\frac{Du}{Dt} = -\frac{1}{6}(3+4\pi\eta R^3)\frac{\partial C_P}{\partial r} \quad ; \quad r \le A(t) \tag{2.2}$$

where $D/Dt \equiv \partial/\partial t + u\partial/\partial r$ is the Lagrangian derivative, $u(r,t)$ is the mixture velocity, $R(r,t)$ is the individual bubble radius, $C_P(r,t)$ is the mixture pressure coefficient defined in Section 2.1, and $A(t)$ is the radius of the cloud. The bubble population per unit liquid volume, η, is related to the void fraction, α, by $(\frac{4}{3}\pi R^3)\eta = \alpha/(1-\alpha)$. The definition of α is the total volume of bubbles per unit mixture volume. Interactions of the bubble dynamics with the flow are modeled by the Rayleigh-Plesset equation (Knapp *et al.* [1970]; Plesset and Prosperetti [1977]) which connects the local mixture pressure coefficient, C_P, to the bubble radius, R:

$$\begin{aligned} R\frac{D^2R}{Dt^2} &+ \frac{3}{2}\left(\frac{DR}{Dt}\right)^2 + \frac{\sigma}{2}\left[1-R^{-3k}\right] + \frac{4}{Re}\frac{1}{R}\frac{DR}{Dt} \\ &+ \frac{2}{We}\left[R^{-1}-R^{-3k}\right] + \frac{1}{2}C_P = 0 \end{aligned} \tag{2.3}$$

where the definitions of cavitation number, σ, Weber number, We, and the Reynolds number, Re, are all given in Section 2.1. It has been assumed that the non-condensable gas inside the bubbles behaves polytropically with an index k. If $k = 1$, a constant bubble temperature is implied and $k = \gamma$, the ratio of specific heats, would model adiabatic behavior. Bubble growth due to rectified diffusion has been ignored since that takes place on a much slower timescale than in the process of violent collapse in cavitating flows. Furthermore, the above Rayleigh-Plesset equation neglects the local pressure perturbations experienced by the individual bubble due to the growth or collapse of its neighbor. In other words, effects of the nonzero volume variation of the neighboring bubbles are excluded in this bubble dynamic model. It has been shown that for randomly distributing bubbles the correction factors are of order of α (Nigmatulin [1991]), or higher (Sangani [1991]). These corrections could be incorporated theoretically or numerically. However, in the present work the void fractions considered are only few percent so that the correction factors are neglected. d'Agostino and Brennen [1989] also estimated the error in neglecting these effects to be very small.

The mathematical model of equations (2.1), (2.2), and (2.3) is complete and after applying appropriate initial and boundary conditions can, in theory, be solved to find the unknowns $C_P(r,t)$, $u(r,t)$, and $R(r,t)$ for any bubbly cavitating flow with spherical symmetry. However, the nonlinearities in the

Rayleigh-Plesset equation and in the Lagrangian derivative, D/Dt, present considerable computational impediments.

The boundary condition on the surface of the cloud, $r = A(t)$, is obtained as follows. The spherically symmetric incompressible liquid flow outside the cloud, $r \geq A(t)$, must have a solution of the form:

$$u(r,t) = \frac{C(t)}{r^2} \quad ; \quad r \geq A(t) \tag{2.4}$$

$$C_P(r,t) = C_{P\infty}(t) + \frac{2}{r}\frac{dC(t)}{dt} - \frac{C^2(t)}{r^4} \quad ; \quad r \geq A(t) \tag{2.5}$$

where $C(t)$ is an integration constant and $C_{P\infty}(t)$ is the imposed driving pressure coefficient at infinity which will be described in Section 2.4. By substituting the values of u and r at the boundary of the cloud in (2.4), $C(t)$ can be determined as

$$C(t) = u(A_0,t)r^2(A_0,t) \tag{2.6}$$

Combining (2.4) and (2.5) and substituting $r = A(t)$, we obtain the time-dependent boundary condition at the surface of the cloud:

$$C_P(A(t),t) = C_{P\infty}(t) + \frac{2}{A(t)}\frac{d[A^2(t)u(A(t),t)]}{dt}u^2(A(t),t) \tag{2.7}$$

At the center of cloud, the symmetry of the problem requires

$$u(0,t) = 0 \tag{2.8}$$

Initial conditions are also required and, in the context of cavitating flows, it is appropriate to assume that, at time $t \leq 0$, the whole flow field is in equilibrium. It is also assumed, for simplicity, that all the bubbles have the same initial size. Therefore, the following initial conditions should be applied:

$$R(r,0) = 1, \quad \frac{DR}{Dt}(r,0) = 0, \quad u(r,0) = 0, \quad C_P(r,0) = 0 \tag{2.9}$$

2.4 The Far-field Driving Pressure, $C_{P\infty}(t)$

In (2.7), $C_{P\infty}(t)$ represents the far-field pressure perturbation experienced by the cloud in a typical cavitating flow. A simple sinusoidal form is chosen for $C_{P\infty}(t)$:

$$C_{P\infty}(t) = \begin{cases} \frac{1}{2} C_{PMIN} \left[1 - \cos(\frac{2\pi}{t_G} t)\right] & 0 < t < t_G \\ 0 & t < 0 \text{ and } t > t_G \end{cases} \tag{2.10}$$

where C_{PMIN} is the minimum driving pressure coefficient and t_G is the non-dimensional duration of the pressure perturbation. Consequently, for a cloud flowing with velocity U^* past a body of size D^*, the order of magnitude of t_G

will be D^*/R_0^*, and C_{PMIN} will be the minimum pressure coefficient of the flow. In order to characterize how $C_{P\infty}(t)$ and the cavitation number, σ, influence the occurrence of cavitation, an example of $C_{P\infty}(t)$ with C_{PMIN} = -0.5 and t_G = 500 is given in Figure 2.2. Any flow, whether cavitating or not, has some value of σ, which is set as 0.4 in the present example. From the definitions of pressure coefficient and cavitation number, we know that when $C_{P\infty}(t) < -\sigma$ the driving pressure is lower than the vapor pressure, p_V^*, and will cause nuclei in the flow to cavitate. Figure 2.3 shows a typical dynamic response of a single bubble to this pressure perturbation by solving the Rayleigh-Plesset equation numerically; it also demonstrates the strong nonlinearity of the equation. The fast growth rate of the cavitating bubble, after $C_{P\infty}(t) < -\sigma$, makes it continue to expand even after the ambient pressure has recovered and is higher than vapor pressure. In other words, the maximum bubble size occurs after the minimum pressure. Then the bubble collapses catastrophically, and this is followed by successive rebounds and collapses. In the absence of dissipation mechanisms such as viscosity, these rebounds would continue indefinitely without attenuation. Each collapse and rebound will result in extremely large radiated pressure pulses and thus cause noise and material damage.

Chapter 3

Numerical Method

3.1 The Lagrangian Integral Method

The natural coordinate system in the present problem is the Lagrangian coordinate system based on the mixture velocity, in which all the nonlinear convective terms in the mixture momentum equation and bubble dynamics are eliminated. A numerical scheme based on the integral representation of the continuity and momentum equations in the Lagrangian coordinates, (r_0, t), has been developed, where r_0 is the radial distance from the center of the cloud at initial time $t = 0$. The values of quantities at $t = 0$ are denoted by a subscript 0. For example, $\rho_0 = \rho(r_0, 0)$ is the mixture density at $t = 0$. Therefore, the local density of a mixture material element, $\rho(r_0, t)$, is related

to its initial density, $\rho_0(r_0)$, by

$$\frac{\rho(r_0,t)}{\rho_0(r_0)} = \frac{1}{J} \tag{3.1}$$

where J is the Jacobian of the coordinate transformation from Lagrangian coordinates to Eulerians: $r_0 \longmapsto r(r_0,t)$, and has the following expression in the spherically symmetric configuration:

$$J = \frac{r^2}{r_0^2}\frac{\partial r}{\partial r_0} \tag{3.2}$$

This also represents the ratio of the current material volume to its initial volume. The position of a mixture particle can be obtained by integrating equation (3.1).

$$r(r_0,t) = \left\{ \frac{3}{3+4\pi\eta} \int_0^{r_0} \xi^2 \left[3 + 4\pi\eta R^3(\xi,t)\right] d\xi \right\}^{1/3} \tag{3.3}$$

where ξ is the dummy variable of the integration and we approximate $\rho(r_0,t)/\rho_0(r_0) \approx [1-\alpha(r_0,t)]/[1-\alpha_0(r_0)]$ due to the fact of large ratio of liquid to vapor density. Note that the boundary condition $r(r_0,t) = 0$ at the center of the cloud has been used to eliminate the integration constant. The

mixture velocity can be obtained by differentiating equation (3.3) as follows:

$$
\begin{aligned}
(3.4) \qquad u(r_0,t) &= \frac{\partial r(r_0,t)}{\partial t} \\
&= \frac{12\pi\eta}{(3+4\pi\eta)r^2(r_0,t)} \int_0^{r_0} \frac{\partial R(\xi,t)}{\partial t} R^2(\xi,t)\xi^2 d\xi
\end{aligned}
$$

The mixture momentum equation, (2.2), and the boundary condition at the surface of the cloud, (2.7), have the following forms in the Lagrangian coordinate framework:

$$
(3.5) \qquad \frac{\partial C_P(r_0,t)}{\partial r_0} = -\frac{6}{3+4\pi\eta R^3(r_0,t)} \frac{\partial u(r_0,t)}{\partial t} \frac{\partial r(r_0,t)}{\partial r}
$$

$$
(3.6) \qquad C_P(A_0,t) = C_{P\infty}(t) + \frac{2}{r(A_0,t)} \frac{d}{dt} \left[r^2(A_0,t) u(A_0,t) \right] - u^2(A_0,t)
$$

After substituting equations (3.3) and (3.4) in the right-hand side of (3.5) and integrating from r_0 to A_0 using the boundary condition (3.6), an integral equation for mixture pressure coefficient, C_P is found:

$$
\begin{aligned}
(3.7) \quad C_P(r_0,t) &= \frac{6}{3+4\pi\eta} \left[\int_{r_0}^{A_0} \frac{f(\xi,t;C_P) - 2r(\xi,t)u^2(\xi,t)}{r^4(\xi,t)} \xi^2 d\xi \right] \\
&\quad + \frac{2f(A_0,t)}{r(A_0,t)} - u^2(A_0,t) + C_{P\infty}(t)
\end{aligned}
$$

where

$$(3.8) \qquad f(\xi,t;C_P) = \frac{12\pi\eta}{3+4\pi\eta}\int_0^{\xi}\left\{\frac{2}{We}\left[R^{1-3k}(\zeta,t)-1\right]\right.$$
$$-\frac{4}{Re}\frac{\partial R(\zeta,t)}{\partial t}+\frac{\sigma}{2}R(\zeta,t)\left[R^{-3k}(\zeta,t)-1\right]$$
$$\left.+\frac{1}{2}R(\zeta,t)\left[(\frac{\partial R(\zeta,t)}{\partial t})^2-C_P\right]\right\}\zeta^2 d\zeta$$

Here the Rayleigh-Plesset equation, (2.3), has been used to substitute for the bubble wall acceleration, $\partial^2 R(r_0,t)/\partial t^2$. As we will see in the next chapter, it is the very large value of this acceleration at the instant of bubble collapse and rebound which causes numerical difficulties.

A complete integration time step therefore proceeds as follows.

1) At each Lagrangian node, r_0, $R(r_0,t+\triangle t)$ and $\partial R(r_0,t+\triangle t)/\partial t$ are calculated using an explicit time marching scheme (a Runge-Kutta scheme) based on the known solution at the previous time step, $R(r_0,t)$, $\partial R(r_0,t)/\partial t$ and $\partial^2 R(r_0,t)/\partial t^2$.

2) With $R(r_0,t+\triangle t)$ and $\partial R(r_0,t+\triangle t)/\partial t$, equations (3.3) and (3.4) can be integrated to obtain $r(r_0,t+\triangle t)$ and $u(r_0,t+\triangle t)$.

3) With the results of steps 2 and 3, we can iterate upon equation (3.7) to find $C_P(r_0,t+\triangle t)$. Then the Rayleigh-Plesset equation (2.3) can be used to find $\partial^2 R(r_0,t+\triangle t)/\partial t^2$.

4) Proceed to next time step.

3.2 Iteration Algorithms to Find C_P

Under-relaxation must be used in the iteration step 3 to achieve convergence. To explain this, rewrite equation (3.7) into the following symbolic form:

$$C_P = T(r, R, u, C_P) + g(r, R, u) \tag{3.9}$$

where operator T represents the double integration in (3.7) combined with (3.8) and the inhomogeneous term $g(r, R, u)$ includes all the other terms without C_P. Recall that, at this stage all the quantities, except C_P, are known so we need to iterate the above equation to find C_P. Denote all quantities at node r_{0j} with subscript j. At each stage in the iteration, the residuals, ϵ_j, are

$$\epsilon_j = T_j(r, R, u, C_P^{old}) + g_j(r, R, u) - C_{Pj}^{old} \tag{3.10}$$

where C_P^{old} is the result of the last iteration. In general, the iteration algorithm assumes the following form:

$$C_{Pj}^{new} = C_{Pj}^{old} + \omega \frac{\epsilon_j}{\gamma_j} \tag{3.11}$$

in which ω is the relaxation factor and γ_j represents the estimation of the rate of the change of the residual ϵ_j with respect to C_{Pj}. If $\gamma_j = 1$, (3.11) corresponds to the algorithm of weighted average. It is found that, in general, ω must be much less than 1 to make the iteration procedure converge. This results in large computational time. The source of this difficulty can be seen from the following discussion. First, approximate equation (3.9) by the set of difference equations:

$$a_j C_{Pj} + \sum_{k=1,\ k\neq j}^{N} b(k) C_{Pk} + g_j = 0, \quad j = 1 \cdots N \tag{3.12}$$

in which the operator of double integral, T, has been approximated by the trapezoidal rule, $a(j)$ and $b(k)$ are the known coefficients, and N is the total number of Lagrangian nodes. Equation (3.12) can be put into a matrix form, $QC_P = g$, with a_j as the diagonal elements of the coefficient matrix Q. This can be used to find the unknown vector C_P. However, in the present computation, the equation is close to being ill-conditioned. The local collapse and rebound of bubbles produce very large bubble wall accelerations which in turn contribute to the magnitude of the off-diagonal coefficient, $b(k)$, at that location and cause the matrix Q to be far from diagonally dominant. As we will see in Section 4.2, the stronger the shock wave, the worse the situation. However, the iteration algorithm (3.11) can still reach convergence by limiting the relaxation factor ω to a very small number, and it is found that the best

choice of γ_j in (3.11) are the diagonal elements in equation (3.12), namely, a_j. The rates of convergence for different γ_j will be shown in Section 4.2.

In addition, the program automatically adjusts the interval of each time step to ensure that the maximum fractional change of bubble radius in the cloud between any two consecutive times does not exceed some specific value (typically, 5%). This is essential for time marching through a violent bubble collapse.

Chapter 4

Results and Discussion

The typical flow condition chosen for illustrated purposes in the present study is as follows. A cloud of nuclei, composed of air bubbles of initial radius R_0^*=100 μm in water at 20^oC, flows with velocity U^*=10 m/sec through a region of low pressure characterized by $C_{PMIN} = -0.75$ and the non-dimensional duration of the low pressure perturbation, t_G (in equation (2.10)), of 50, 100, 500, and 1000. The computation is performed for different combinations of the following parameters: initial void fraction, α_0, of 0.03%, 0.3%, and 3%; cavitation number, σ, of 0.45, 0.55, and 0.65; the non-dimensional cloud radius, A_0, of 32, 100, and 312. These ranges of values of A_0 and t_G correspond to the ratio of the length scale of the low pressure perturbation to the initial radius of the cloud, D/A_0, of 0.5 to 31.25. The Reynolds number, $Re = U^* R_0^* \rho_L^* / \mu_E^*$, based on the reference flow velocity, initial bubble radius, the liquid density, and the effective viscosity, is 20 in all the cases presented.

As mentioned in Chapter 2, the effective liquid viscosity, μ_E, is used in place of actual liquid viscosity to incorporate the various bubble damping mechanisms (Chapman and Plesset [1971]).

4.1 Nonlinear Dynamics of the Spherical Cloud

Figure 4.1 presents typical bubble-size time histories for five different Lagrangian locations within the cloud, from the surface, $r_0 = A_0$, to the center, $r_0 = 0$. The characteristics of the growth of the cloud are similar to those of a single bubble and that all bubbles in the cloud grow in phase. However, because of the strong bubble interaction effects, bubble growth is severely restrained and the bubble growth rate within the cloud is much smaller than that near the surface. Under these circumstances all bubbles away from the near-surface region grow to a smaller maximum size. In other words, the bubbles in the interior are shielded to some extent by the outer shell of bubbles. The shielding effect is typical of the bubble-bubble interacting phenomenon appearing in the earlier investigations of cloud dynamics (Omta [1987]; d'Agostino and Brennen [1989]; Chahine and Duraiswami [1992]). After the recovery of the ambient pressure, bubbles on the surface of the cloud start to collapse first. The flow acceleration

induced by the collapse of the surface bubbles promotes more violent collapse of the neighboring bubbles and then the strengthening collapse spreads inward, as shown in Figure 4.1. The shielding effect causes the bubbles in the interior region to continue to grow even after the surface-layer bubbles have totally collapsed.

As a result of the collapse of the surface layer, a bubbly shock wave develops and propagates inward through the cloud. A typical structure of this shock wave is illustrated in Figures 4.2 and 4.3. The wave front of the shock can be easily identified by the collapse front of bubbles. Unlike aerodynamic shock waves, the bubbly shock has an oscillatory structure behind the shock front which involves a series of rebounds and secondary collapses and is very similar to that of the gas/liquid shocks investigated by Noordzij and van Wijngaarden [1974] and other investigators (see, for example, Kameda and Matsumoto [1995]). The series of zones with small bubble size represent regions of low void fraction and higher pressure due to the local bubble collapse. A schematic representation of the spherical shock is shown in Figure 4.4. Parenthetically, Mørch, Kedrinskii and Hanson (Mørch [1980], [1980]; Hanson *et al.* [1981]) first speculated that the collapse of a cloud of bubbles is driven by an inwardly propagating shock wave. Results of the present analysis confirm this idea (see also Wang and Brennen [1994], [1995b], [1995a]).

As the shock front passes bubbles and causes them to collapse, a very large pressure pulse can be produced, as shown in Figure 4.5. This pressure peak, which has a typical magnitude of about 40 *atm* in practice, corresponds to the violent collapse of bubbles at the shock front (located at 50% of the cloud radius at the moment of time depicted in Figure 4.4). The shock wave strengthens considerably as it propagates into the cloud primarily because of the focusing effect of the spherical configuration.

4.2 Inherent Numerical Difficulties

As mentioned in Section 3.2, there is an inherent numerical difficulty associated with the cavitating flows with bubble dynamic effects. In the computational procedures developed in Section 3.1, an essential step was the solution of an integral equation for the mixture pressure coefficient. It is shown in Part II of this thesis that, instead of the integral equation, mathematically, we can derive a Poisson-type second order differential equation for the pressure coefficient. But, in either method, we need to integrate the pressure field through the very large local pressure pulse produced by the violent bubble collapse where the spatial derivative of the pressure is discontinuous. An example of this can be seen in Figure 4.5. The pressure pulse increases in amplitude as the shock propagates inwards and is focused geometrically. The instantaneous non-dimensional magnitude can be as high as $O(10^5)$ with discontinuity of

slope.

Figure 4.6 shows a typical convergence history for solving the integral equation (3.7) by the iteration algorithm (3.11) in which γ_j=1 is used. In this example the cloud reaches its maximum size at about t=220 and then collapses. As a part of this collapse, we know that a shock wave is developed and is focused into the cloud. Each local peak of the fast oscillation in Figure 4.6 corresponds the presence of a large pressure pulse in the cloud which in turn requires larger number of iterations. As the shock moves toward the cloud center, the iteration number increases with the increase of the magnitude of the pressure pulse. At $t \approx 370$, when the shock arrives to the center of the cloud, the number of iteration reaches its maximum and then reduces suddenly as a result of cloud rebound. Comparison of the convergence history for different combinations of ω and γ_j in (3.11) are shown in Figure 4.7. The choice of ω=0.03 and $\gamma_j = a(j)$, the diagonal element in equation (3.12), results in better convergence.

4.3 The Bubble/Cloud Interaction Parameter

In Wang and Brennen [1995a], parameters such as the cavitation number, σ, initial void fraction, α_0, ratio of initial cloud size to bubble size, A_0/R_0, ratio of the low pressure perturbation length scale to cloud size, D/A_0, and C_{PMIN} were exercised in order to explore the range of possible phenomena. The char-

acteristics dynamics were found to be strongly dependent on the parameter, $\beta \equiv \alpha_0(1-\alpha_0)A_0^2/R_0^2$, which will be termed the "bubble/cloud interaction parameter." Earlier linear and weakly nonlinear studies of cloud dynamics (see d'Agostino and Brennen [1983], [1989], Kumar and Brennen [1991], [1992], [1993]) show that this parameter is crucial in determination of the cloud natural frequency. If this parameter is much less than order of unity, the natural frequency of the cloud is close to that of the individual bubbles in the cloud. In other words, the bubbles in the cloud tend to behave as individual voids in an infinite fluid and the bubble/bubble interaction effects are minor. These imply that the dynamic effects of the cloud are approximately the direct sum of the effects of the individual bubbles in the cloud. On the other hand the bubble interaction effects in the cloud are dominant when the value of β is greater than order one. The collective oscillation of bubbles in the cloud can result in a cloud natural frequency which is much lower than the natural frequency of individual bubbles.

The complexity of multiphase flows comes from the existence of different characteristic times or length scales in the flows and the interactions between them. The fluid dynamic phenomena are different for the flow fields with different interaction effects. In cloud cavitation one of the most important effect is that of the bubble dynamics on the global flow fields and the control parameter of this effect is β. In the expression of β, A_0 is the macroscopic

length scale in the flow, R_0 characterizes the microscale, and $\alpha_0(1-\alpha_0) \approx \alpha_0$ represents the concentration of the dispersed phase. The physical meaning of β is more clear if we rewrite it into another form. The sonic speed in a bubbly mixture of void fraction α_0 without viscosity and surface tension effects is approximately (see, for example, Brennen [1995], Section 6.2)

$$c^* = \sqrt{\frac{kp^*}{\alpha_0\left(1-\alpha_0\right)\rho_L^*}} \tag{4.1}$$

where p^* is the mixture pressure and k is the polytropic index of the gas inside the bubble. (Recall that all quantities with * are dimensional). The natural frequency of bubbles in the mixture is approximately

$$\omega_B^* = \sqrt{\frac{3kp^*}{\rho_L^* R_0^*}} \tag{4.2}$$

where R_0^* is the bubble radius. But the global length scale of the flow is the radius of the cloud, A_0^* and, consequently, there are two dynamic time scales in the flow: the time scale of bubble dynamics, $T_B^* \equiv 1/\omega_B^*$, and the time scale of wave propagation given by

$$T_C^* \equiv \frac{1}{\omega_C^*} = \frac{A_0^*}{c^*} \tag{4.3}$$

The ratio of these two characteristic times has the expression of

$$\frac{T_C^*}{T_B^*} \approx \sqrt{\frac{\alpha_0 \left(1-\alpha_0\right) A_0^{*2}}{R_0^{*2}}} = \sqrt{\frac{\alpha_0 \left(1-\alpha_0\right) A_0^2}{R_0^2}} = \sqrt{\beta} \tag{4.4}$$

Therefore, β determines the ratio of the two characteristic times in the flow. If β is small, the bubbles will not feel the large scale perturbation in the flow and there is no interaction from bubble dynamics. On the contrary, if β is larger than order one, the bubble dynamics can effectively influence the large scale perturbation and contribute to the global dynamics of the cloud.

4.4 Cloud Collapse Modes

Depending on the magnitude of β, three modes of collapse have been identified and are described as follows. Figure 4.1 presents the first mode of collapse for $\beta \gg 1$ ($\beta \approx 300$). Time histories of bubble radius at five different Lagragian locations, from the cloud surface, $r_0 = A_0$, to the cloud center, $r_0 = 0$, are presented to illustrate this collapse mode. Because of the strong bubble/cloud interaction effects, bubble growth is severely restrained and the bubble growth rate within the cloud is quite uniform. All bubbles away from the cloud surface grow to about the same maximum size. During the collapse phase, bubbles on the surface of the cloud collapse first and then the collapse propagates and strengthens inward. As a result of these collapses, a shock wave develops and

propagates inward through the cloud. The structure of the shock has been described in Figures 4.2 and 4.3. Figure 4.1 also shows that the closer the bubbles are to the cloud center, the smaller size they collapse. This is due to the strengthening of the shock. Very complicated bubble-bubble interactions are observed when the focusing shock reaches the center of the cloud (at $t \approx 746$), produces very high pressures, and then causes a rebound of the cloud. An outspreading expansion wave causes all bubbles to grow and starts the next dynamic cycle of the cloud.

On the other hand, when $\beta \ll 1$, the bubbles tend to behave as they would in an infinite fluid and as illustrated in Figure 4.8. The behavior of the cloud is quite different under this circumstance. The bubbles can grow more "freely" to larger sizes than when $\beta \gg 1$. However, the bubbles closer to cloud center grow more slowly than the bubbles near the surface and, therefore, the bubbles with the smallest maximum size occur at the center of the cloud. The maximum size of the bubbles on the surface can be up to an order of magnitude larger than that of the bubbles near the center. As a result, the central bubbles collapse first and the collapse spreads outward as an innocuous expansion wave. There is no shock-enhancing process involved and the resulting acoustic impulse is much smaller than that of the previous mode of collapse as is shown in Section 4.6.

There is an intermediate type of collapse when β has an intermediate value,

as illustrated in Figure 4.9. The collapse starts at mid-radius (about $0.7A_0$ in Figure 4.9) and spreads inward and outward from this location. From the figure we know that the shielding effect is still strong in the core region of the cloud so that the growth of core bubbles continues even after outer bubbles have collapsed. The outward moving collapse front tends to cancel the inward acceleration of the flow caused by the collapse of the bubbles on the surface of the cloud. The inward moving collapse has a structure similar to the shock wave described earlier. However, the shock- focusing effect is weaker due to the reduced "effective collapse size" of the cloud. The resulting acoustic impulse will be an intermediate value between the previous two modes.

4.5 The Far-field Acoustic Noise

It is important to determine the acoustic consequences associated with the cloud dynamics. For this reason we shall examine the far-field acoustic noise produced by the volumetric acceleration of the cloud. The noise is a consequence of the large momentary mass flux involved in the process of cloud collapse and rebound. Acoustic effects generateded by individual bubbles are minor in the far-field and will be neglected. If we denote the dimensional time-varying volume of the cloud by $V^*(t^*)$, it follows that the dimensional form of the time-varying far-field acoustic pressure is given by (see

Dowling and Williams [1983]; Blake [1986])

$$p_a^*(t^*) = \frac{\rho_L^*}{4\pi r^*}\frac{d^2V^*}{dt^{*2}} \tag{4.5}$$

where p_a^* is the radiated acoustic pressure and r^* is the distance from the cloud center to the point of measurement. In considering the far-field noisethe noise radiated by individual bubble is neglected

A non-dimensional far-field acoustic pressure can be defined by

$$p_a(t) = \frac{p_a^* r^*}{\frac{1}{2}\rho_L^* U^{*2} D^*} = \frac{2R_0}{D}\left[A^2(t)\frac{d^2A(t)}{dt^2} + 2A(t)\left(\frac{dA(t)}{dt}\right)^2\right] \tag{4.6}$$

where the normalizing length scale was chosen to be D^*, the typical length of low pressure perturbation experienced by the cloud (see Section 2.4). In real flows, D^* can be the size of the body or the chord of propeller blade. The time history of the radius of the cloud is shown in Figure 4.10. Note that, unlike single bubbles, the cloud radius, $A(t)$, only decreases to a size marginally smaller than its equilibrium size during the collapse process. However, the local void fraction within the cloud undergoes large changes due to the sweep of the shock. This is consistent with the recent experimental observation for cloud collapse by Reisman and Brennen [1996]. When the enhanced shock wave moves to the center of the cloud, extremely high pressures are produced; an outwardly expanding wave then follows. This process can result in very large

volumetric accelerations and thus cause a large peak in the radiated acoustic noise as illustrated in Figure 4.10. The magnitudes of the subsequent peaks decay with time with each cloud collapse and rebound. After several cycles, the cloud begins to oscillate at its natural frequency (for natural frequency of the cloud, see d'Agostino and Brennen [1983], [1989]).

The power spectral density of the acoustic noise in Figure 4.10 is shown as a function of dimensionless frequency in Figure 4.11. This spectrum exhibits the f^{-2} behavior for the frequency range below 0.2 (or 20 kHz in dimensional value) which is typical of cavitation noise (see, for example, Arakeri and Shangumanathan [1985], Blake *et al.* [1977]). Other cases exhibited an f^{-n} behavior with n in the range of 0.5 to 2. The spectrum has large peaks at the lowest cloud natural frequency and its higher harmonics. The first large peak in Figure 4.11 corresponds to the first natural frequency of the cloud which is located at f=0.02 (or 2 kHz) in the present case. It is contributed by the regular oscillations of the cloud which occur toward the end of the collapse and rebound process. The higher harmonics have large amplitudes and indicate high degree of nonlinearity of the cloud dynamics. Note that the natural frequency of the individual bubble in the cloud is 0.158 (15.8 kHz) in this case. The most significant feature of the spectrum is that most of the energy is in the lower frequency range (with respect to the bubble natural frequency), and is due to the coherent dynamics of the cloud. It is

noted that Marboe *et al.* [1986] and Arakeri and Shangumanathan [1985] observed the tendency of the noise spectrum to shift towards lower frequencies than expected from single bubble dynamics considerations. The effects of bubble interactions in cavitating flows were suspected to be the source of this phenomenon. The linear analyses by d'Agostino and Brennen [1983], [1989] confirmed that the cloud can indeed have much lower natural frequency than that of the individual bubble. Furthermore, the present analysis shows that the shift of the spectrum is also caused by the nonlinear harmonics in cloud dynamics.

4.6 Acoustic Impulses of the Cloud

A good measure of the strength of the collapse noise is the acoustic impulse, I, defined as the area under the acoustic pulse or

$$I = \int_{t_1}^{t_2} p_a(t)dt \tag{4.7}$$

where t_1 and t_2 are times before and after the pulse at which p_a is zero. Figures 4.12 to 4.15 illustrate the acoustic impulses as a function of the bubble/cloud interation parameter, β, for flows with different cavitation number, σ, and different ratio of the low pressure perturbation length to initial cloud size, D/A_0. In all cases, the impulse increases with increasing β and the rate of increase

is more pronounced as β transitions from order one to order ten. Moreover, for larger D/A_0, the difference of the impulse levels for different cavitation numbers is obvious, as shown in Figures 4.12 and 4.13. This is because the recovery of the ambient pressure of the cloud is slower and, therefore, the bubbles have more time to cavitate. Under this circumstance the degree of the cavitation in the cloud and the resulting acoustic impulse increases with the decrease of the cavitation number. On the other hand, if D/A_0 is small (Figures 4.14 and 4.15), the cloud will not have cavitated much before the recovery of the ambient pressure. Therefore, the influence of the cavitation number is smaller.

To investigate the relationship of the acoustic impulses to various parameters of the flow, calculations using a wide variety of parameter choices (45 permutations) are performed. It is found that the acoustic impulses are linearly correlated with the maximum total volume of the bubbles in the cloud normalized by the length of the low pressure perturbation, $V_{BMAX}/(0.5D)^3$, as shown in Figure 4.16. Moreover, as illustrated in Figure 4.17, this total volume decreases with increasing cavitation number and with increase in initial void fraction. It also varies with D/A_0.

4.7 Shock Speed

Figure 4.18 shows the inward propagation speed of the spherical bubbly shock wave as a function of the location of the shock front for three different initial void fractions, α_0, of 0.03%, 0.3% and 3%. Note that the shock speed has been non-dimensionalized by the reference velocity U^*=10 m/sec. In each case, the speed of the shock when it is initially formed in the surface layer of the cloud is of the order of 10 m/sec. However, the speed increases as it propagates into the cloud. The rate of the increase of the speed is quite linear as the shock moves in and is very pronounced over the last 20% of the collapse. This shows the strong focusing of the shock especially in the inner region of the cloud.

The shock speed near the center of the cloud is an order of magnitude larger than that in the outer region. The speed can reach about 800 m/sec for the cases of larger void fractions and can be as large as 1000 m/sec in the case of small void fraction (α_0=0.03%). If these moving pulses passed over some pressure transducer in a cavitating flow, the typical durations of the output signals will be the order of tenths of milliseconds to the order of tenths of microseconds. Furthermore, Figure 4.18 shows that the shock speed is smaller for larger initial void fraction. This trend is consistent with the void fraction dependence of the sonic speed in bubbly mixtures.

4.8 Comparisons of Experiments and Analytical Results

Earlier measurements of noise produced by cloud cavitation are characterized by pressure pulses of very short duration and large magnitude (see, for example, Bark and Berlekom [1978]; Shen and Peterson [1978], [1980]; Bark [1985]; Le *et al.* [1993]; Reisman *et al.* [1994]). However, the basic mechanisms for the production of these pulses were not clear. The present theory suggests that the formation and concentration of the bubbly shock waves should be responsible for these phenomena. Recently, experimental investigations of the large unsteady and impulsive pressures which are experienced on the suction surface of an oscillating hydrofoil as a result of cloud cavitation were conducted at California Institute of Technology (Reisman and Brennen [1996]; Brennen *et al.* [1996]). The experiments used piezo-electric transducers to measure the unsteady pressures at four locations along the chord of the foil and at two locations along the walls of the tunnel test section. The transducers on the foil surface registered very large positive pressure pulses with amplitudes of the order of tens of atmospheres and with durations of the order of tenths of milliseconds. These orders of magnitudes are in the range of present theoretical results. Correlation of the transducer output with high speed movies of the cavitation revealed that these pulses were produced by

the large scale collapse of a cloud of bubbles. Experiments also showed that substantial local pressure pulses were produced by the passage of low void fraction regions over pressure transducers. These regions appear to be bounded by bubbly shock waves which were propagating within the massive sheet cavitation on the foil suction surface. The transducers on the wall recorded the far-field acoustic pulses produced by the collapse of clouds. The magnitudes of these far-field pulses were of the order of one atmosphere which are also in the same order of magnitude as the theoretical far-field acoustic noise described in Section 4.5. Propagation speeds of the experimental pressure pulses were also studied by Brennen *et al.* [1996]. It was found that the pressure pulses moved with speeds from 10-100 m/sec in agreement with the range predicted by the present theory (see Figure 4.18). Furthermore, the present analysis shows that the pressure pulse increases in amplitude as the shock propagates inwards. The magnitudes of the pressure pulses in the present analysis for the case of low void fraction have an average value of hundreds of Mpa and can be as high as thousands of Mpa. While such predictions may seem excessively large, it should be noted that Avellan and Farhat [1989] recorded very large magnitude pressure pulses with average of 900 Mpa in magnitude (and extreme values of 2200 Mpa) during a study of cavitation vortex collapse.

Chapter 5

Concluding Remarks

The nonlinear growth and collapse of a spherical cloud of cavitation bubbles has been studied. Fully nonlinear mixture equations coupled with the Rayleigh-Plesset equation for the dynamics of the bubbles are solved by a Lagrangian integral method. It has been shown that a bubbly shock wave can develop as part of the nonlinear collapse of the bubble cloud. The shock forms on the surface of the cloud and strengthens both in magnitude and speed as it propagates into the cloud. Very high pressure pulses are produced when the shock wave passes the bubbles in the cloud and causes them to collapse. Moreover, the focusing of the shock produces very high pressures at the center of the cloud and then causes the rebound of the cloud. The volumetric acceleration of the cloud induces a large pulse in the far-field noise. Understanding such bubbly flow and shock wave processes is important because these flow structures propagate the noise and produce the impulsive loads on nearby solid

surfaces in a cavitating flow. The present results suggest that bubbly shock formation and focusing is one of the major mechanisms for the enhanced noise and damage potential associated with cloud cavitation.

The theoretical results shed some light on the previous experimental observations (Bark and Berlekom [1978]; Shen and Peterson [1978], [1980]; Bark [1985]; Franc and Michel [1988]; Kubota *et al.* [1989]; Le *et al.* [1993]; Reisman *et al.* [1994]; Reisman and Brennen [1996]; Brennen *et al.* [1996]). Experimental measurements of the far-field noise noise produced by cloud cavitation all exhibit pressure pulses of very short duration and large amplitude. These pulses can have magnitudes on the order of tens of atmospheres with typical durations of the order of tens of milliseconds. Even magnitudes as high as thousands of Mpa had been recorded. High-speed movies have also demonstrated that the passage of low void fraction regions over pressure transducers causes large pressure pulses, which are attributed to propagating shock waves. Correlation of the movie and the transducer outputs showed that the collapse of a large scale bubble cloud results in very large pressure pulses with propagating speeds ranging from tens of m/sec to hundreds of m/sec. These speeds are consistent with the present theory. Comparisons of the magnitudes of the pulses in the experiments and the theoretical analyses also show consistency.

The characteristics of the nonlinear cloud dynamics are shown to be

strongly dependent on the parameter $\beta = \alpha_0(1-\alpha_0)A_0^2/R_0^2$ where α_0 is the initial void fraction of the cloud, A_0 is the initial cloud radius and R_0 is the initial bubble radius. Physically, $\beta = T_C^2/T_B^2$ is the square of the ratio of two dynamic characteristic times in the two-phase flow where T_C is the global dynamic time scale for wave propagation through the cloud and T_B is the characteristic time of bubble pulsation. Three modes of collapse have been identified for a spherical cloud. Most notably, the formation and inward focusing of the shock and the intensity of the generated acoustic impulse is most pronounced when $\beta \gg 1$. Fundamentally, this requires either the initial void fraction or the ratio of cloud size to bubble size be sufficiently large and this, in turn, is qualitatively in accord with the observation that cavitation must be quite extensive for the cloud phenomenon to be manifest. Furthermore, this implies that bubble interaction effects play a crucial role in cloud cavitation noise and damage.

Another important issue is the scaling for cloud cavitation. Up to now, the scaling laws between the experiments of model scale and full scale are still unknown. This is because the precise physical phenomena in cloud cavitation has not been properly understood. This thesis has explored the collapse dynamics of nonlinear cavitating clouds and the resulting pressure pulses responsible for noise and erosion. It appears that an understanding of the collapse shock dynamics and acoustics has important consequences and implications

for the scaling of cloud cavitation noise and damage. For example, the far-field acoustic impulses were found to have strong correlation with the normalized maximum total volume of cavitating bubbles in the cloud. Further verification of this result will require the invention of reliable experimental techniques for the measurement of the void fraction in the cloud.

The scaling problem arises from the possiblity that the model test could have very different β values than the prototype. Even if the nuclei have the same size distribution, population and void fraction in the model and prototype, the bubble/cloud interaction effects could be much larger in the prototype due to the larger value of β.

Of course, most clouds are not spherical. Nevertheless the collapse of all or part of non-spherical clouds will produce points at which shock waves focus to produce large local and radiated pulses. Sturtevant and Kulkarny [1976] (see also Howard [1996]) present a useful review of the various foci of gasdynamic shock waves including shocks traveling in inhomogeneous media. However, it is not currently clear what three-dimensional forms or what types of foci the propagating bubbly shocks might take in the highly non-uniform bubbly environments which occur in real flows.

Bibliography

Arakeri, V. H., and Shangumanathan, V. [1985] On the evidence for the effect of bubble interference on cavitation noise. *J. Fluid Mech.*, **159**, 131–150.

Avellan, F., and Farhat, M. [1989] Shock pressure generated by cavitation vortex collpase. *Pages 199–125 of: ASME Int. Symp. on Cavitation Noise and Erosion in Fluid Systems*, volume FED 88.

Bark, G. [1985] Developments of distortions in sheet cavitation on hydrofoils. *Pages 470–493 of: Proc. ASME Int. Symp. on Jets and Cavities.*

Bark, G., and Berlekom, W. B. [1978] Experimental investigations of cavitation noise. *Pages 470–493 of: Proc. 12th ONR Symp. on Naval Hydrodynamics.*

Biesheuvel, A., and van Wijngaarden, L. [1984] Two phase flow equations for a dilute dispersion of gas bubbles in liquid. *J. Fluid Mech.*, **148**, 301–318.

Blake, W. K. [1986] *Mechanics of flow-induced sound and vibration.* Academic Press.

Blake, W. K., Wolpert, M. J., and Geib, F. E. [1977] Cavitation noise and inception as influenced by boundary-layer development on a hydrofoil. *J. Fluid Mech.*, **80**, 617–640.

Brennen, C. E. [1995] *Cavitation and bubble dynamics.* Oxford University Press.

Brennen, C. E., Reisman, G. E., and Wang, Y.-C. [1996] (June) Shock waves in cloud cavitation. *In: Proc. 21th ONR Symp. on Naval Hydrodynamics.*

Chahine, G. L. [1982a] Cloud cavitation: theory. *Pages 165–194 of: Proc. 14th ONR Symp. on Naval Hydrodynamics.*

Chahine, G. L. [1982b] Pressure filed generated by the collective collapse of caviation bubbles. *In: IAHR Symp. on Operating Problems of Pump Stations and Power Plants*, volume 1.

Chahine, G. L., and Duraiswami, R. [1992] Dynamical interactions in a multi-bubble cloud. *ASME J. Fluids Eng.*, **114**, 680–686.

Chahine, G. L., Duraiswami, R., and Rebut, M. [1992] Analytical and numerical study of large bubble/bubble and bubble/flow interactions. *In: Proc. 19th ONR Symp. on Naval Hydrodynamics.*

Chapman, R. B., and Plesset, M. S. [1971] Thermal effects in the free oscillation of gas bubbles. *ASME J. Basic Eng.*, **93**, 373–376.

d'Agostino, L., and Brennen, C. E. [1983] On the acoustical dynamics of bubble clouds. *Pages 72–75 of: ASME Cavitation and Multiphase Flow Forum.*

d'Agostino, L., and Brennen, C. E. [1988] Acoustical absorption and scattering cross-sections of spherical bubble clouds. *J. Acoust. Soc. Am.*, **84**, 2126–2134.

d'Agostino, L., and Brennen, C. E. [1989] Linearized dynamics of spherical bubble clouds. *J. Fluid Mech.*, **199**, 155–176.

d'Agostino, L., Brennen, C. E., and Acosta, A. J. [1988] Linearized dynamics of two-dimensional bubbly and cavitating flows over slender surfaces. *J. Fluid Mech.*, **192**, 485–509.

Dowling, A. P., and Williams, J. E. F. [1983] *Sound and sources of sound.* Ellis Horwood Ltd. and John Wiley and Sons.

Franc, J. P., and Michel, J. M. [1988] Unsteady attached cavitation on an oscillating hydrofoil. *J. Fluid Mech.*, **193**, 171–189.

Hanson, I., Kedrinskii, V. K., and Mørch, K. A. [1981] On the dynamics of cavity clusters. *J. Appl. Phys.*, **15**, 1725–1734.

Howard, D. D. [1996] (April) *Mechanisms of injury associated with extracorporeal shock wave lithotripsy.* Ph.D. thesis, California Institute of Technology, Pasadena, California.

Kameda, M., and Matsumoto, Y. [1995] Structure of shock waves in a liquid containing gas bubbles. *Pages 117–126 of: IUTAM Symposium on Waves in Liquid/Gas and Liquid/Vapour Two-Phase Systems.*

Knapp, R. T., Daily, J. W., and Hammit, F. G. [1970] *Cavitation.* McGraw Hill.

Kubota, A., Kato, H., Yamaguchi, H., and Maeda, M. [1989] Unsteady structure measurement of cloud cavitation on a foil section using conditional sampling. *ASME J. Fluids Eng.*, **111**, 204–210.

Kubota, A., Kato, H., and Yamaguchi, H. [1992] A new modelling of cavitating flows: a numerical study of unsteady cavitation on a hydrofoil section. *J. Fluid Mech.*, **240**, 59–96.

Kumar, S., and Brennen, C. E. [1991] Non-linear effects in the dynamics of clouds of bubbles. *J. Acoust. Soc. Am.*, **89**, 707–714.

Kumar, S., and Brennen, C. E. [1992] Harmonic cascading in bubble clouds. *Pages 171–179 of: Proc. Int. Symp. on Propulsors and Cavitation.*

Kumar, S., and Brennen, C. E. [1993] Some nonlinear interactive effects in bubbly cavitating clouds. *J. Fluid Mech.*, **253**, 565–591.

Le, Q., Franc, J. M., and Michel, J. M. [1993] Partial cavities: global behaviour and mean pressure distribution. *ASME J. Fluids Eng.*, **115**, 243–248.

Marboe, R. C., Billet, M. L., and Thompson, D. E. [1986] Some aspects of traveling bubble cavitation and noise. *In: Int. Symp. on Cavitation and Multiphase Flow Noise.*

Mørch, K. A. [1980] On the collapse of cavity cluster in flow cavitation. *Pages 95–100 of: Proc. First Int. Conf. on Cavitation and Inhomogenieties in Underwater Acoustics.* Springer Series in Electrophysics, volume 4.

Mørch, K. A. [1981] Cavity cluster dynamics and cavitation erosion. *Pages 1–10 of: Proc. ASME Cavitation and Polyphase Flow Forum.*

Mørch, K. A. [1982] Energy considerations on the collpase of cavity cluster. *Appl. Sci. Res.*, **38**, 313.

Nigmatulin, R. I. [1991] *Dynamics of Multiphase Media.* Hemisphere, New York.

Noordzij, L. [1973] *Shock in mixtures of liquid and air bubbles.* Ph.D. thesis, Technishe Hogeschool, Twente, Netherlands.

Noordzij, L., and van Wijngaarden, L. [1974] Relaxation effects, caused by relative motion, on shock waves in gas-bubble/liquid mixtures. *J. Fluid Mech.*, **66**, 115–143.

Omta, R. [1987] Oscillations of a cloud of bubbles of small and not so small amplitude. *J. Acoust. Soc. Am.*, **82**, 1018–1033.

Plesset, M. S. [1948] The dynamics of cavitation bubbles. *ASME J. Appl. Mech.*, **16**, 228–231.

Plesset, M. S., and Prosperetti, A. [1977] Bubble dynamics and cavitation. *Ann. Rev. Fluid Mech.*, **9**, 145–185.

Prosperetti, A. [1975] Nonlinear oscillations of gas bubbles in liquids: transient solutions and the connection between subharmonic signal and cavitation. *J. Acoust. Soc. Am.*, **57**, 878–885.

Prosperetti, A. [1988] Bubble-related ambient noise in the ocean. *J. Acoust. Soc. Am.*, **84**, 1042–1054.

Reisman, G. E., and Brennen, C. E. [1996] (July) Pressure pulses generated by cloud cavitation. *In: ASME Symposium on Cavitation and Gas-Liquid Flows in Fluid Machinery and Devices.*

Reisman, G. E., McKenney, E. A., and Brennen, C. E. [1994] Cloud cavitation on an oscillating hydrofoil. *Pages 78–89 of: Proc. 20th ONR Symp. on Naval Hydrodynamics.*

Sangani, A. S. [1991] A pairwise interaction theory for determining the linear acoustic properties of dilute bubbly liquids. *J. Fluid Mech.*, **232**, 221–284.

Shen, Y., and Peterson, F. B. [1978] Unsteady cavitation on an oscillating hydrofoil. *Pages 362–384 of: Proc. 12th ONR Symp. on Naval Hydrodynamics.*

Shen, Y., and Peterson, F. B. [1980] The influence of hydrofoil oscillation on boundary layer transition and cavitation noise. *Pages 221–241 of: Proc. 13th ONR Symp. on Naval Hydrodynamics.*

Soyama, H., Kato, H., and Oba, R. [1992] Cavitation observations of severely erosive vortex cavitation arising in a centrifugal pump. *Pages 103–110 of: Proc. Third I.Mech.E. Int. Conf. on Cavitation.*

Sturtevant, B., and Kulkarny, V. J. [1976] The focusing of weak shock waves. *J. Fluid Mech.*, **73**, 651–680.

van Wijngaarden, L. [1964] On the collective collapse of a large number of gas bubbles in water. *Pages 854–861 of: Proc. 11th Int. Conf. Appl. Mech.*

van Wijngaarden, L. [1972] One-dimensional flow of liquids containing small gas bubbles. *Ann. Rev. Fluid Mech.*, **4**.

Wade, R. B., and Acosta, A. J. [1966] Experimental observations on the flow past a plano-convex hydrofoil. *ASME J. Basic Eng.*, **88**, 273–283.

Wang, Y.-C., and Brennen, C. E. [1994] Shock wave development on the collapse of a cloud of bubbles. *Pages 15–19 of: Cavitation and Multiphase Flow Forum*, volume FED 194.

Wang, Y.-C., and Brennen, C. E. [1995a] The noise generated by the collapse of a cloud of cavitation bubbles. *Pages 17–29 of: ASME/JSME Symposium on Cavitation and Gas-Liquid Flow in Fluid Machinery and Devices*, volume FED 226.

Wang, Y.-C., and Brennen, C. E. [1995b] Shock wave and noise in the collapse of a cloud of cavitation bubbles. *In: 20th International Symposium on Shock Waves.* Pasadena: California Institute of Technology, for GALCIT. (in press).

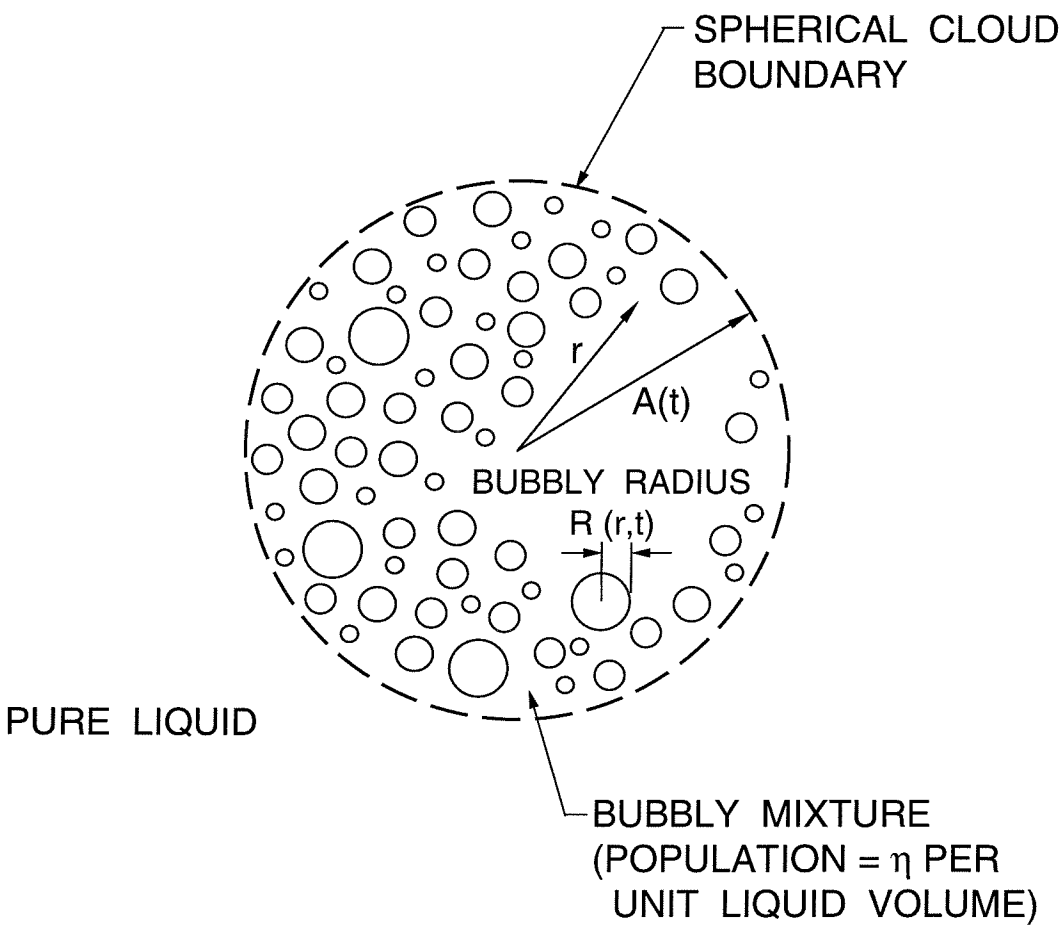

Figure 2.1 Schematic of a spherical cloud of bubbles.

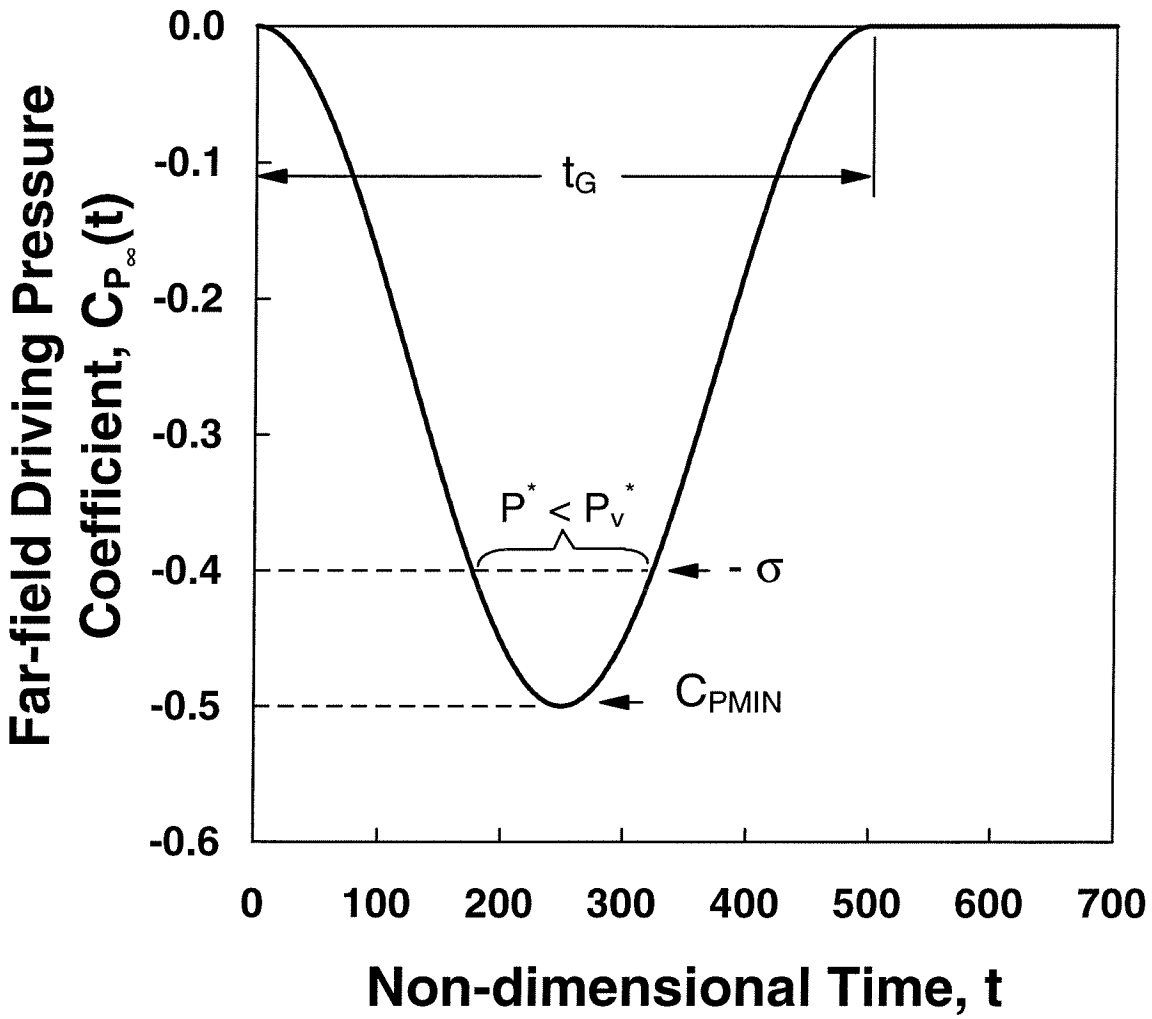

Figure 2.2 An example of the sinusoidal low pressure region, $C_{P\infty}(t)$, (equation (2.10)), with $t_G = 500$, $C_{PMIN} = -0.5$. Cavitation number, σ shown is 0.4.

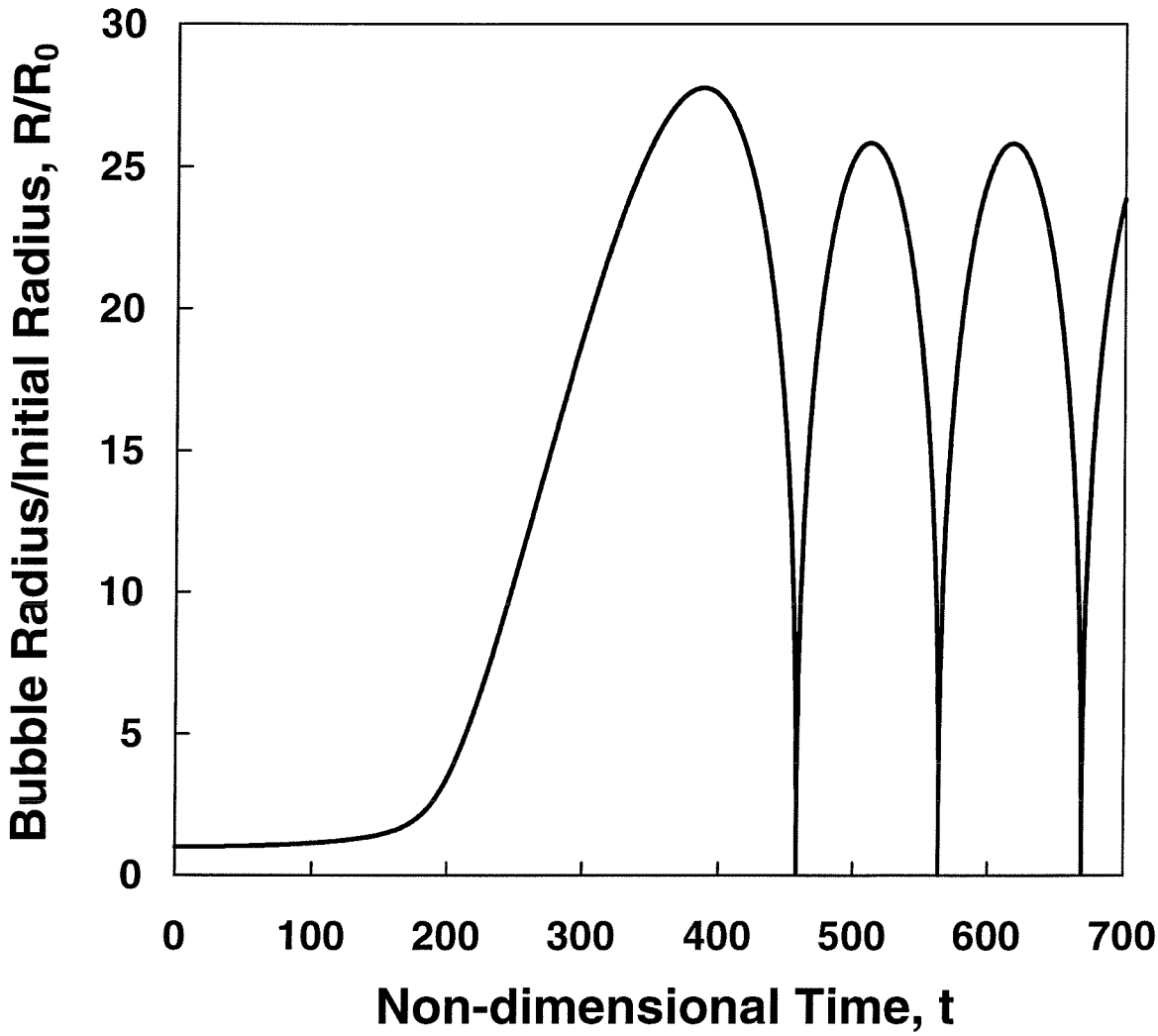

Figure 2.3 Typical solution of the Rayleigh-Plesset equation (2.3) for spherical bubble size/initial size, R/R_0. The nuclei enters a low-pressure region as shown in Figure 2.2.

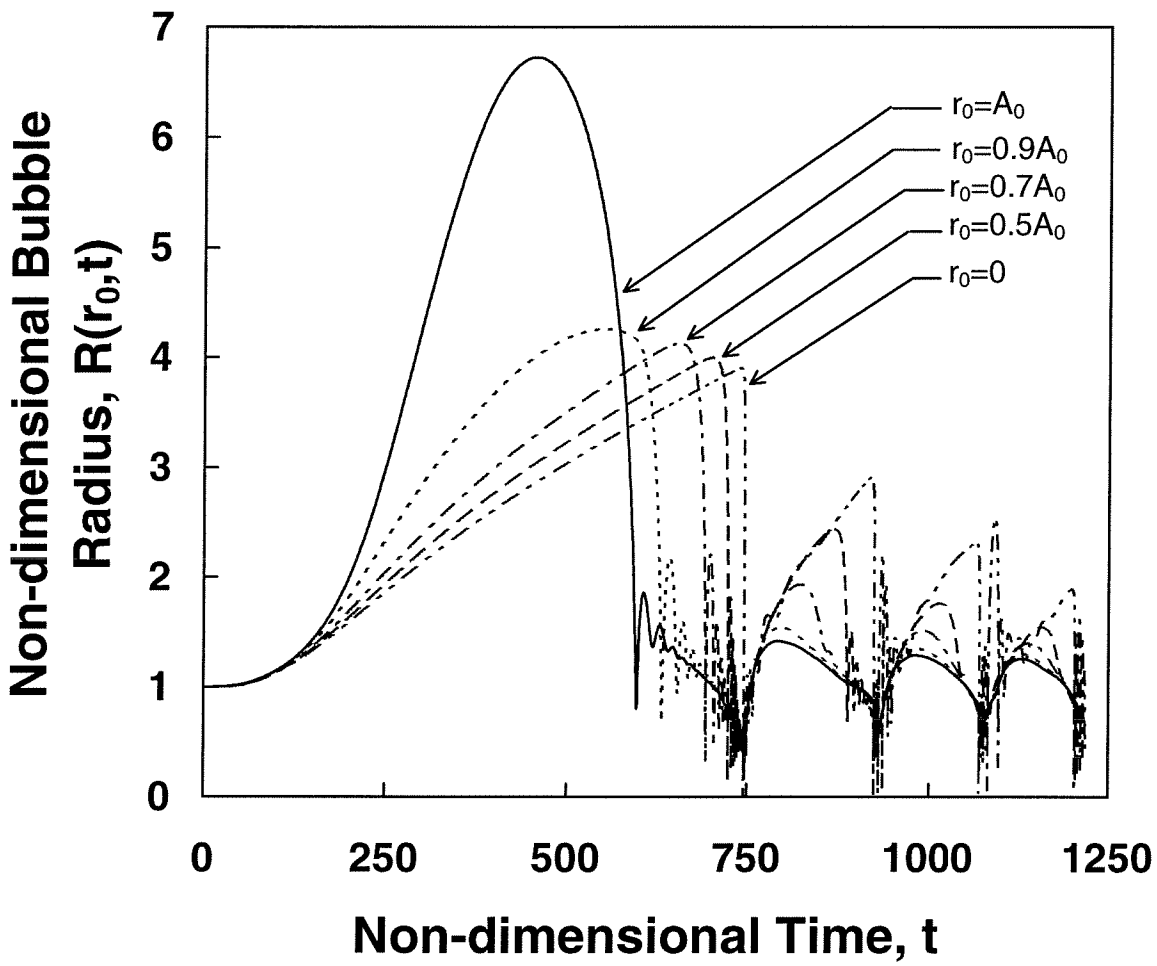

Figure 4.1 The time history of the dimensionless bubble size at five different positions in the cloud. Parameters used are $\sigma = 0.45$, $C_{PMIN} = -0.75$, $\alpha_0 = 3\%$, $A_0 = 100$, and the ratio of the low pressure perturbation length to initial cloud radius, $D/A_0 = 5$ (corresponds to $t_G = 500$). The bubble interactive parameter, β, is approxmately 300 in this case.

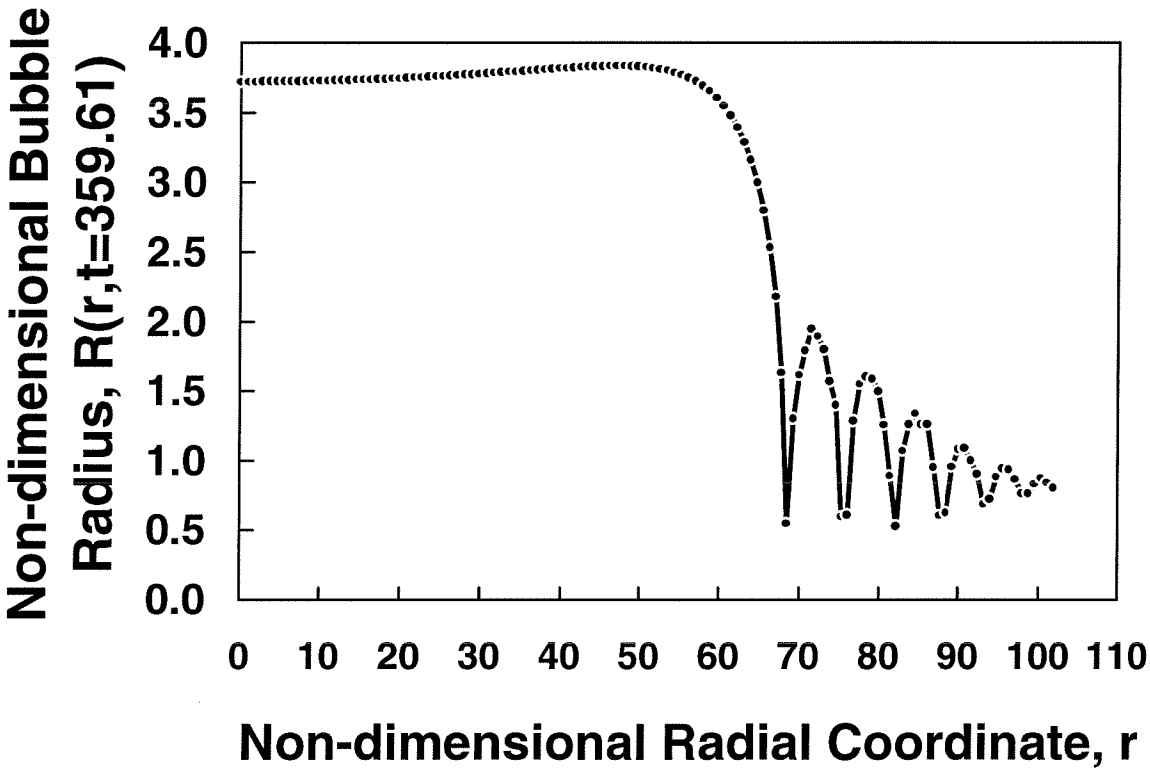

Figure 4.2 The structure of a bubbly shock wave accompanying the collapse of the spherical cloud of cavitation bubbles. Shown are the dimensionless bubble-size distribution, $R(r,t)$, in the cloud as a function of the dimensionless radial coordinate, r, at the dimensionless time, t = 359.61. Parameters used are σ=0.45, C_{PMIN}=-0.75, α_0=0.5%, A_0=100, and the ratio of the low pressure perturbation length to initial cloud radius, D/A_0 = 2.5, which corresponds to the duration of the low pressure perturbation, t_G=250.

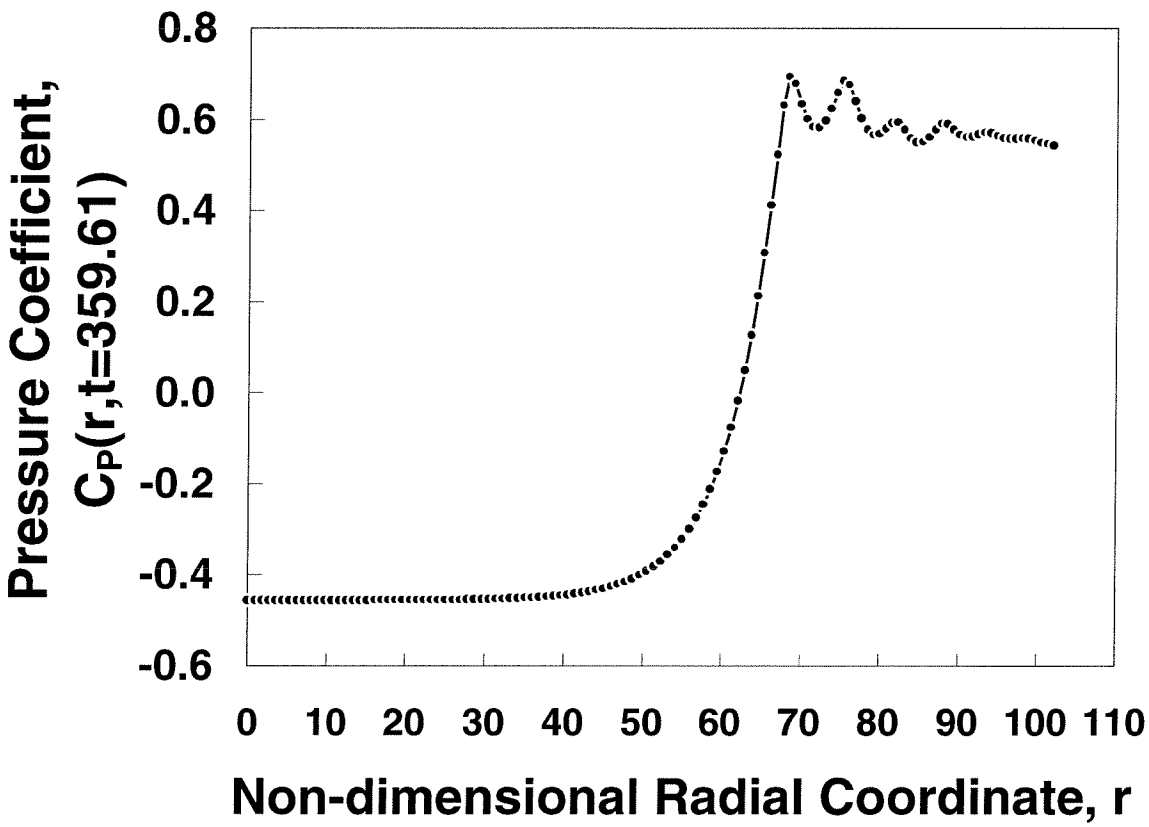

Figure 4.3 The structure of a shock wave accompanying the collapse of the spherical cloud of cavitation bubbles. Shown are the pressure coefficient distribution, $C_P(r,t)$, in the cloud as a function of the dimensionless radial coordinate, r, at the same time as in Figure 4.2. Parameters as in Figure 4.2.

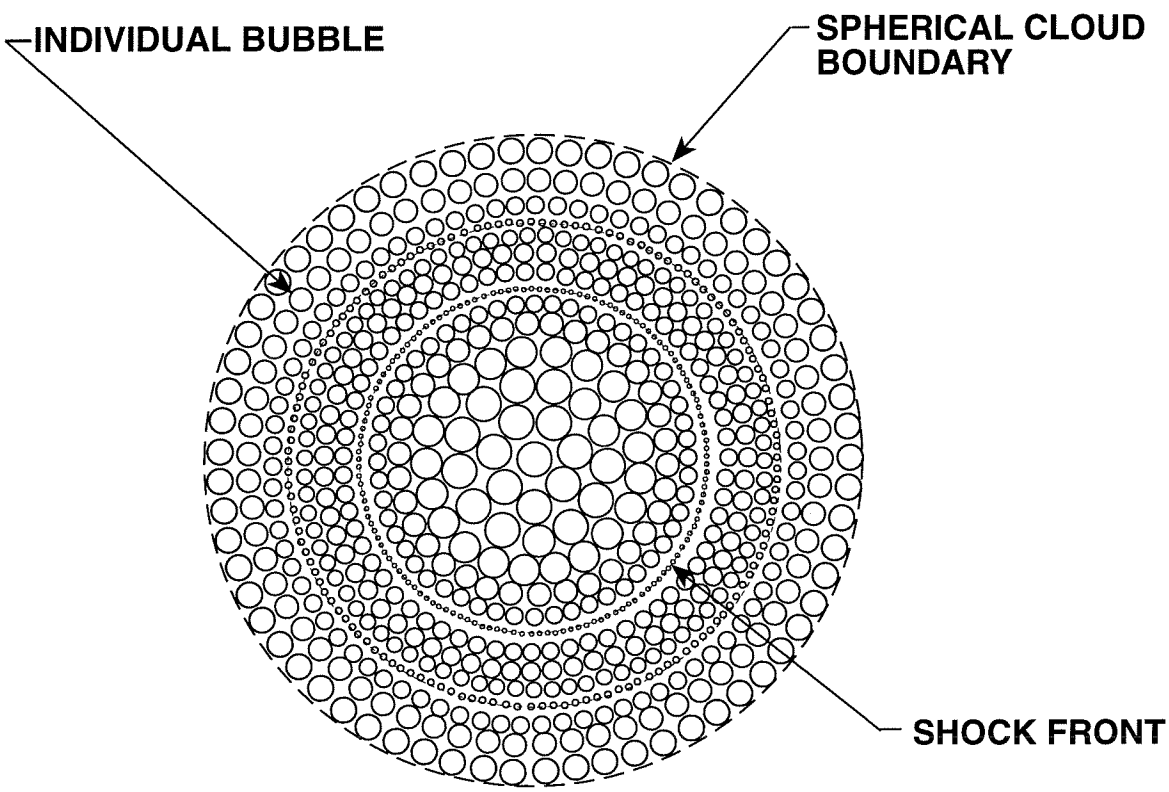

Figure 4.4 Notation for the structure of an inwardly propagating bubbly shock wave in a spherical cloud of cavitating bubbles.

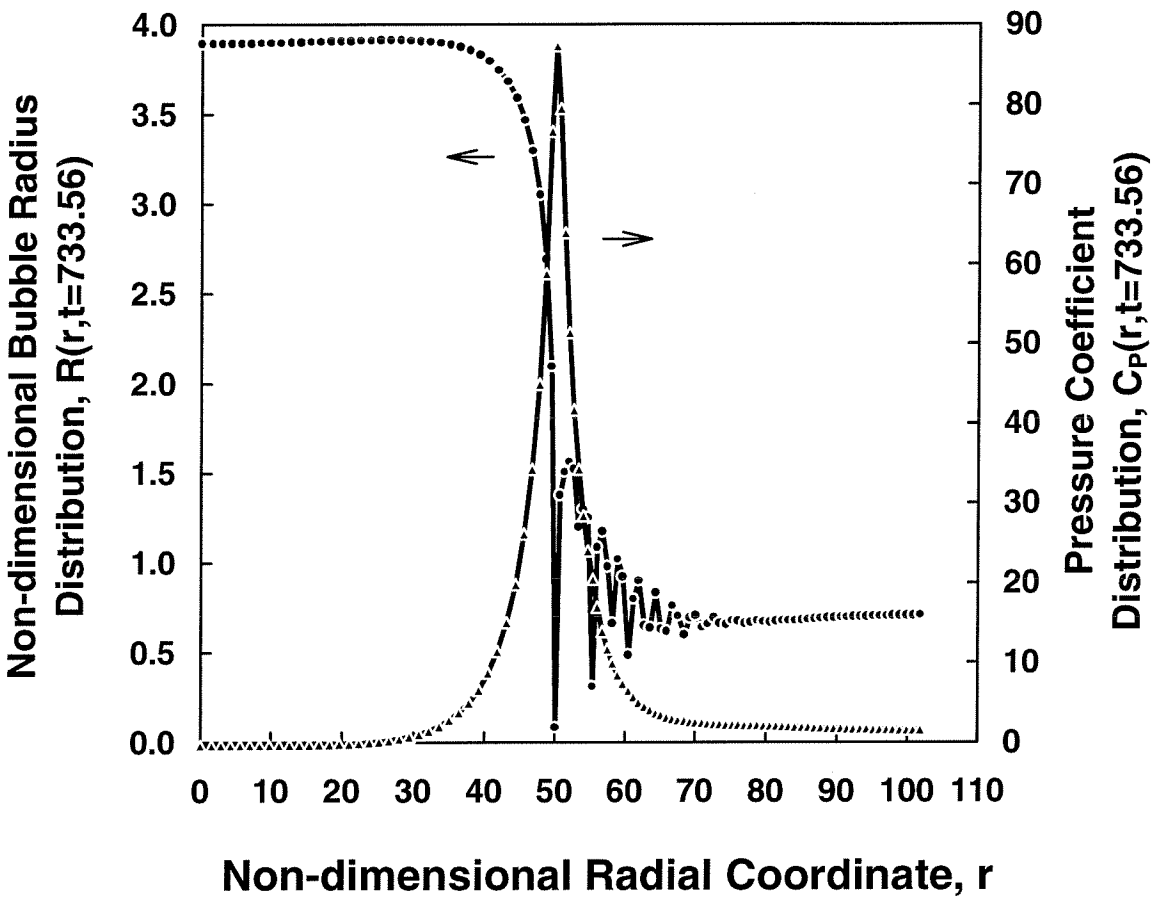

Figure 4.5 Bubble size distribution in the shock and pressure pulse produced by shock-induced bubble collapse at the moment of $t = 733.56$. Parameters as in Figure 4.1.

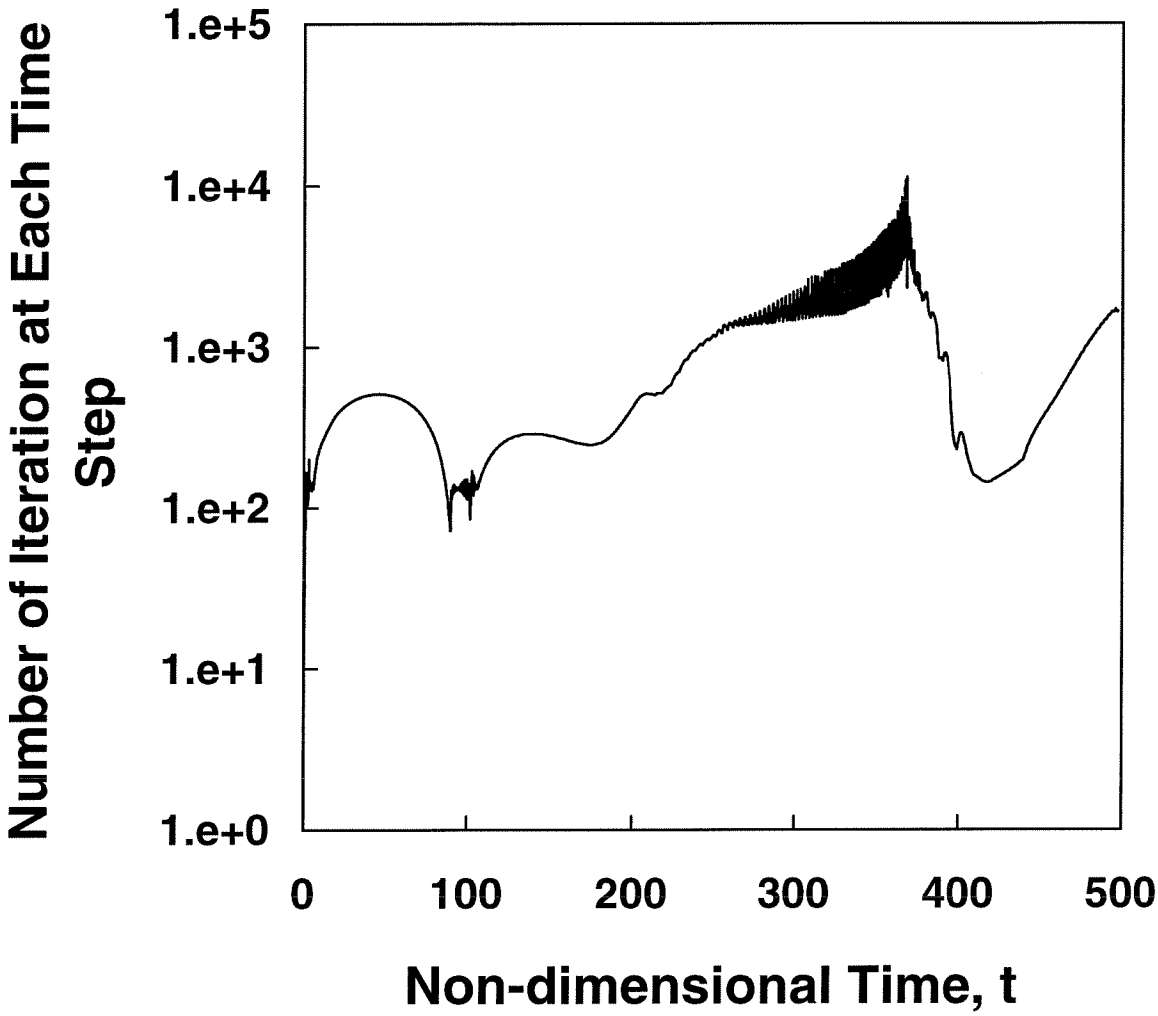

Figure 4.6 A typical convergence history for integrating the mixture pressure equation (3.7) using iteration parameters, $\omega = 0.002$ and $\gamma_j = 1$. Other parameters are $D/A_0 = 2$ (corresponds to t_G=200) and the rest as in Figure 4.1.

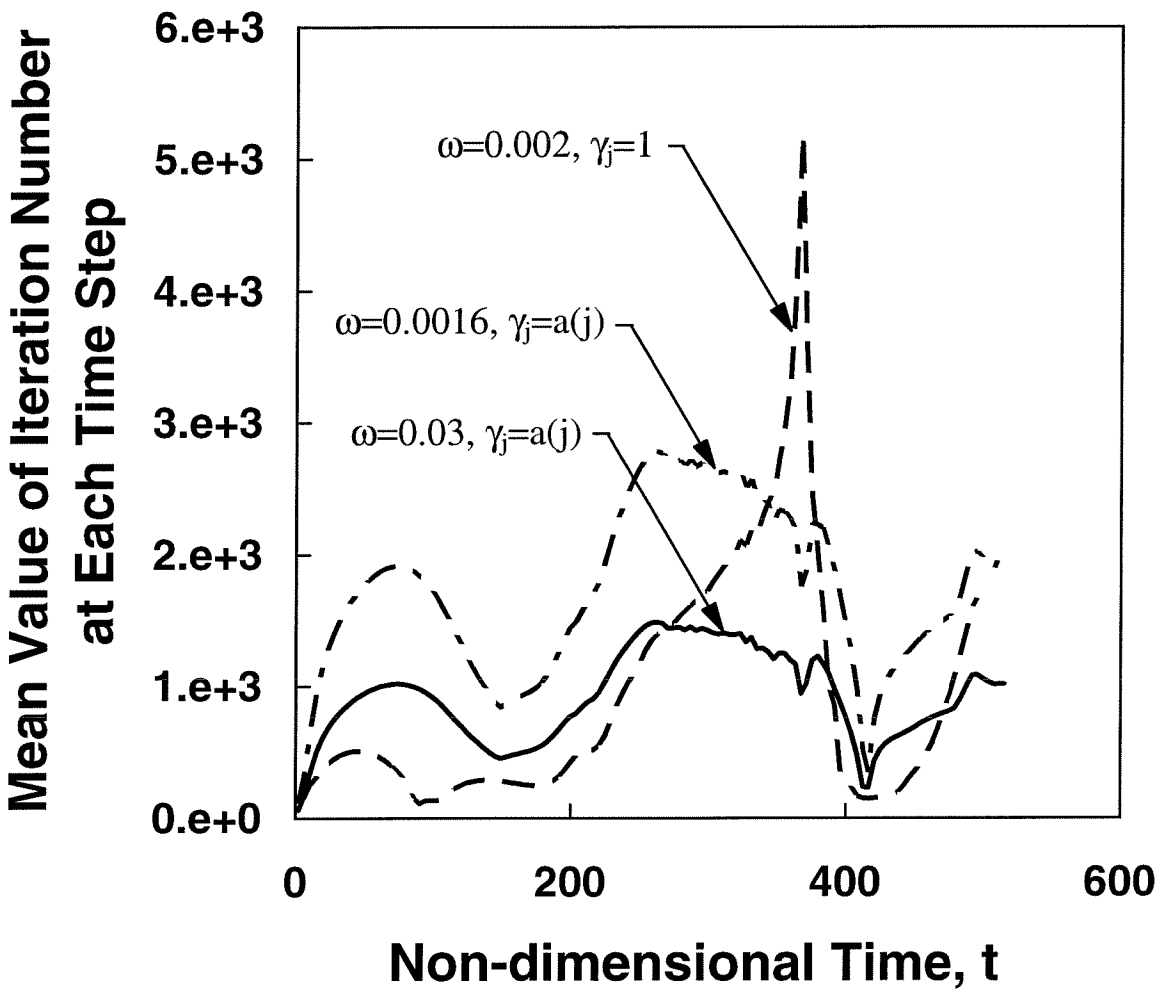

Figure 4.7 Comparisons of the convergence history for integrating the mixture pressure equation (3.7) using different iteration parameters. Other parameters as in Figure 4.6.

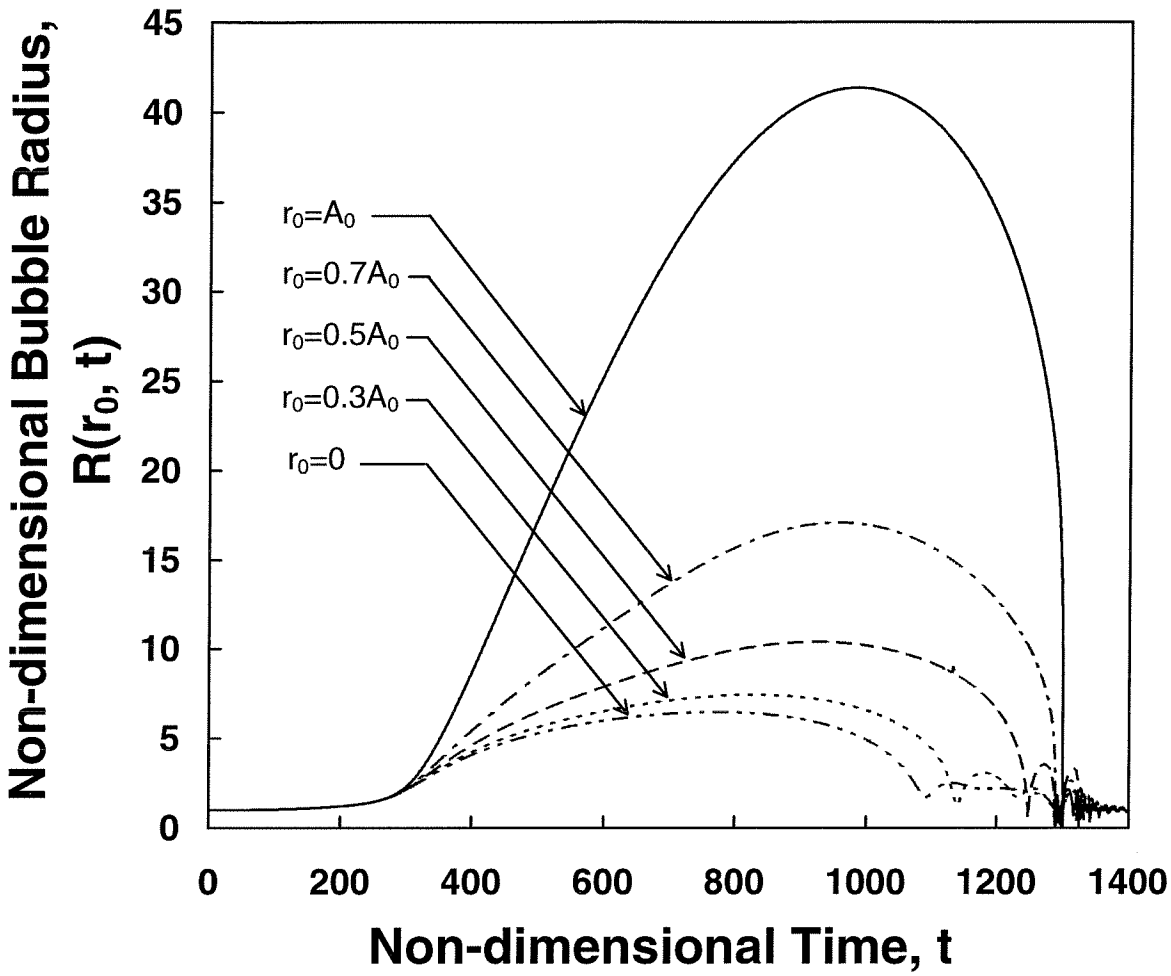

Figure 4.8 The time history of the dimensionless bubble size at five different positions in the cloud. Parameters used are $\alpha_0 = 0.03\%$, $D/A_0 = 10$ (corresponds to $t_G = 1000$). Other parameters as in Figure 4.1. The bubble interative parameter, β, is approxmately 3 in this case.

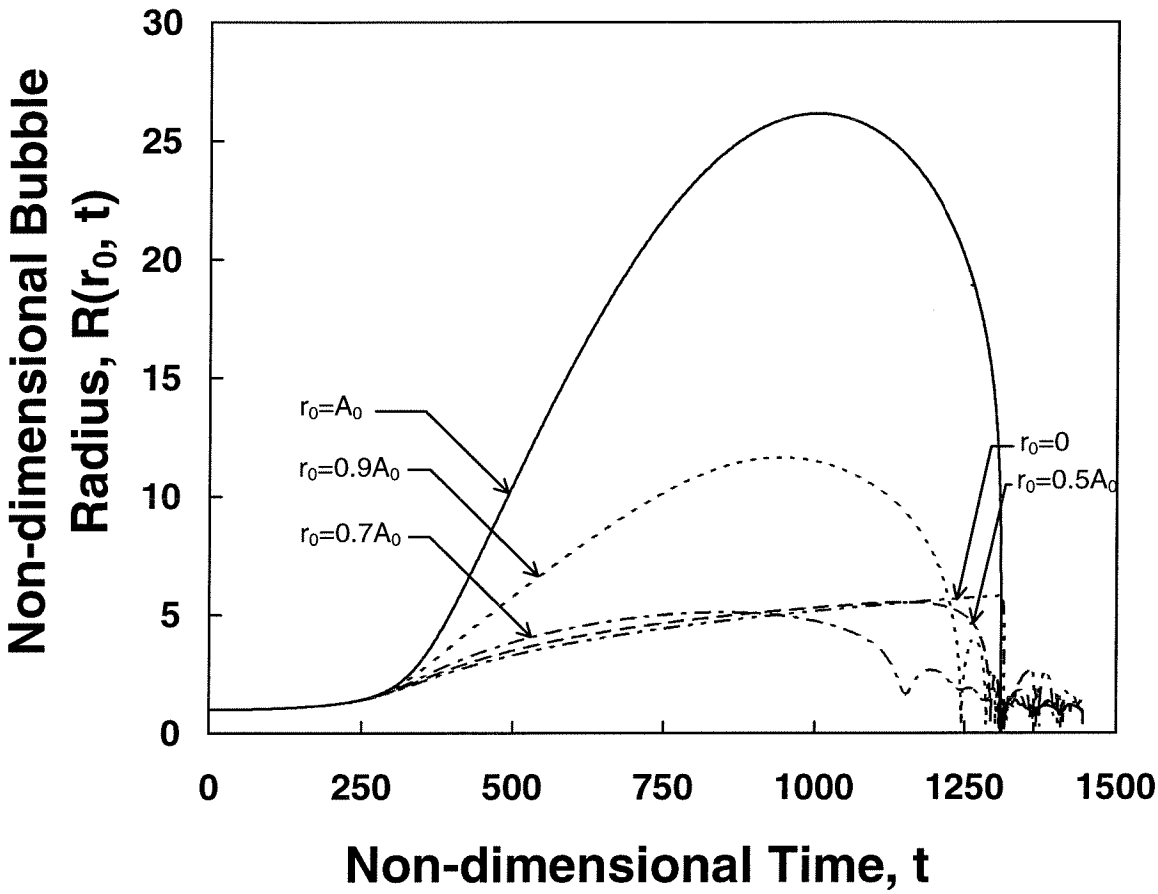

Figure 4.9 The time history of the dimensionless bubble size at five different positions in the cloud. Parameters used are $\alpha_0 = 0.3\%$, $D/A_0 = 10$ (corresponds to $t_G = 1000$). Other parameters as in Figure 4.4. The bubble interative parameter, β, is approxmately 30 in this case.

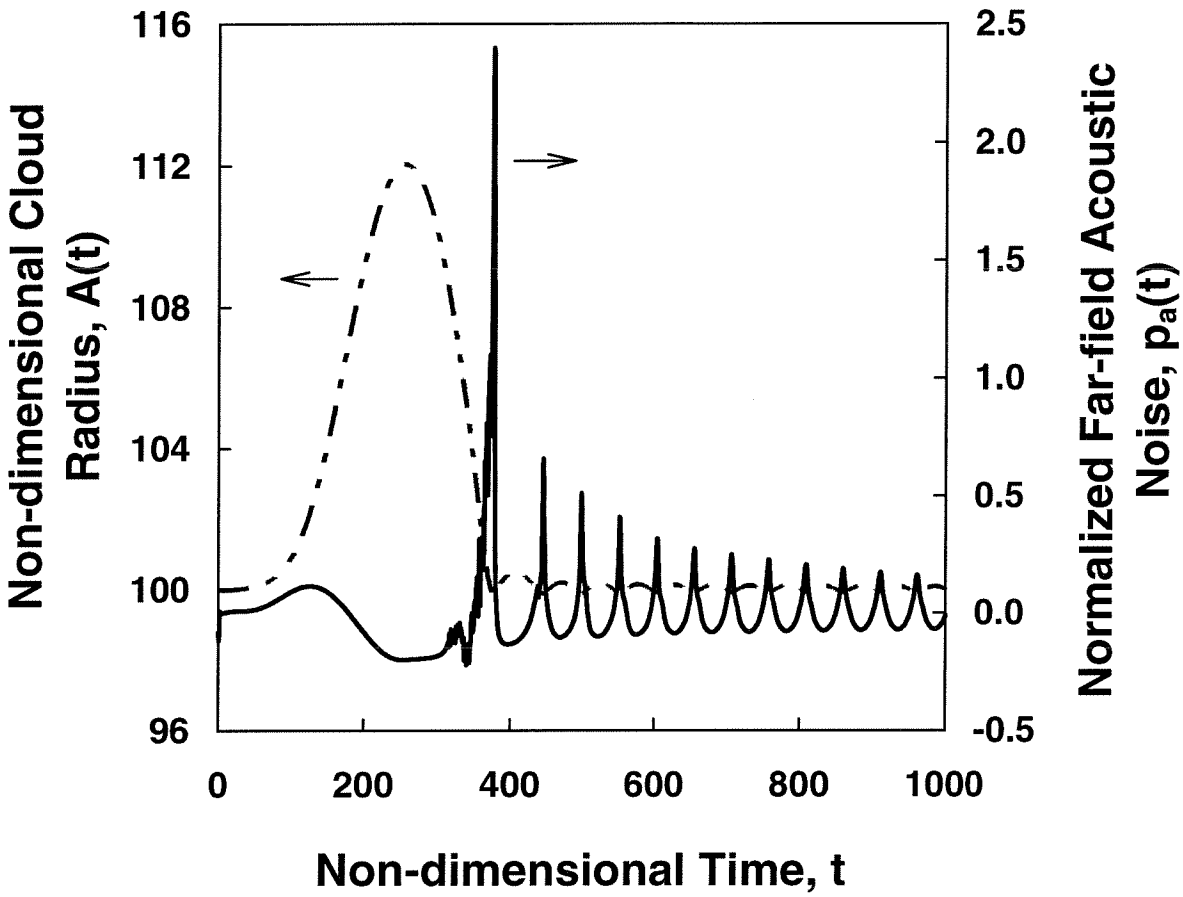

Figure 4.10 The time history of the dimensionless cloud radius and the resulting far field acoustic noise for the case of Figure 4.2.

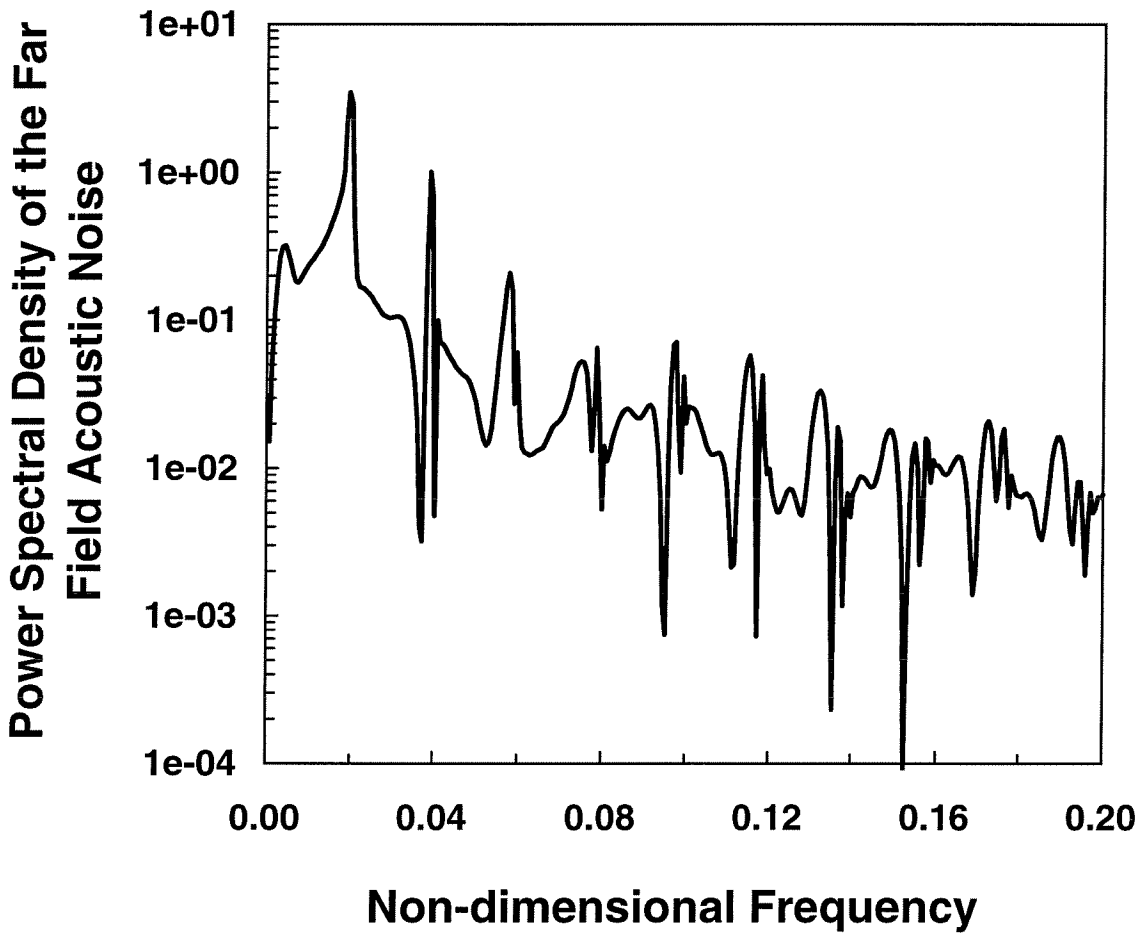

Figure 4.11 The non-dimensional power spectral density of the far-field acoustic noise in Figure 4.10 as a function of dimensionless frequency. The lowest cloud natural frequency is about 0.02. The natural frequency of bubbles in the cloud is 0.158.

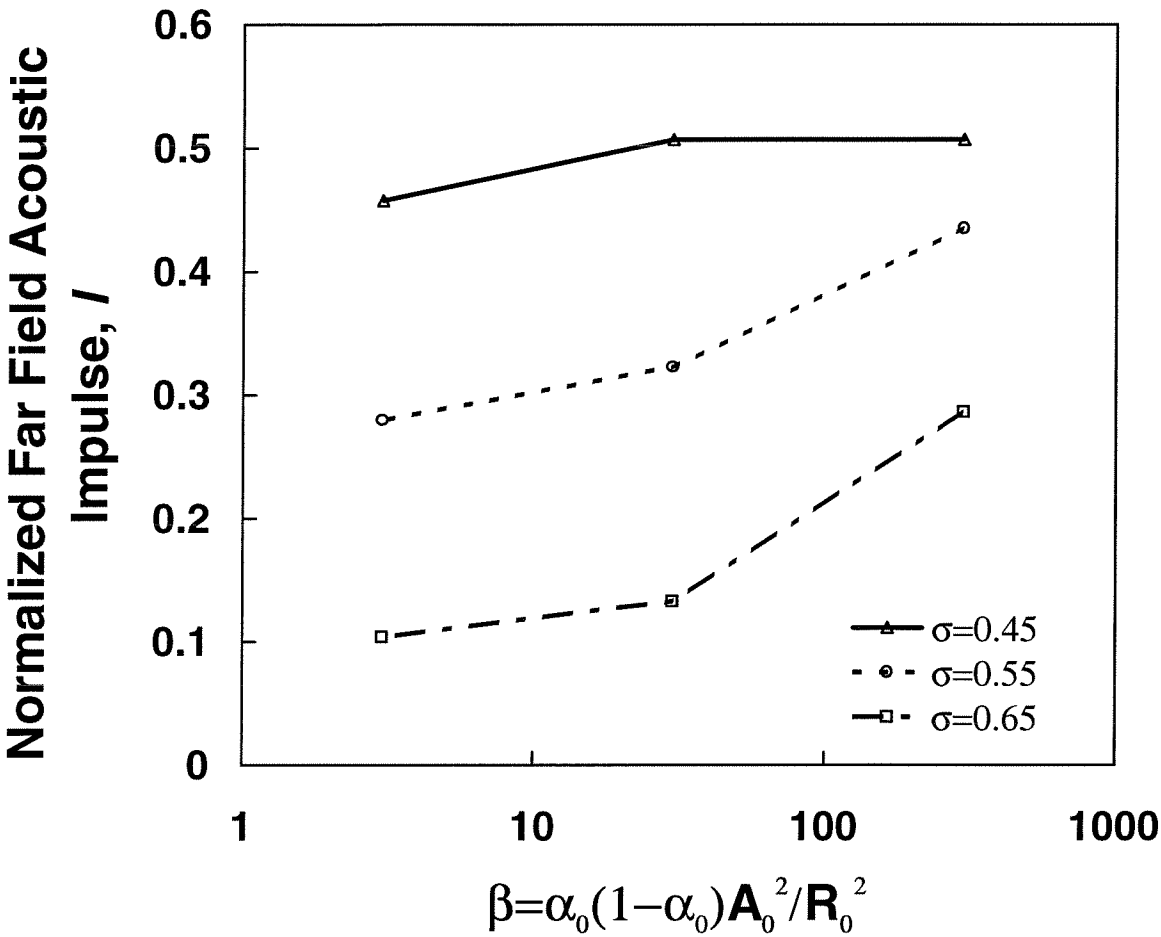

Figure 4.12 The impulse of the normalized far field acoustic noise as a function of the bubble interactive parameter, β. The ratio of the length scale of the low pressure perturbation to initial cloud radius, D/A_0, is 10 (corresponds to $t_G = 1000$). Data is shown for three different cavitation numbers, σ. Other parameters used are $C_{PMIN} = -0.75$ and $A_0/R_0 = 100$.

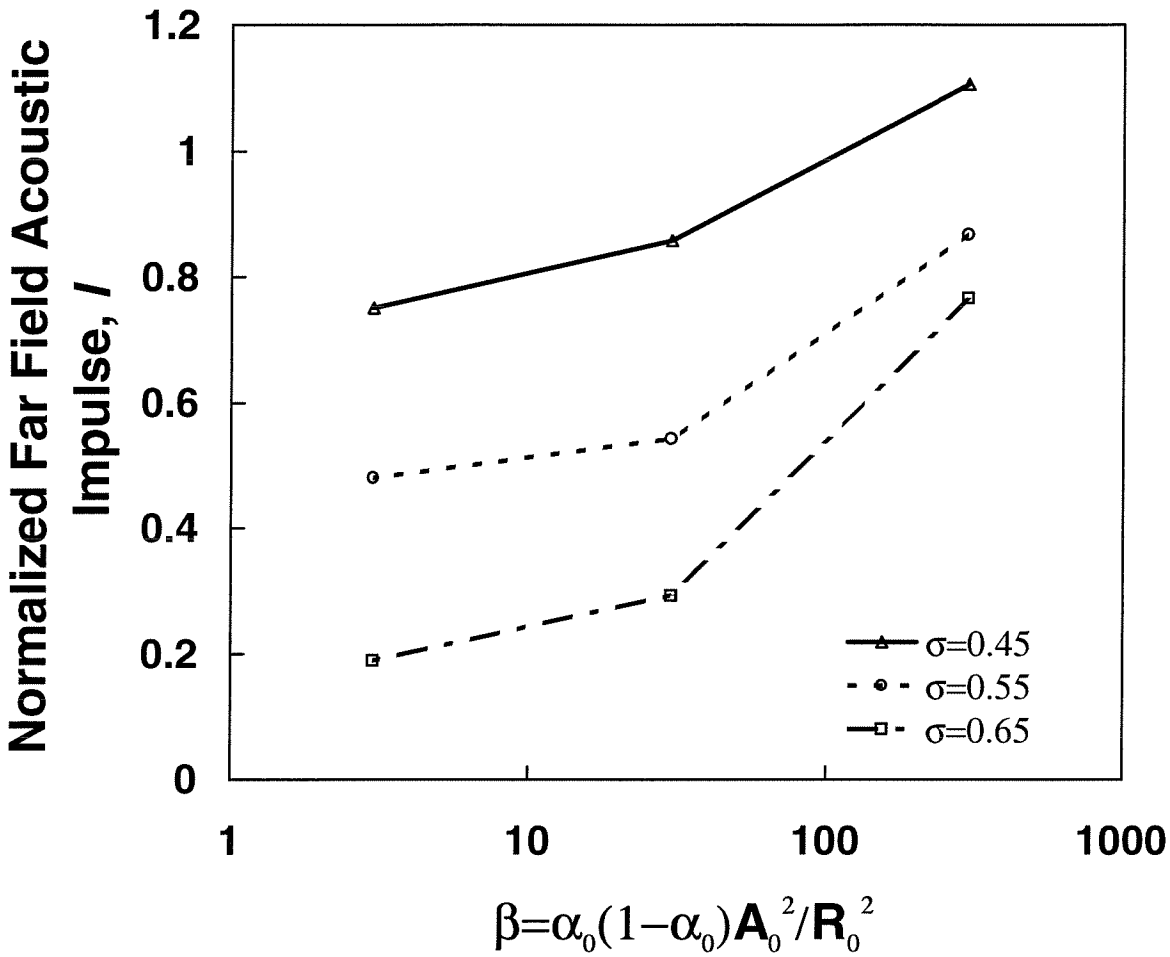

Figure 4.13 The impulse of the normalized far field acoustic noise as a function of the bubble interactive parameter, β. The ratio of the length scale of the low pressure perturbation to initial cloud radius, D/A_0, is 5 (corresponds to $t_G = 500$). Data is shown for three different cavitation numbers, σ. Other parameters as in Figure 4.12.

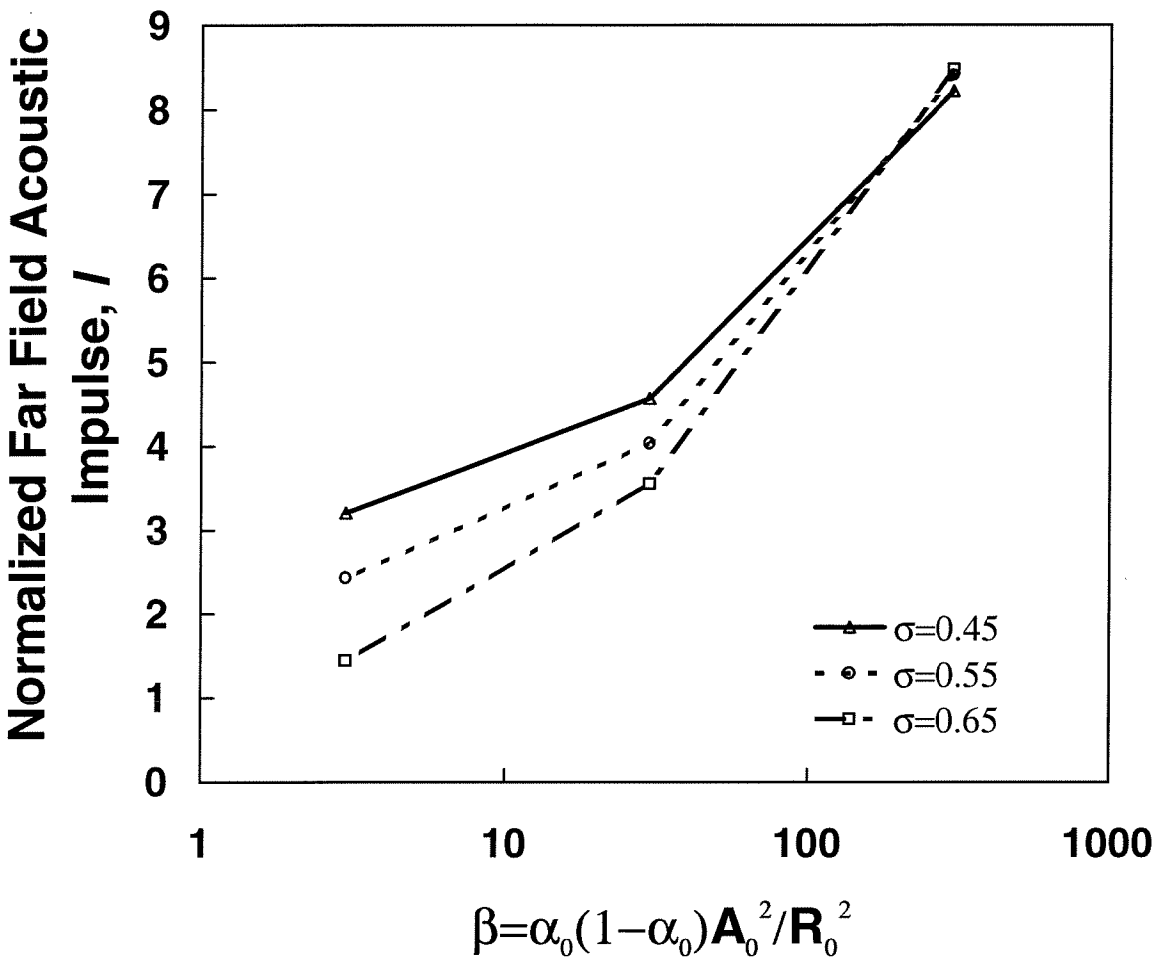

Figure 4.14 The impulse of the normalized far field acoustic noise as a function of the bubble interactive parameter, β. The ratio of the length scale of the low pressure perturbation to initial cloud radius, D/A_0, is 1 (corresponds to $t_G = 100$). Data is shown for three different cavitation numbers, σ. Other parameters as in Figure 4.12.

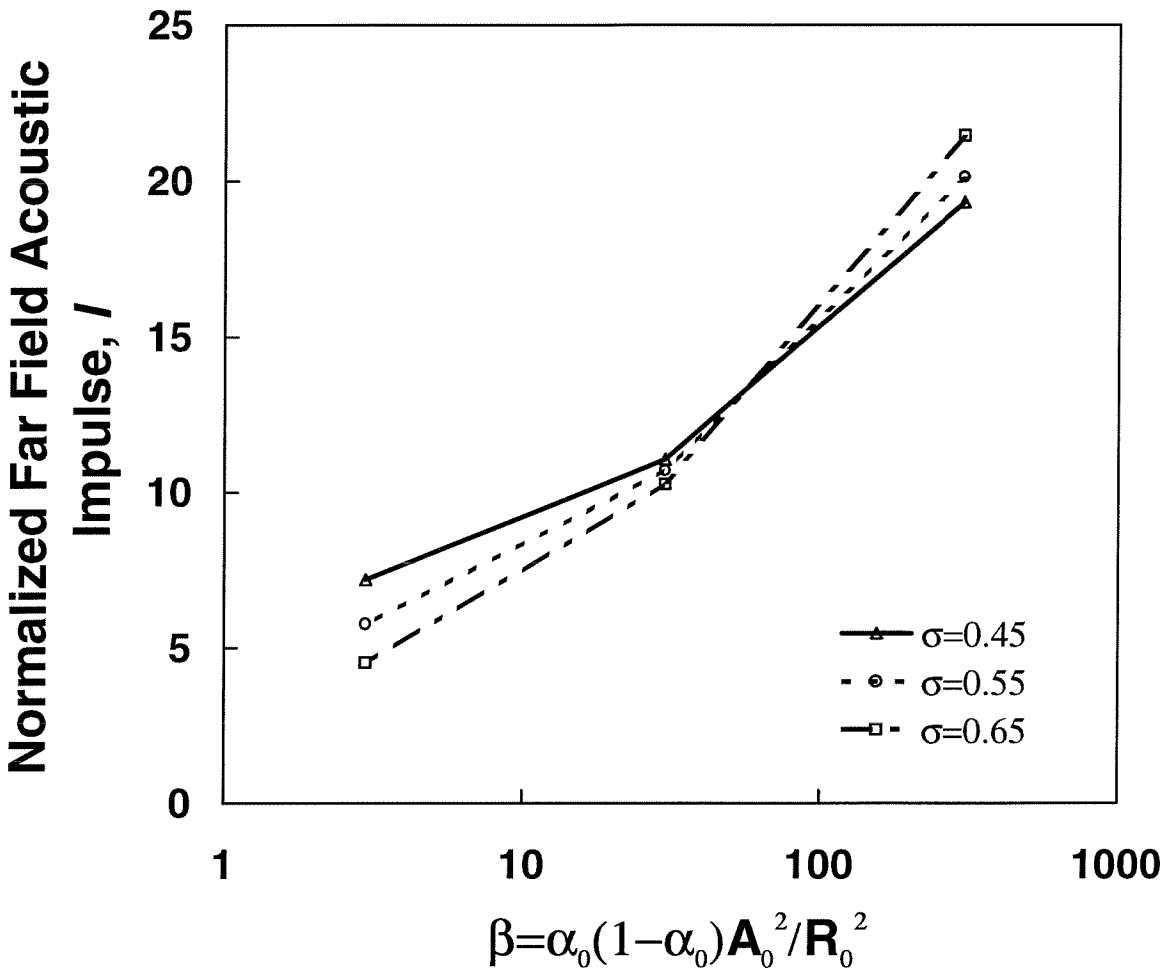

Figure 4.15 The impulse of the normalized far field acoustic noise as a function of the bubble interactive parameter, β. The ratio of the length scale of the low pressure perturbation to initial cloud radius, D/A_0, is 0.5 (corresponds to $t_G = 50$). Data is shown for three different cavitation numbers, σ. Other parameters as in Figure 4.12.

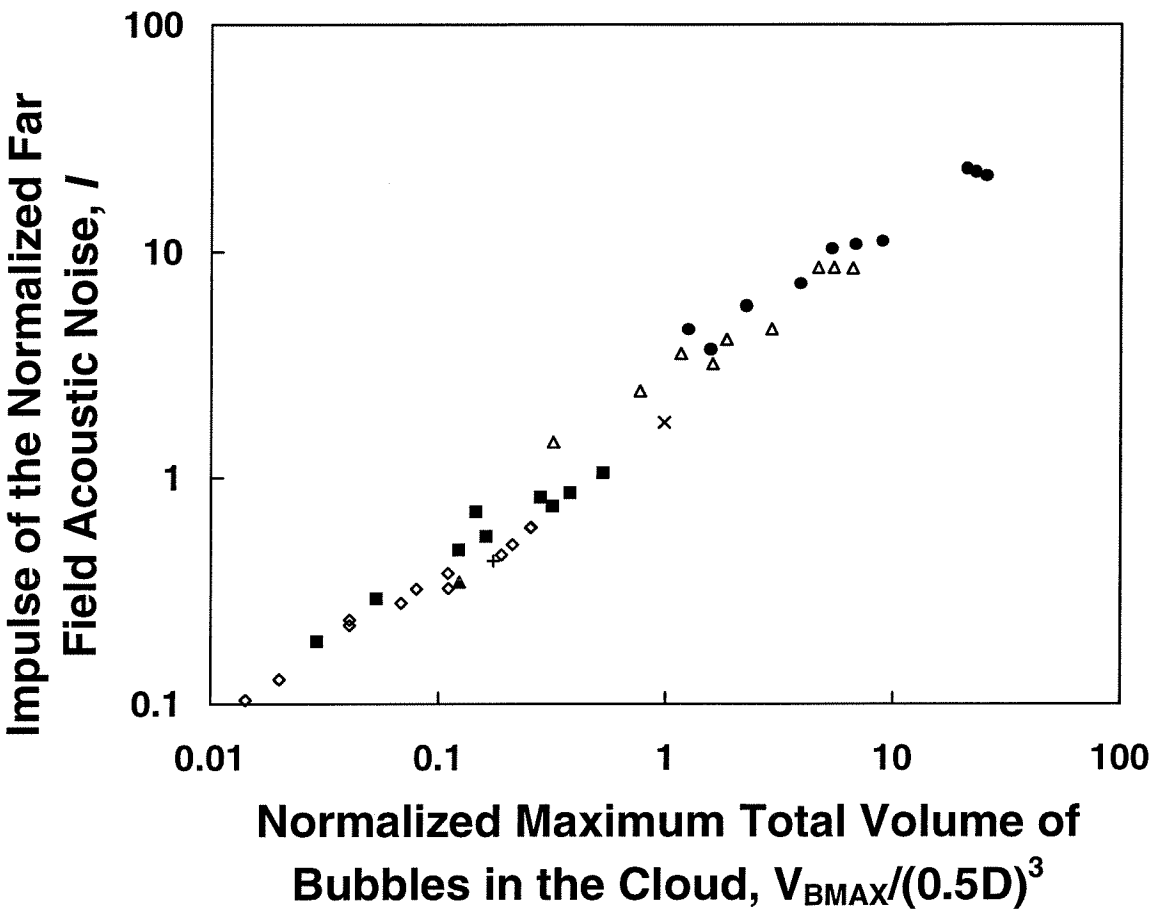

Figure 4.16 The impulse of the normalized far field acoustic noise correlated with the normalized maximum total volume of bubbles in the cloud at different ratio of the length scale of the low pressure perturbation to the initial radius of the cloud, D/A_0 (31.25 = solid $\triangle$, 15.625 = +, 10 = $\Diamond$, 5 = solid $\square$, 3.125 = $\times$, 1 = $\triangle$, 0.5 = $\bullet$). Three different cavitation number, σ, of 0.45, 0.55, and 0.65, and three different initial void fraction, α_0, of 0.03%, 0.3%, and 3% are used permutatively. Other parameters used are $C_{PMIN} = -0.75$ and three different initial cloud radius, A_0/R_0, of 31, 100, and 312.

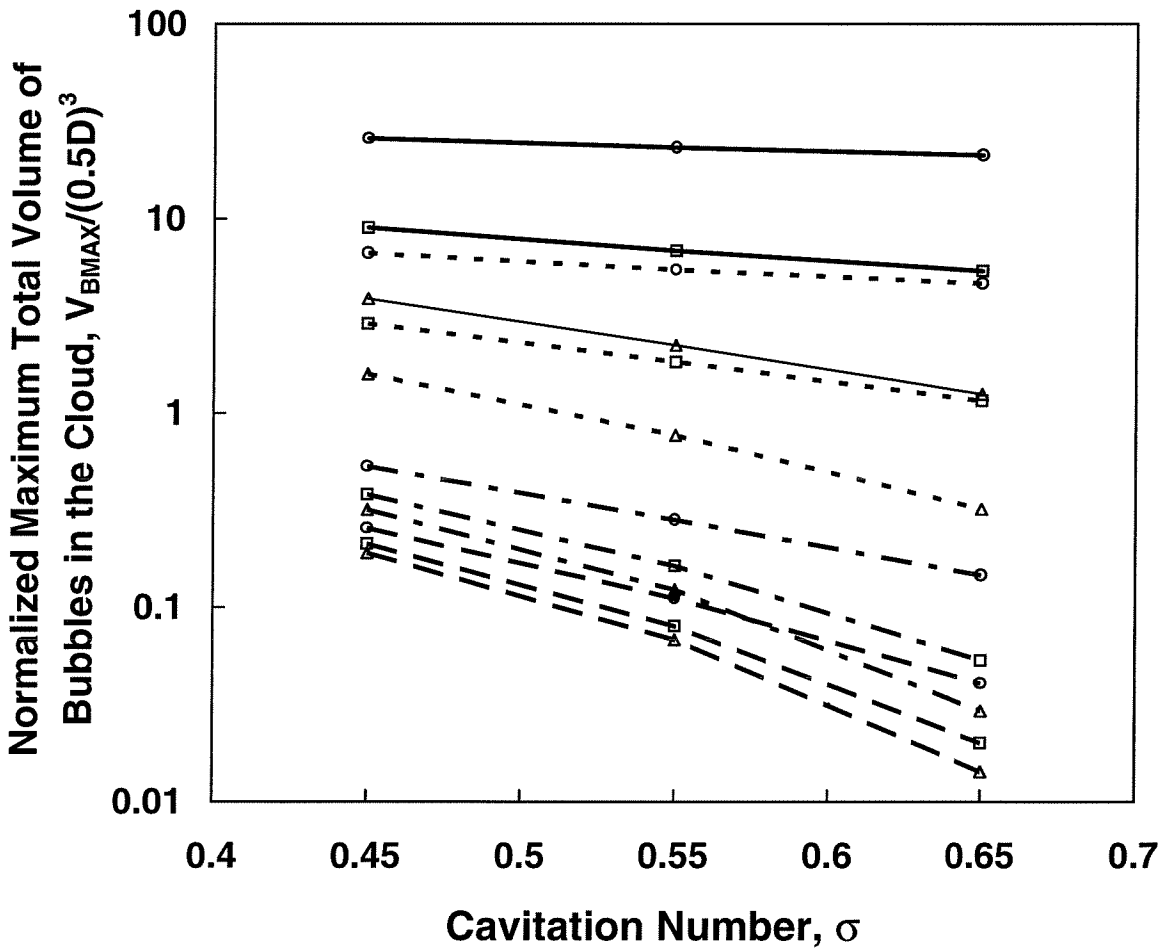

Figure 4.17 The normalized maximum total volume of bubbles in the cloud as a function of cavitation number. Data is shown for four different values of D/A_0 (0.5 = solid lines, 1.0 = dotted lines, 5.0 = dash-dot lines, 10 = dashed lines) and three initial void fractions, α_0 (3% = ○, 0.3% = □, 0.03% = △). Other parameters as in Figure 4.1.

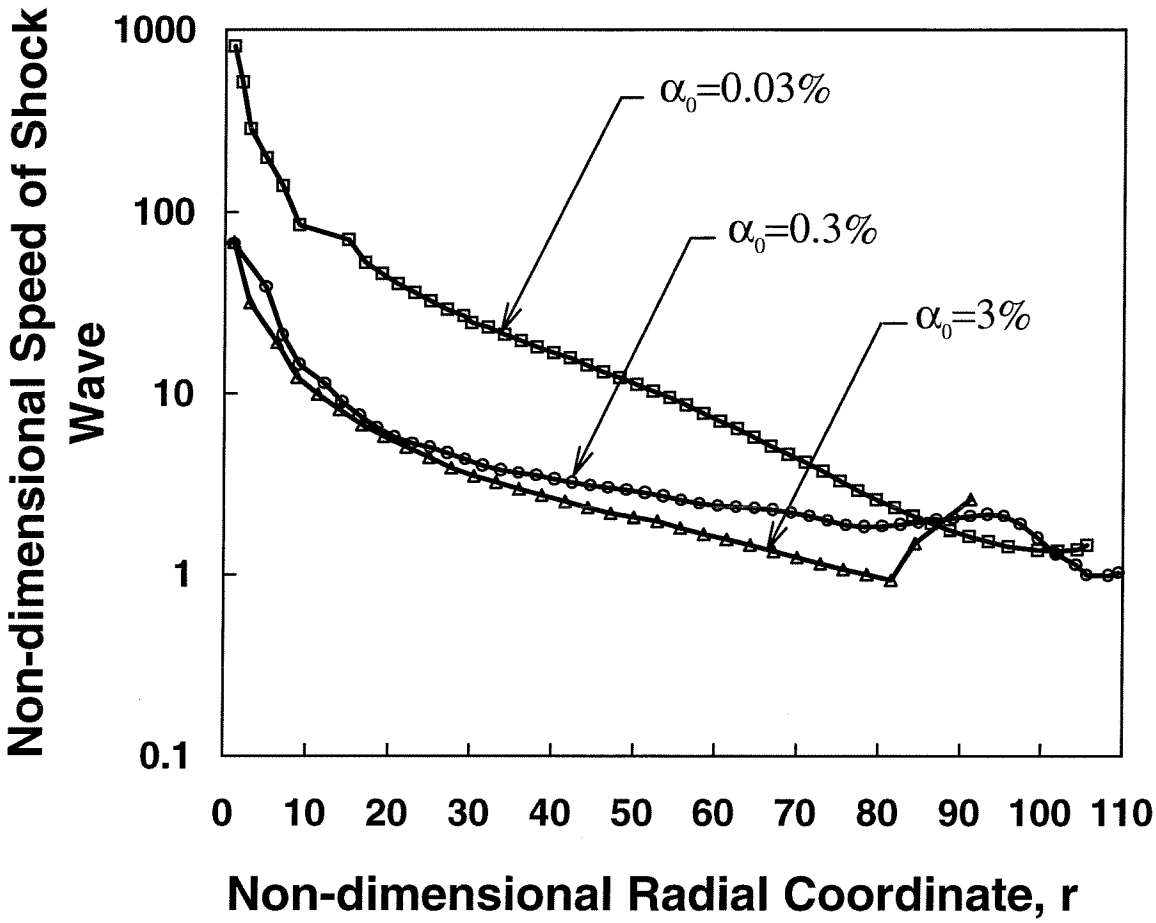

Figure 4.18 The speeds of the shock wave as a function of shock front position in the cloud for three different initial void fraction. Other parameters as in Figure 4.1.

Part II

Bubbly Cavitating Flows Through a Converging-diverging Nozzle

Chapter 1

Introduction

One-dimensional bubbly liquid flows in ducts and nozzles represent the simplest confined gas-liquid flow configurations. Understanding of the characteristics of these flows is important not only for the practical applications such as gas-liquid pipeline transport, liquid metal MHD propulsion, industrial bubble columns and so on, but for the development of appropriate analytical models for other types of cavitating flow.

It is well known that a very small number of bubbles can have a substantial effect on the fluid dynamics of the suspending liquid. Furthermore, the dynamics of the mixture both in the linear and in the nonlinear regimes are strongly dependent on the concentration of the bubbles and on the interface interactions, namely the mass, momentum and energy interactions between the two phases. Therefore, different interactive effects will produce different phenomena. For example, the friction and the relative motion between the

bubbles and the liquid often cause wave dispersion in the mixture. If the frequency of the wave is close to the natural frequency of the bubbles, in addition to further dispersion, an oscillatory structure will occur on the wave because of the bubble radial pulsations. In some flows it is possible to establish a barotropic relation, $p = f(\rho)$, which assumes that the mixture pressure is the function of mixture density only. This implies that all effects caused by bubble content are disregarded except for the compressibility and that the mixture can be regarded as a new single-phase compressible substance. Then the equations of motion of the flow will become purely hyperbolic. In this case one can anticipate that the flow phenomena and the methods used to solve the equations will be similar to those in single-phase gas dynamics. In practice this would only be the case if the typical frequencies experienced by the bubbles in the flow are very much smaller than the natural frequencies of the bubbles themselves and if the perturbation imposed on the flow is small enough such that the bubbles do not cavitate. Under these circumstances the bubbles would behave quasistatically and the mixture would be barotropic. Tangren *et al.* [1949] first addressed the barotropic nozzle flow. A summary of this subject can be found, for example, in Brennen [1995]. In many practical flows, however, the barotropic criterion is not met. Then the dynamics of individual bubbles have to be incorporated into the dynamics of the mixture.

The present paper addresses a cavitating bubbly flow through a converging-

diverging nozzle. The dynamic effects of the flow acceleration in the nozzle cause bubbles to cavitate so that they do not behave quasistatically. Under this circumstance the mixture is not barotropic. The growth and collapse of cavitating bubbles may dramatically change or destabilize the flow.

The flow model used here is similar to that discussed in Part I. Namely, the continuum mixture equations coupled with the Rayleigh-Plesset equation for bubble dynamics. This model was proposed first by van Wijngaarden [1968], [1972] and has been used for studying steady and transient shock wave propagation in bubbly liquids without the acceleration of the mean flow (see, for example, Noordzij and van Wijngaarden [1974], Kameda and Matsumoto [1995]). Only a few papers have addressed problems with flowing bubbly liquids. Ishii *et al.* [1993] studied steady bubbly flows through a converging-diverging nozzle but with the assumption that the gas pressure inside the bubbles is equal to the ambient fluid pressure so that the bubble radial dynamics (as represented by the Rayleigh-Plesset equation) are neglected. Morioka and Matsui [1980] and Morioka and Toma [1984] investigated the acoustic dispersion relation for a flowing bubbly liquid using van Wijngaarden's model. Toma and Morioka [1986] examined characteristics of different acoustic modes in flowing bubbly liquid using the same model. However, for an accelerating flow, the linearization of the equations of motion is impossible since the mean flow quantities are changing with both space and

time and the perturbation with respect to constant mean values can not be performed. Of course, one can perturb the flow equations with respect to the steady state solutions to make the equations linear. However, the steady state solutions are complicated enough (see Chapter 3) so that an analytical analysis is intractable. Toma *et al.* [1988] conducted the experiments with bubbly liquid flows in a converging-diverging nozzle and recorded the temporal fluctuation characteristics of this kind of flow. However, fully nonlinear solutions of the accelerating bubbly flows with bubble cavitation effects have not, previously, been obtained.

Nonlinear solutions for a cavitating nozzle flow are presented here. It is found that the characteristics of the flow change dramatically even when the upstream void fraction is very small. Large downstream spatial fluctuations can be induced by the pulsations of cavitating bubbles. When the flow is unsteady, the effects of bubble dynamics cause instant large pressure pulses which move back and forth downstream of the throat.

Chapter 2 describes the basic equations for the present problem. Chapter 3 describes steady state solutions. Two different flow regime are found. Bifurcation occurs as the bubbles grow to a critical size and the flow transitions from a quasistatically stable regime to the quasistatically unstable regime. An analytical expression of this critical bubble size is derived in Section 3.3.

Chapter 4 addresses the problem of the unsteady cavitating nozzle flow.

The system of the unsteady equations is rewritten based on the Lagrangian formulation and are described in Section 4.1. An explicit computational procedure for solving the equations is suggested in Section 4.2. Section 4.3 presents some solutions obtained for a particular case. These solutions are characterized by downstream spatial fluctuations coupled with large pressure pulses changing in both magnitude and location with time. The characteristics of these pulses are similar to the shock pulses shown in Part I and are produced by the local violent collapse of the bubbles in the flow.

Chapter 2

Basic Equations

The variables and equations in this part of thesis are all in dimensionless form. The definitions of the non-dimensional quantities are similar to those in Section 2.1, Part I, but are now based on the upstream conditions of the nozzle: $x = x^*/R_s^*$ is the non-dimension Eulerian coordinate, $R = R^*/R_s^*$ is the non-dimensional bubble radius, $u = u^*/u_s^*$ is the non-dimensional mixture velocity, $C_P = (p^* - p_s^*)/\frac{1}{2}\rho_L^* u_s^{*2}$ is the mixture pressure coefficient, and $A = A^*/A_s^*$ is the normalized cross-sectional area of the nozzle. Here R_s^* is upstream bubble radius, u_s^* is the upstream mixture velocity, p_s^* is the upstream pressure, A_s^* is the upstream cross-sectional area of the duct, and ρ_L^* is the liquid density. Again, all quantities with superscript * denote dimensional values.

Referring to Figure 2.1, consider a one-dimensional converging-diverging nozzle with length L and cross-sectional area $A(x)$. Here the non-dimensional Eulerian coordinate, x, is positive in the direction of the flow. The inlet of the

nozzle is located at x_n. The mixture continuity and momentum equations are

$$\frac{\partial}{\partial t}[(1-\alpha)A] + \frac{\partial}{\partial x}[(1-\alpha)uA] = 0 \tag{2.1}$$

$$\frac{\partial u}{\partial t} + u\frac{\partial u}{\partial x} = -\frac{1}{2(1-\alpha)}\frac{\partial C_P}{\partial x} \tag{2.2}$$

where $\alpha(x,t)$, the bubble void fraction, is related to the bubble radius, $R(x,t)$, by $\alpha(x,t) = \frac{4}{3}\pi\eta R^3(x,t)/[1+\frac{4}{3}\pi\eta R^3(x,t)]$ and η is the bubble population per unit liquid volume. The non-dimensional mixture density has been approximated by $\rho \approx (1-\alpha)$ by neglecting the density of gas phase. It is also assumed that the liquid phase is incompressible. The dynamics of the individual bubbles are modeled by the Rayleigh-Plesset equation:

$$\begin{aligned} R\frac{D^2R}{Dt^2} &+ \frac{3}{2}\left(\frac{DR}{Dt}\right)^2 + \frac{\sigma}{2}\left[1-R^{-3k}\right] + \frac{4}{Re}\frac{1}{R}\frac{DR}{Dt} \\ &+ \frac{2}{We}\left[R^{-1}-R^{-3k}\right] + \frac{1}{2}C_P = 0 \end{aligned} \tag{2.3}$$

where $D/Dt = \partial/\partial t + u\partial/\partial x$ is the Lagrangian derivative. The definitions of cavitation number, σ, Weber number, We, and the Reynolds number, Re, can be found in Section 2.1, Part I, but now are based on the upstream velocity and pressure. As before, the index k is used to model the polytropic behavior of the permanent gas inside the bubble. All the basic assumptions used to write

down the above equations are the same as in Section 2.2, Part I. Furthermore, friction between the mixture and the duct wall is neglected.

Equations (2.1), (2.2) and (2.3) represent a simple model of one-dimensional flowing bubbly mixture with nonlinear bubble dynamics. Previous investigations have resulted in the dispersion and stability properties of this model in the linear regimes (see, for example, Biesheuvel and van Wijngaarden [1984]; Morioka and Matsui [1980]; Morioka and Toma [1984]; Toma and Morioka [1986]; Toma *et al.* [1988]). These results helped to identify the propagation modes and the dispersion characteristics of the acoustic waves in a flowing bubbly liquid. However, if the flow is accelerating, simple linearization of the equations of motion is impossible since the mean flow quantities are changing rapidly with both space and time and the perturbation with respect constant and uniform mean values can not be performed. Analyses of the dynamics of this model then become significantly more complicated and new phenomena may be manifest due to the coupling of flow acceleration and bubble pulsation.

Chapter 3

Steady State Solutions

The first question which arises concerns the existence of steady state solutions and their characteristics. For an unsteady nozzle flow, the system of equations (2.1), (2.2) and (2.3) set up an initial boundary value problem. The problem could be ill-posed since the dispersion relation of this system results in complex acoustic wave numbers and makes the system non-hyperbolic. However, when steady solutions are considered, the problem becomes an initial value problem and is free from ill-posedness.

3.1 Steady Equations

Assume that equations (2.1), (2.2) and (2.3) have steady state solutions for a constant mass flow rate with upstream conditions denoted by p_s^*, u_s^*, and $\rho_s^* \approx \rho_L^*(1-\alpha_s) = \rho_L^*/(1+\frac{4}{3}\pi\eta R_s^{*^3})$, where R_s^* and α_s are the upstream nuclei size and void fraction respectively. After dropping all the time derivative terms,

the governing equations become a system of ordinary differential equations with one independent variable, x:

$$(1-\alpha)uA = (1-\alpha_s) = constant \tag{3.1}$$

$$u\frac{du}{dx} = -\frac{1}{2(1-\alpha)}\frac{dC_P}{dx} \tag{3.2}$$

$$\begin{aligned} R\left(u^2\frac{d^2R}{dx^2} + u\frac{du}{dx}\frac{dR}{dx}\right) + \frac{2u^2}{3}\left(\frac{dR}{dx}\right)^2 + \frac{4}{Re}\frac{u}{R}\frac{dR}{dx} \\ + \frac{2}{We}\left(\frac{1}{R} - \frac{1}{R^{3k}}\right) + \frac{\sigma}{2}\left(1 - \frac{1}{R^{3k}}\right) + \frac{1}{2}C_P = 0 \end{aligned} \tag{3.3}$$

The non-dimensional initial conditions arise from the upstream conditions and are given by:

$$R(x=0) = 1, \quad u(x=0) = 1, \quad C_P(x=0) = 0 \tag{3.4}$$

We choose to examine a simple nozzle, $A(x)$, such that

$$A(x) = \begin{cases} \sqrt{1 + \frac{1}{2}C_{PMIN}\left[1 - cos\left(\frac{2\pi x}{L}\right)\right]} & ;\ x_n \leq x \leq L \\ 1 & ;\ x < x_n \text{ and } x > L \end{cases} \tag{3.5}$$

This profile will produce a simple sinusoidal pressure distribution in the case

of incompressible flow with the minimum pressure coefficient, C_{PMIN}, located at the nozzle throat. The value of $-C_{PMIN}$ relative to the cavitation number, σ, represents the intensity of tension in the flow. If $-C_{PMIN}$ is greater than the cavitation number, σ, the minimum mixture pressure experienced by the individual bubbles will be lower than vapor pressure and the bubbles will cavitate (see also Section 2.4, Part I).

3.2 Results and Discussion

A fourth order Runge-Kutta scheme was used to integrate equations (3.2) and (3.3). The following flow conditions were chosen to illustrate the structures of the steady state solutions in flows which might occur in practice. A bubbly liquid, composed of air bubbles ($k = 1.4$) in water at 20°C ($\rho_L^* = 1000kg/m$, $S^* = 0.073N/m$), is flowing through a nozzle with profile given by equation (3.5). The inlet of the nozzle is located at $x = 0$ (or $x_n = 0$ in Figure 2.1) and the non-dimensional length of the nozzle is $L = 500$. The minimum pressure coefficient, C_{PMIN}, for a pure liquid flow is chosen as -1. The upstream cavitation number, σ, is set at 0.8 smaller than $-C_{PMIN}$ and cavitation will occur. The Reynolds number, Re, is taken as 1000 in which only the liquid viscosity are considered. Other damping mechanisms can be included by using an "effective viscosity" (Chapman and Plesset [1971]). Five different upstream void fractions, α_s, of the order of 10^{-6} are used in the computation and the results

are shown in Figures 3.1 to 3.4.

Flows which are both quasistatically stable and quasistatically unstable were found. Furthermore, it was found that a bifurcation occurs between the two types of flow. Figure 3.1 illustrates the mixture velocity in the flow. The case of $\alpha_s = 0$ corresponds to the incompressible pure liquid flow. It is notable that even for an upstream void fraction as small as 2×10^{-6}, the characteristics of the flow are changed. Radial pulsation of bubbles results in the downstream fluctuations of the flow. The amplitude of the velocity fluctuation is 10% of that of the incompressible flow in this case. As α_s increases further, the amplitude as well as the wavelength of the fluctuations increase. However, the velocity dose eventually return to the upstream value. In other words, the flow is still quasistatically stable. However, as α_s increases to a critical value, α_b (about 2.862×10^{-6} in the present calculation), a bifurcation occurs. The velocity increases dramatically and the flow becomes quasistatically unstable. The physical picture of this instability is quite simple indeed: Growth of the cavitation bubbles will increase the mixture velocity according to the mass conservation of the flow. The increase of the velocity then cause the mixture pressure to decrease due to the Bernoulli effect. The decrease of the pressure is fed back to the Rayleigh-Plesset dynamics and results in more bubble growth.

The corresponding variations in the mixture pressure coefficient are shown in Figure 3.2. In addition to the two different flow regimes, another important

feature in the quasistatically stable flow is the typical frequency associated with the downstream periodicity. This "ringing" will result in acoustic radiation at frequencies corresponding to this interval. How this ring frequency relates to the upstream flow condition remains to be studied. Furthermore, since some energy is contained in the oscillatory structure, the downstream pressure coefficient has a lower level than that of the upstream value except in the case of pure liquid flow.

Figure 3.3 illustrates the void fraction distribution in the flow. When the flow becomes quasistatically unstable, the bubble void fraction, $\alpha(x)$, quickly approaches unity. This means that the flow is flashing to vapor. When α becomes large, our model equations, which are limited to flows with small void fraction, lose their validity.

Figure 3.4 indicates the non-dimensional bubble radius distribution in the flow. The bubbles grow without bound after reaching a critical radius, R_c, which is found to be dependent on the cavitation number and the upstream void fraction. The analytical expression for R_c is derived in the next section.

3.3 Bifurcation Parameters of the Steady Solutions

Due to the time lag of bubble growth phase, bubbles reach the maximum size after passing the nozzle throat (Figure 3.4). With increase in the upstream void fraction, the maximum size of the bubbles increases and is shifted further downstream. The bifurcation occurs when a critical value, R_c, is reached. From Figure 3.4 we know that dR/dx and d^2R/dx^2 both vanish at $R = R_c$. Substitution of these conditions into (3.3) gives

$$\frac{2}{We}\left[R_c^{-1} - R_c^{-3k}\right] + \frac{1}{2}C_{Pc} = 0 \tag{3.6}$$

Here C_{Pc} can be found by integrating (3.1) and (3.2) by putting $A = 1$ (assuming that the flow exits the nozzle into a length of constant area duct downstream of the nozzle):

$$C_{Pc} = -\frac{24\pi\eta R_c^3}{(3+4\pi\eta)^2}\left(1 - \frac{1}{R_c^3}\right) \tag{3.7}$$

Since $R_c \gg 1$, all the higher order terms ($1/R_c^{3k}$ in (3.6) and $1/R_c^3$ in (3.7)) can be neglected. After combining these two equations, one can write

$$R_c^4 - \frac{\sigma}{2\alpha_s(1-\alpha_s)}R_c - \frac{2}{\alpha_s(1-\alpha_s)We} = 0 \tag{3.8}$$

in which $\frac{4}{3}\pi\eta = \alpha_s/(1-\alpha_s)$ has been used. The third term in (3.8) can be neglected because, in addition to $R_c \gg 1$, practical values for $2/We$ are about an order of magnitude less than the values of $\sigma/2$ in the second term. Thus, finally we have:

$$R_c = \left[\frac{\sigma}{2\alpha_s(1-\alpha_s)}\right]^{1/3} \approx \left[\frac{\sigma}{2\alpha_s}\right]^{1/3} \tag{3.9}$$

If $R > R_c$, the flow becomes quasistatically unstable. In the cases presented here $(\sigma/2\alpha_s)^{1/3} \approx 51$. Examination of Figure 3.4 shows that this value is accurate. With known R_c, the expressions for the critical pressure coefficient can be obtained from (3.7):

$$C_{Pc} = 2\alpha_s(1-\alpha_s) - \sigma \approx -\sigma \tag{3.10}$$

Chapter 4

Unsteady Flows

In this chapter, a method for the numerical modeling of bubbly cavitating flows will be developed and used to investigate the one-dimensional unsteady bubbly cavitating flows in ducts or nozzles. The numerical approach was first used by Nigmatulin and his coworkers (Nigmatulin [1991]) to study the nonstationary wave motions of bubbly liquids in a straight pipe without mean flow. The method presented here is based on the same idea but is extended to the accelerating flows in ducts with variable cross-section area.

The natural coordinate system for an individual bubble in the flow is the Lagrangian coordinate system. It is much easier to calculate the effects of bubble volume pulsation on the global fluid dynamics by moving with the bubbles. In this way, all the nonlinear convective terms contained in the Lagrangian derivative, D/Dt, in equation (2.3) can be transformed into regular time derivatives in the moving coordinate system. However, the boundary con-

ditions of the nozzle flow are essentially Eulerian. In order to solve equations (2.1), (2.2), and (2.3), two Eulerian boundary conditions must be prescribed at each end of the flow. In practice, these may be reservoir conditions with known values of pressure. Therefore, the situation here is unlike that in Part I, in which the boundary of the cloud is moving with the Lagrangian grid.

4.1 Lagrangian Formulation

The non-dimensional Lagrangian coordinates are denoted by (x_0, t), where x_0 is the distance from a Lagrangian particle to the origin of an inertial frame at initial time, $t = 0$. The origin is set at the inlet to the pipe. All quantities with subscript 0 denote values at $t = 0$. For example, $A_0 = A(x_0)$ is the cross-section area felt by a Lagrangian particle located at x_0 at $t = 0$, $\alpha_0 = \alpha(x_0, 0)$ is the bubble void fraction distribution at $t = 0$, $R_0 = R(x_0, 0)$ is the bubble size distribution at $t = 0$, and so on. The coordinate transformation from the Lagrangian coordinate, x_0, to the Eulerian position, x, namely $x_0 \longmapsto x(x_0, t)$, is given by

$$\frac{\partial x}{\partial x_0} = \frac{A_0 \rho_0}{A \rho} \approx \frac{A_0(1-\alpha_0)}{A(1-\alpha)} \tag{4.1}$$

After some algebra, instead of equations (2.1), (2.2), and (2.3), the following system of equations are obtained in the Lagrangian coordinates:

$$\frac{\partial^2 C_P}{\partial x_0^2} + K\frac{\partial C_P}{\partial x_0} + NC_P + M = 0 \tag{4.2}$$

where

$$\begin{aligned}
K(x_0,t;x) &= \frac{2(1-\alpha_0)A_0}{(1-\alpha)A^2}\frac{dA}{dx} - \frac{1}{A_0}\frac{dA_0}{dx_0} + \frac{1}{1-\alpha_0}\frac{d\alpha_0}{dx_0} \\
N(x_0,t;x) &= -\frac{3\alpha\left(1-\alpha_0\right)^2 A_0^2}{(1-\alpha)A^2R^2} \\
M(x_0,t;x) &= -\frac{2\left(1-\alpha_0\right)^2 A_0^2 u^2}{(1-\alpha)A^3}\left[\frac{2}{A}\left(\frac{dA}{dx}\right)^2 - \frac{d^2A}{dx^2}\right] \\
&\quad + \frac{6\alpha\left(1-\alpha_0\right)^2 A_0^2}{(1-\alpha)A^2R^2}\left[\frac{\sigma}{2}\left(R^{-3k}-1\right) + \frac{2}{We}\left(R^{-3k}-R^{-1}\right)\right. \\
&\quad \left. -\frac{4}{Re}\frac{w}{R} - \frac{1}{2}w^2 - 2Ruw\frac{1}{A}\frac{dA}{dx}\right]
\end{aligned}$$

$$\begin{cases}
\dfrac{DR}{Dt} = w \\
\dfrac{Dw}{Dt} = \dfrac{1}{R}\left[\dfrac{\sigma}{2}\left(R^{-3k}-1\right) + \dfrac{2}{We}\left(R^{-3k}-R^{-1}\right) - \dfrac{4}{Re}\dfrac{w}{R} - \dfrac{3}{2}w^2 - \dfrac{1}{2}C_P\right]
\end{cases} \tag{4.3}$$

$$\frac{Dx}{Dt} = u \tag{4.4}$$

$$\frac{Du}{Dt} = -\frac{A}{2A_0(1-\alpha_0)}\frac{\partial C_P}{\partial x_0} \tag{4.5}$$

The derivation of equation (4.2) is given in Appendix A. Equations (4.3) constitute the Rayleigh-Plesset equation, (2.3), where the Lagrangian bubble wall velocity, $w = DR/Dt$, is used as a new variable. Equation (4.4) is a simple kinematic relation. Equation (4.5) is the Lagrangian expression of the mixture momentum equation, equation (2.2). Note that equations (4.3) to (4.5) only contain the Lagrangian time derivative and can therefore be integrated by any time-marching scheme in the Lagrangian coordinate system. On the other hand, equation (4.2) contains only spatial derivatives and is a second order Poisson equation. If all of the quantities, α, x, R, w, and u, are known at an instance of time, this equation can be integrated to obtain the pressure distribution at that time. This result is due to the incompressibility of the liquid phase. Recall that for incompressible flow one can always combine the continuity and momentum equations to obtain a Poisson equation for the pressure field. For a bubbly flow with incompressible carrier liquid, suppose that, at some point in time, all the other quantities mentioned above are known by some method. Then, at that instant, all the bubbles in the flow have known size and the mixture is simply an incompressible substance with many unchanging voids. The separation of the spatial and Lagrangian time derivatives in the above formulation makes it possible to solve the problem by an explicit numerical scheme, as shown in the next section.

4.2 Numerical Method to Solve Equations (4.2) to (4.5)

Assume that the computational domain is $[0, x_e]$ in the Eulerian space. Also assume that at time t, a Lagrangian grid is generated in this domain with N grid points located at $x_{01} = 0, x_{02}, \ldots, x_{0N-1}, x_{0N} = x_e$ and that the value of the quantities, $R(x_0, t)$, $w(x_0, t)$, $x(x_0, t)$, and $u(x_0, t)$, are known at these points. Note that the void fraction, α, is related to the bubble radius, R, by

$$\alpha = \frac{\frac{4}{3}\pi\eta R^3}{1 + \frac{4}{3}\pi\eta R^3} \tag{4.6}$$

A complete integration time step from t to $t + \triangle t$ then proceeds as follows.

1) With the prescribed pressure boundary conditions, $C_P(0, t)$ and $C_P(x_e, t)$, equation (4.2) can be integrated to find $C_P(x_0, t)$ at the grid points. A relaxation method (see, for example, Press *et al.* [1992]) is used in the integration of this boundary value problem.

2) With known $C_P(x_0, t)$, $\frac{\partial C_P}{\partial x_0}(x_0, t)$, equations (4.3) to (4.5) can be integrated by time-marching schemes to find $R(x_0, t + \triangle t)$, $w(x_0, t + \triangle t)$, $x(x_0, t + \triangle t)$, and $u(x_0, t + \triangle t)$, at each Lagrangian node. A fifth order Runge-Kutta method is used in the present computation. Note that the Eulerian end point x_e may not coincide with the Eulerian position of

any of new grid locations. Assume that $x_M \leq x_e \leq x_{M+1}$, $M < N$.

3) Before proceeding to the next time step, we re-define the new Lagrangian grid by $x_{01} = 0, x_{02} = x_1, \ldots, x_{0M} = x_M, x_{0M+1} = x_e$, where x_i ($i = 1 \ldots M$) are the Eulerian positions at time $t + \triangle t$. In other words, the total number of Lagrangian nodes is now changed to $M+1$. However, the values of R (and thus α), w, and u are unknown at the end points, $x_{01} = 0$ and $x_{0M+1} = x_e$. Polynomial interpolation is used to find these values at x_{0M+1} based on the known values at the neighboring points. For the inlet point, $x_{01} = 0$, the values of $R(x_{01}, t + \triangle t) = 1$ and $w(x_{01}, t + \triangle t) = 0$ are used. Physically, this means that all the entering nuclei have the same initial size and are assumed stable (with zero initial bubble wall velocities). However, the inlet mixture velocity, $u(x_{01}, t + \triangle t)$, can not be prescribed since the flow is going to adjust itself in an unsteady way. Polynomial extrapolation is used to find $u(x_{01}, t + \triangle t)$ in the present computation.

4) With the new value of $u(x_{01}, t + \triangle t)$, the values of w, u, C_P, σ, Re, and We are re-normalized by this new upstream velocity. (Recall that the non-dimensionalization is based on the upstream conditions.)

5) Proceed to next time step.

A numerical difficulty similar to that experienced in Part I (see Section 3.2 and

Section 4.2, Part I) is found when integrating equation (4.2). Large number of iterations are necessary if there is a violent bubble collapse in the flow.

4.3 Results and Discussion

One selective case is chosen to illustrate the unsteady characteristics of the flow. In practice, solutions with a downstream oscillating structure are more interesting since these are the flows which manifest bubble dynamic effects. Surprisingly, the oscillation solutions are only found in the cases of very small upstream void fraction (2×10^{-6} in the current case). For time $t < 0$ the flow is assumed to be in a steady state; the pressure coefficient at the exit end is about - 0.066 (see Figure 4.1 (a)). At t=0, the exit pressure coefficient is lowered suddenly to -0.2. We will examine the response of the flow to this sudden change.

Figures 4.1 (a) to (h) show the results of the unsteady mixture pressure coefficient at a series of consecutive times, $0 < t_1 < t_2 < \cdots < t_{20}$. The unsteady solutions are characterized by alternating growth and decay of the individual pressure pulses in the flow downstream of the throat. The instantaneous magnitudes of these pulses can be very large. Their location is changing with time; typically they move back and forth between the nozzle exit and x_e. The characteristics of these pulses are similar to the shock pulses shown in Part I (see Figure 4.5, Part I). They are produced by the local collapse of

the bubbles in the flow.

During the same series of times, the distributions of mixture velocity and bubble size do not change much from the steady state solution. Interesting questions one may ask are: Is there any new steady state solution for the flow? Are the above unsteady phenomena transient? Unfortunately, the questions can not be answered yet. The inherent numerical difficulty mentioned before strongly impedes the progress of the computation. This generic problem must be solved before more unsteady characteristics can be explored.

Chapter 5

Concluding Remarks

Cavitating bubbly flows through a converging-diverging nozzle have been examined in this part of thesis. It was found that the nonlinear dynamics of bubbles coupled with the equations of motion of the mixture strongly affect the structure of the flow even for very small bubble populations. Both steady state and unsteady solutions were investigated. Two different flow regimes, determined by the parameter $R_c = (\sigma/2\alpha_s)^{1/3}$, (where σ is the cavitation number of the flow and α_s is the upstream void fraction) are revealed in the steady state solutions. The flow becomes quasistatically unstable if the radius of the cavitating bubbles is greater than R_c. In this circumstance, the growth of bubbles increases the mixture velocity due to mass conservation of the flow. The velocity increase then causes the mixture pressure to decrease according to the momentum equation. The decrease of the pressure is fed back to the Rayleigh-Plesset equation and results in further bubble growth. In this

case velocity and void fraction of the mixture increase and pressure coefficient of the flow decreases significantly beyond the upstream values and the flow is flashing. On the other hand, if the bubbles do not grow beyond R_c, the flow is quasistatically stable and is characterized by large amplitude spatial fluctuations downstream of the throat.

An explicit computational method was proposed to explore the features of the unsteady solutions. This method is based on the re-formulation of the governing equations in the Lagrangian coordinate system. The Lagrangian time derivative and the spatial derivative were separated in this approach. Due to the incompressibility of the liquid phase, the mixture pressure equation was found to have the form of Poisson equation at any instant of time. Actually, this method is very similar to that in Part I in which the pressure equation was put into the form of an integral equation.

An unsteady solution was presented showing the evolution of the flow through a series of consecutive times. These solutions are characterized by downstream spatial fluctuations coupled with large pressure pulses changing with time in both magnitude and location. Further numerical experiments were impeded because of an inherent numerical difficulty; these should be focused on in the future.

Appendix A

Derivation of Equation (4.2)

Three useful relations are:

$$\frac{\partial u}{\partial x_0} = \frac{A_0\rho_0}{A\rho}\left(\frac{3\alpha}{R}\frac{DR}{Dt} - \frac{1}{A}\frac{DA}{Dt}\right) \tag{A.1}$$

$$\frac{D\rho}{Dt} = -\frac{3\alpha\rho}{R}\frac{DR}{Dt} \tag{A.2}$$

$$\frac{D\alpha}{Dt} = \frac{3\alpha(1-\alpha)}{R}\frac{DR}{Dt} \tag{A.3}$$

where $DA/Dt = udA/dx$ since $A(x)$ is not function of time. Now we present the proofs of these relations. First write the continuity equations for the liquid

and gas phases in Lagrangian coordinates:

$$\frac{D}{Dt}[(1-\alpha)A] + \frac{(1-\alpha)A^2\rho}{A_0\rho_0}\frac{\partial u}{\partial x_0} = 0 \tag{A.4}$$

$$\frac{D}{Dt}(\rho_g \alpha A) + \frac{\rho_g \alpha A^2 \rho}{A_0\rho_0}\frac{\partial u}{\partial x_0} = 0 \tag{A.5}$$

in which the coordinate transformation (4.1) has been used to substitute $\partial/\partial x$ by $\partial/\partial x_0$ and $\rho_g = \rho_g^*/\rho_L^*$ is the non-dimensional density of the gaseous phase inside the bubble. Since mass transfer between phases is neglected, one has

$$\frac{D(\rho_g R^3)}{Dt} = 0 \tag{A.6}$$

Expanding the first terms in equations (A.4) and (A.5) and adding the two equations, one can have

$$\frac{\partial u}{\partial x_0} = -\frac{A_0\rho_0}{A\rho}\left(\frac{\alpha}{\rho_g}\frac{D\rho_g}{Dt} + \frac{1}{A}\frac{DA}{Dt}\right) \tag{A.7}$$

Substituting equation (A.6) into equation (A.7), one can get equation (A.1). Equation (A.2) can be obtained by rewriting the mixture continuity equation, (2.1), in the Lagrangian coordinates and by substituting equation (A.1) into it. Equation (A.3) is obtained immediately by differentiating (4.6).

Now we derive equation (4.2). The Lagrangian form of the mixture mo-

mentum equation, (2.2), is

$$\frac{Du}{Dt} = -\frac{A}{2A_0\rho_0}\frac{\partial C_P}{\partial x_0} \tag{A.8}$$

Differentiating (A.8) with respect to x_0 gives

$$\begin{aligned}\frac{\partial}{\partial x_0}\left(\frac{Du}{Dt}\right) &= -\frac{A}{2A_0\rho_0}\frac{\partial^2 C_P}{\partial x_0^2} \\ &\quad + \frac{A}{2A_0\rho_0}\left(\frac{1}{\rho_0}\frac{d\rho_0}{dx_0} + \frac{1}{A_0}\frac{dA_0}{dx_0} - \frac{1}{A}\frac{\partial A}{\partial x_0}\right)\frac{\partial C_P}{\partial x_0}\end{aligned} \tag{A.9}$$

where

$$\frac{\partial A}{\partial x_0} = \frac{\partial}{\partial x_0}A(x(x_0,t)) = \frac{dA}{dx}\frac{\partial x}{\partial x_0} = \frac{A_0\rho_0}{A\rho}\frac{dA}{dx} \tag{A.10}$$

Taking the Lagrangian derivative of equation (A.1) and then substituting equations (A.2) and (A.3) into it, one can obtain

$$\begin{aligned}\frac{\partial}{\partial x_0}\left(\frac{Du}{Dt}\right) &= \left(\frac{1}{2\rho A}\frac{dA}{dx}\right)\frac{\partial C_P}{\partial x_0} + \frac{\rho_0 A_0 u^2}{\rho A^2}\left[\frac{2}{A}\left(\frac{dA}{dx}\right)^2\right. \\ &\quad \left. - \frac{d^2A}{dx^2}\right] + \frac{3\alpha\rho_0 A_0}{\rho A R^2}\left(R\frac{Dw}{Dt} - 2Ruw\frac{1}{A}\frac{dA}{dx} + 2w^2\right)\end{aligned} \tag{A.11}$$

where the order of D/Dt and $\partial/\partial x_0$ on the left-hand side has been exchanged since they are independent in the Lagrangian coordinate system; also the variable $w = DR/Dt$ has been used.

Substituting the Rayleigh-Plesset equation (2.3) into the right-hand side of (A.11), equating (A.9) and (A.11), and rearranging the result, one can finally have equation (4.2):

$$\frac{\partial^2 C_P}{\partial x_0^2} + K\frac{\partial C_P}{\partial x_0} + NC_P + M = 0 \tag{A.12}$$

where

$$\begin{aligned}
K(x_0,t;x) &= \frac{2(1-\alpha_0)A_0}{(1-\alpha)A^2}\frac{dA}{dx} - \frac{1}{A_0}\frac{dA_0}{dx_0} + \frac{1}{1-\alpha_0}\frac{d\alpha_0}{dx_0} \\
N(x_0,t;x) &= -\frac{3\alpha\left(1-\alpha_0\right)^2 A_0^2}{(1-\alpha)A^2R^2} \\
M(x_0,t;x) &= -\frac{2\left(1-\alpha_0\right)^2 A_0^2 u^2}{(1-\alpha)A^3}\left[\frac{2}{A}\left(\frac{dA}{dx}\right)^2 - \frac{d^2A}{dx^2}\right] \\
&\quad + \frac{6\alpha\left(1-\alpha_0\right)^2 A_0^2}{(1-\alpha)A^2R^2}\left[\frac{\sigma}{2}\left(R^{-3k}-1\right) + \frac{2}{We}\left(R^{-3k}-R^{-1}\right)\right. \\
&\quad \left. - \frac{4}{Re}\frac{w}{R} - \frac{1}{2}w^2 - 2Ruw\frac{1}{A}\frac{dA}{dx}\right]
\end{aligned}$$

Bibliography

Biesheuvel, A., and van Wijngaarden, L. [1984] Two phase flow equations for a dilute dispersion of gas bubbles in liquid. *J. Fluid Mech.*, **148**, 301–318.

Brennen, C. E. [1995] *Cavitation and bubble dynamics.* Oxford University Press.

Chapman, R. B., and Plesset, M. S. [1971] Thermal effects in the free oscillation of gas bubbles. *ASME J. Basic Eng.*, **93**, 373–376.

Ishii, R., Umeda, Y., Murata, S., and Shishido, N. [1993] Bubbly flows through a converging-diverging nozzle. *Phys. Fluids A*, **5**(7), 1630–1643.

Kameda, M., and Matsumoto, Y. [1995] Structure of shock waves in a liquid containing gas bubbles. *Pages 117–126 of: IUTAM Symposium on Waves in Liquid/Gas and Liquid/Vapour Two-Phase Systems.*

Morioka, S., and Matsui, G. [1980] Mechanism and effect of dispersion and dissipation in nozzle flows of bubbly liquid. *Page 54 of: Proc. 1st Asian Cong. Fluid Mech.*, volume A.

Morioka, S., and Toma, T. [1984] Stability of two-phase liquid metal mhd channel flows. *Prog. Astronaut. Aeronaut.*, **100**, 317.

Nigmatulin, R. I. [1991] *Dynamics of Multiphase Media.* Hemisphere, New York.

Noordzij, L., and van Wijngaarden, L. [1974] Relaxation effects, caused by relative motion, on shock waves in gas-bubble/liquid mixtures. *J. Fluid Mech.*, **66**, 115–143.

Press, W. H., Teukolsky, S. A., Vetterling, W. T., and Flannery, B. P. [1992] *Numerical Recipes.* Second edition. Cambridge University Press.

Tangren, R. F., Dodge, C. H., and Seifert, H. S. [1949] Compressibility effects in two-phase flow. *J. Appl. Phys.*, **20**(7), 637–645.

Toma, T., and Morioka, S. [1986] Acoustic waves forced in flowing bubbly liquid. *J. Phys. Soc. Japan*, **55**(2).

Toma, T., Yoshino, K., and Morioka, S. [1988] Fluctuation characteristics of bubbly liquid flow in converging-diverging nozzle. *Fluid Dyn. Res.*, **2**, 217–228.

van Wijngaarden, L. [1968] On the equations of motion for mixtures of liquid and gas bubbles. *J. Fluid Mech.*, **33**.

van Wijngaarden, L. [1972] One-dimensional flow of liquids containing small gas bubbles. *Ann. Rev. Fluid Mech.*, **4**.

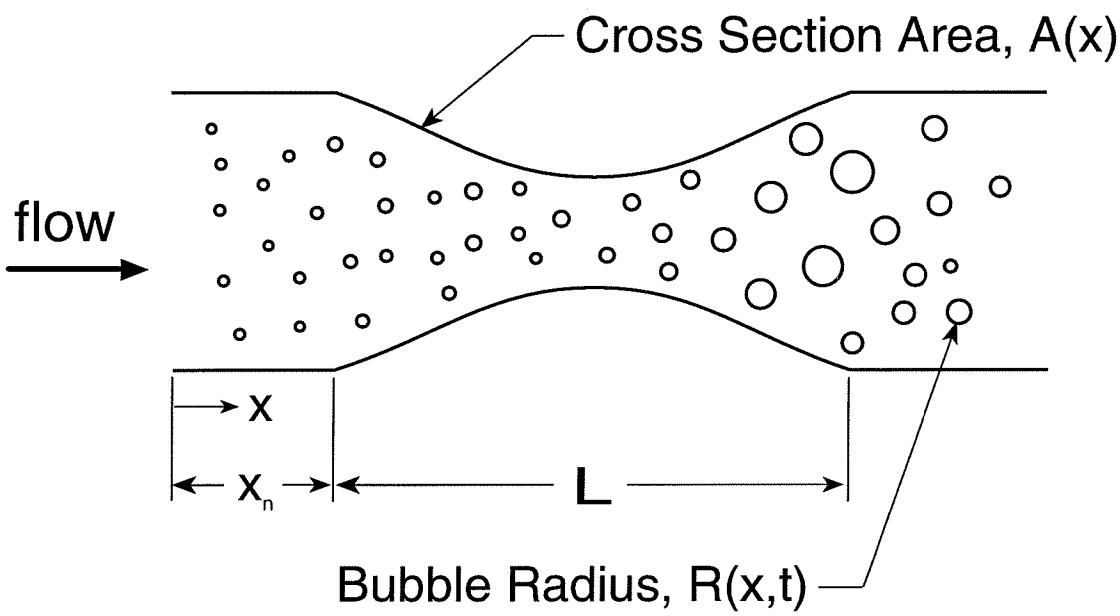

Figure 2.1 Notation for bubbly liquid flow in a converging-diverging nozzle.

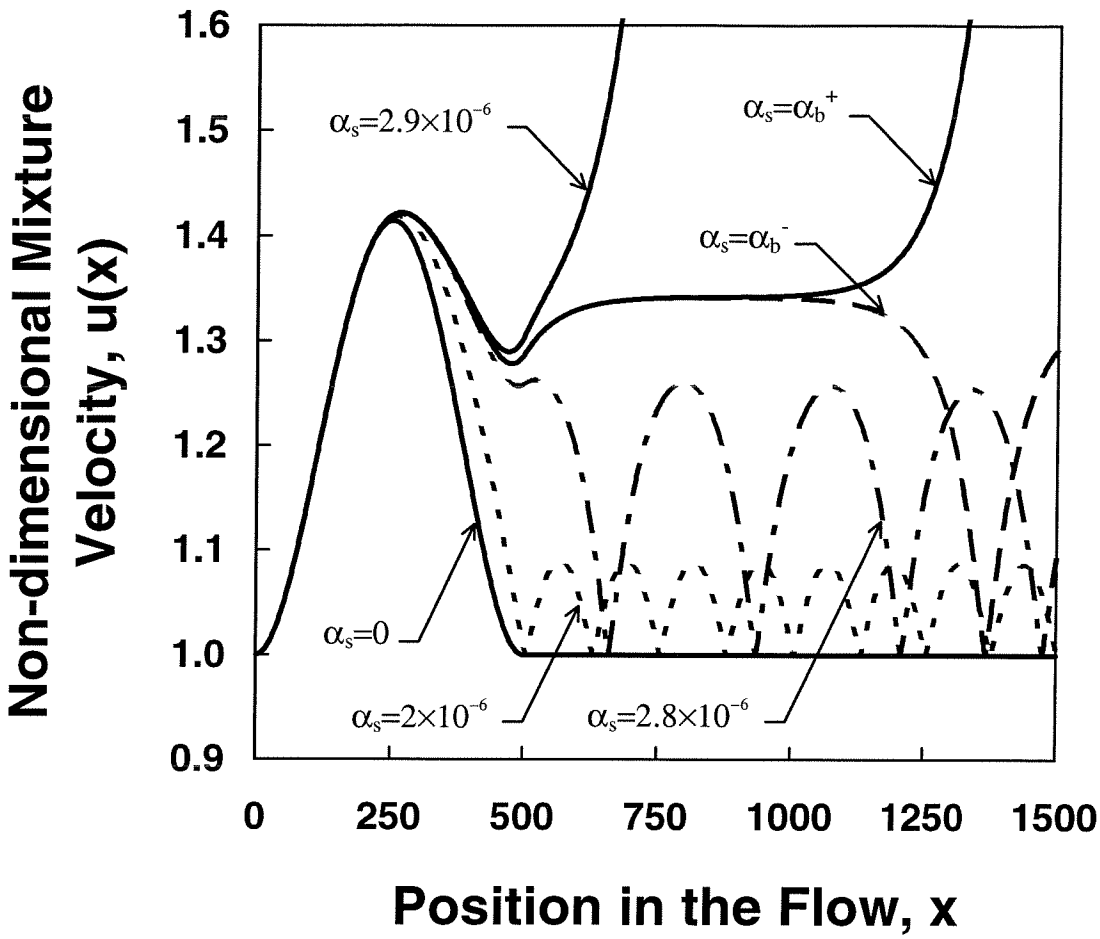

Figure 3.1 The non-dimensional mixture velocity distribution as a function of the non-dimensional position in the flow for five different upstream void fractions. Labels of $\alpha_s = \alpha_b^-$ and $\alpha_s = \alpha_b^+$ correspond to α_s just below and above the critical value $\alpha_b = 2.862 \times 10^{-6}$. The dimensionless length of the nozzle, L, is 500 with the throat located at 250. Other parameters are $\sigma = 0.8$, $C_{PMIN} = -1.0$, $Re = 1000$, and $We = 137$.

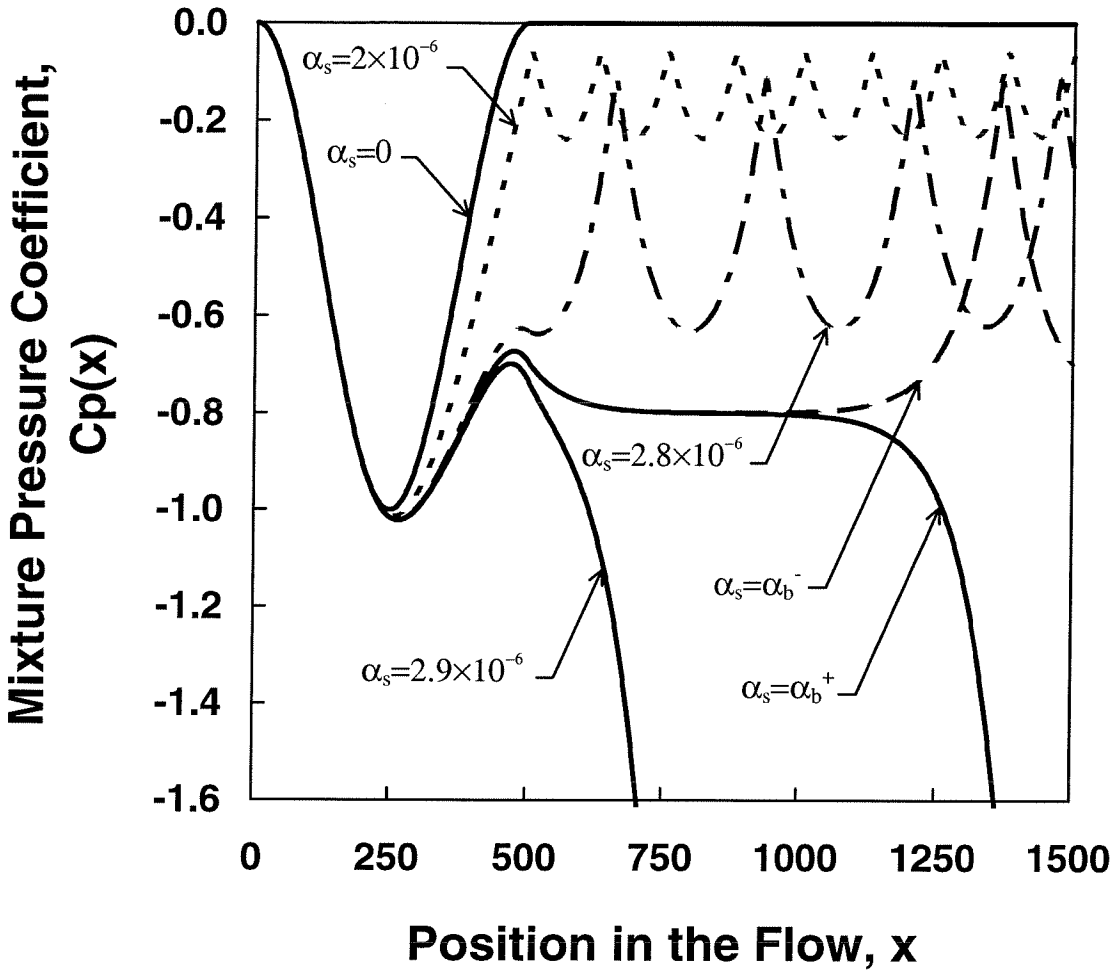

Figure 3.2 The mixture pressure coefficient as a function of the non-dimensional position in the flow for five different upstream void fractions. Labels of $\alpha_s = \alpha_b^-$ and $\alpha_s = \alpha_b^+$ correspond to α_s just below and above the bifurcation value $\alpha_b = 2.862 \times 10^{-6}$. All parameters as in Figure 3.1.

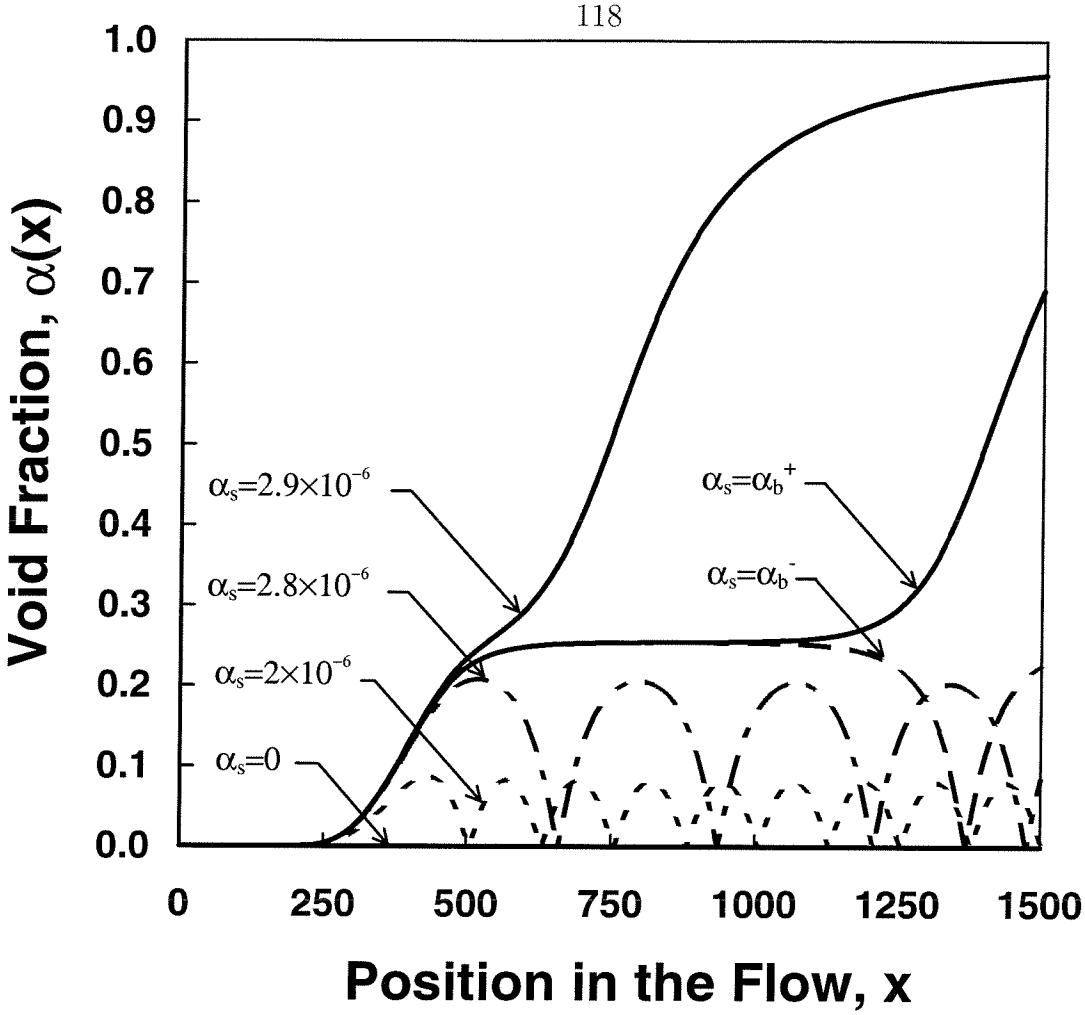

Figure 3.3 The void fraction distribution as a function of the non-dimensional position in the flow for five different upstream void fractions. Labels of $\alpha_s = \alpha_b^-$ and $\alpha_s = \alpha_b^+$ correspond to α_s just below and above the critical value $\alpha_b = 2.862 \times 10^{-6}$. All parameters as in Figure 3.1.

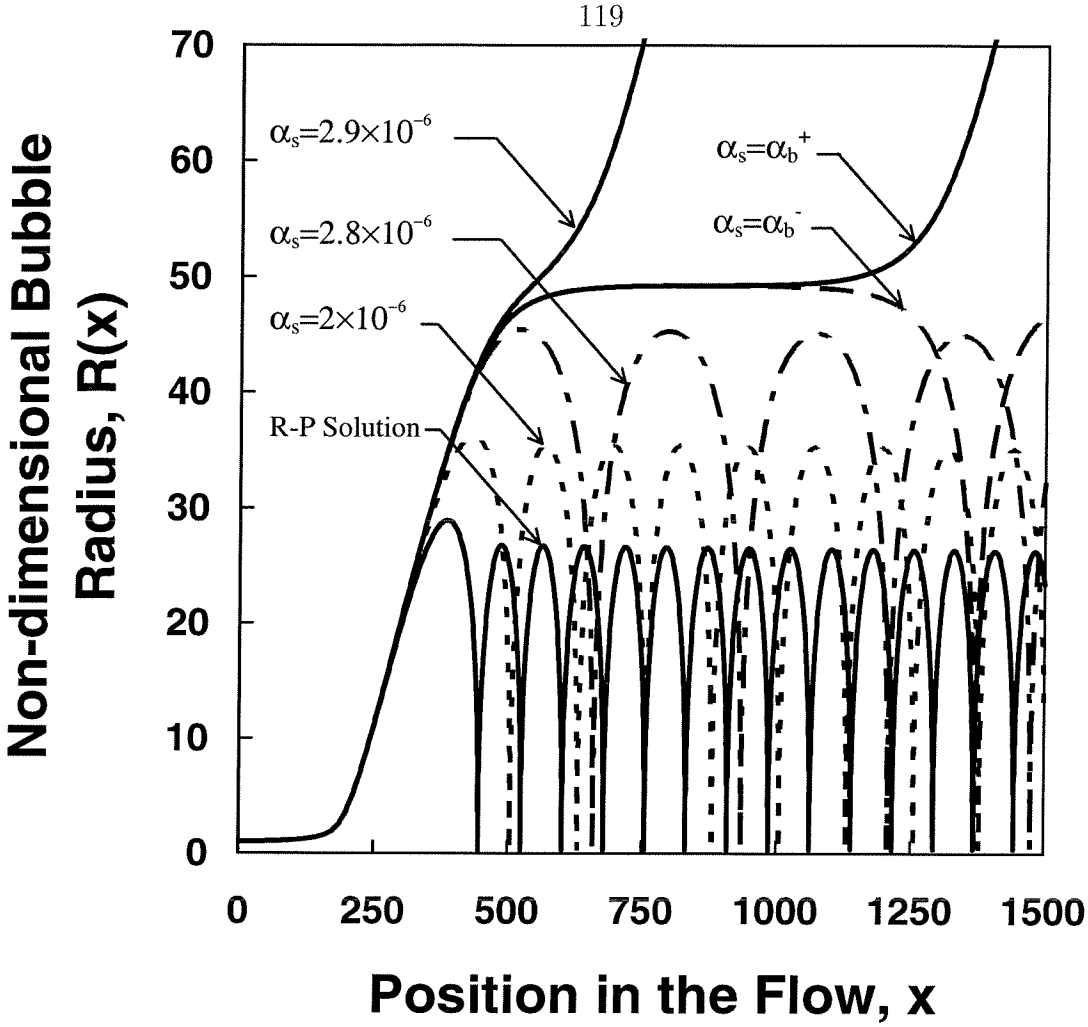

Figure 3.4 The non-dimensional bubble radius distribution as a function of the non-dimensional position in the flow for four different upstream void fractions and the solution from Rayleigh-Plesset equation (labeled by R-P solution). Labels of $\alpha_s = \alpha_b^-$ and $\alpha_s = \alpha_b^+$ correspond to α_s just below and above the critical value $\alpha_b = 2.862 \times 10^{-6}$. All parameters as in Figure 3.1

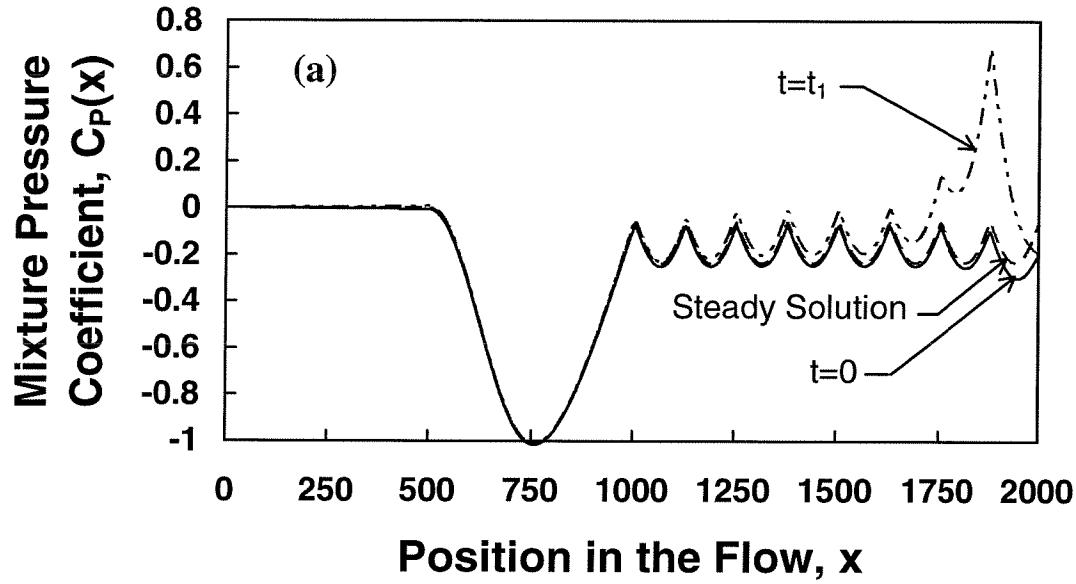

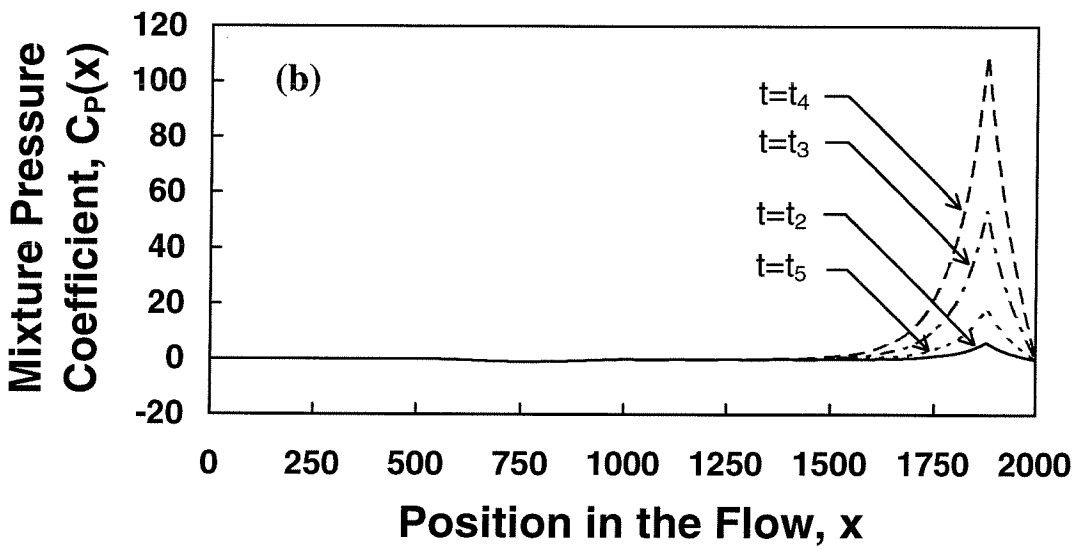

Figure 4.1 (a)–(h): The distribution of the mixture pressure coefficient at a series of consecutive times: $0 < t_1 < t_2 < \cdots < t_{20}$. The initial condition of the flow is labeled $t = 0$. Parameters of the nozzle are: $L = 500$, $x_n = 500$, and $C_{PMIN} = -1.0$. The pressure coefficient at $x_e = 2000$ is initially set as 0.2. The upstream void fraction is 2×10^{-6}. Other parameters have the following initial values: $\sigma = 0.8$, $Re = 1000$, and $We = 137$.

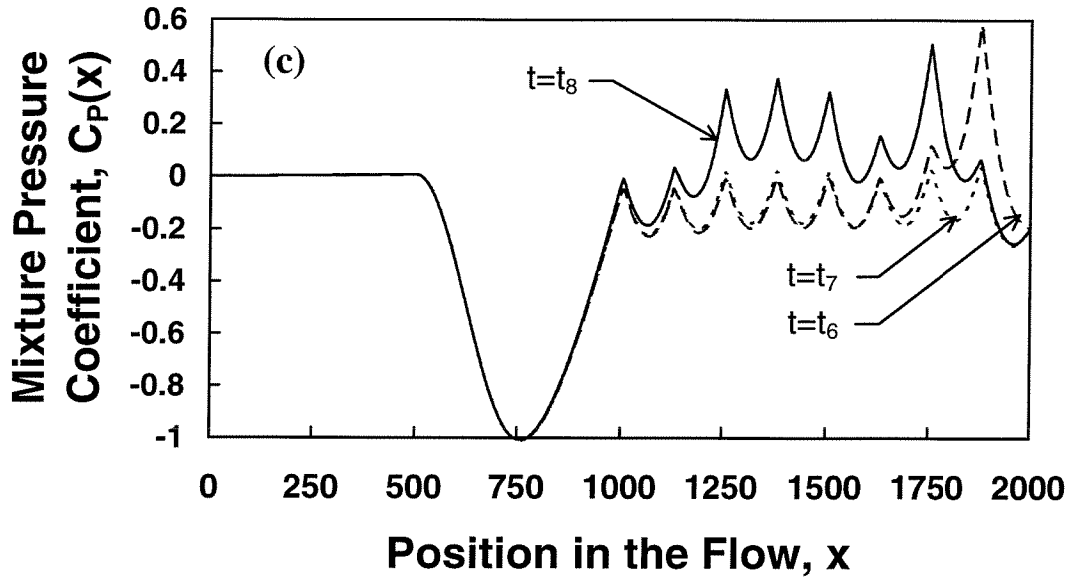
(c)
t=t8
t=t7
t=t6
Mixture Pressure Coefficient, CP(x)
0.6
0.4
0.2
0
-0.2
-0.4
-0.6
-0.8
-1
0
250
500
750
1000
1250
1500
1750
2000
Position in the Flow, x

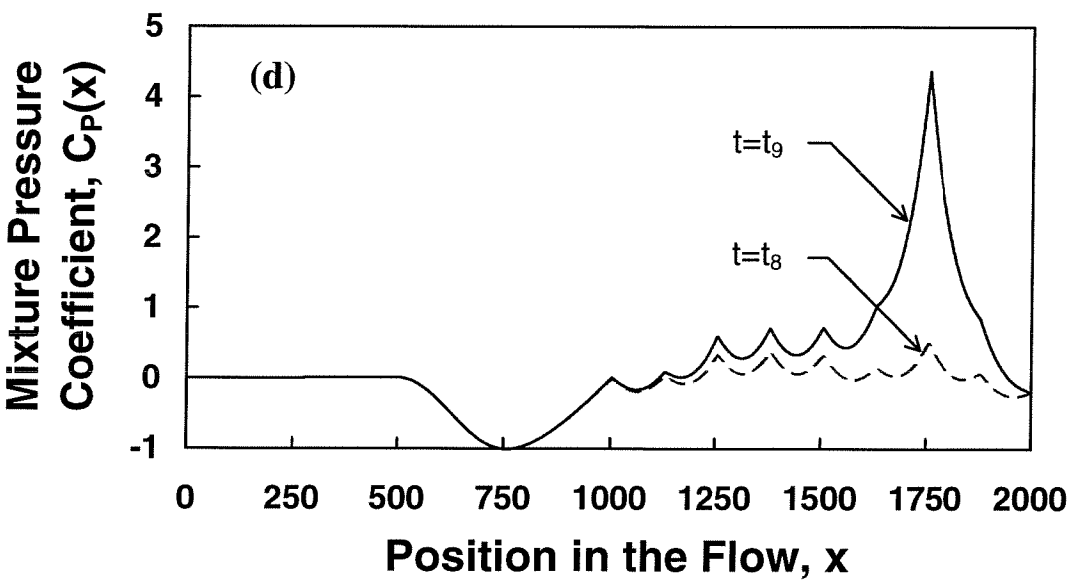
(d)
t=t9
t=t8
Mixture Pressure Coefficient, CP(x)
5
4
3
2
1
0
-1
0
250
500
750
1000
1250
1500
1750
2000
Position in the Flow, x

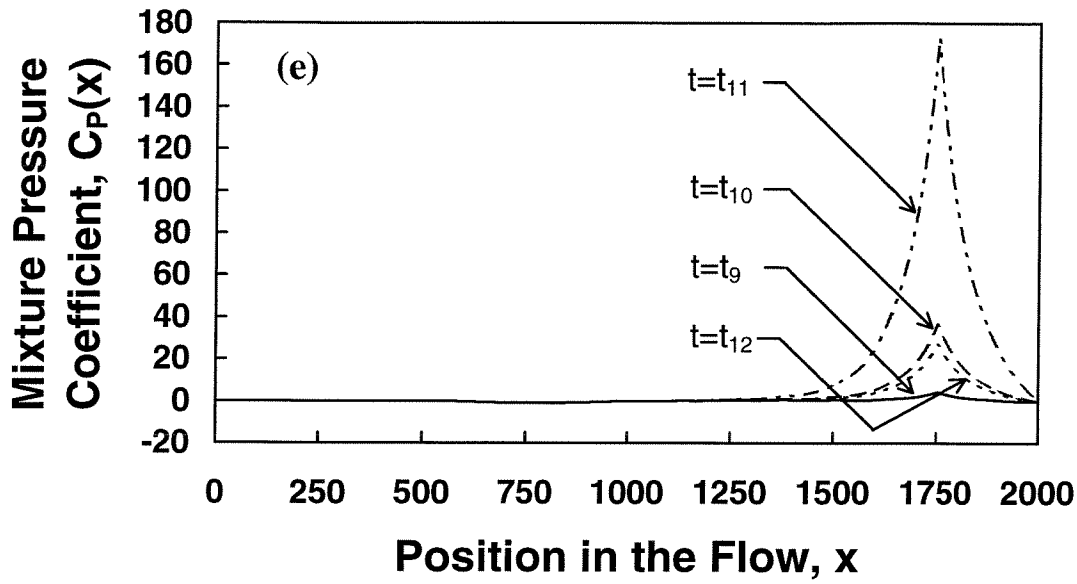
(e)
Mixture Pressure Coefficient, $C_P(x)$
180
160
140
120
100
80
60
40
20
0
-20
0
250
500
750
1000
1250
1500
1750
2000
Position in the Flow, x
$t=t_{11}$
$t=t_{10}$
$t=t_9$
$t=t_{12}$

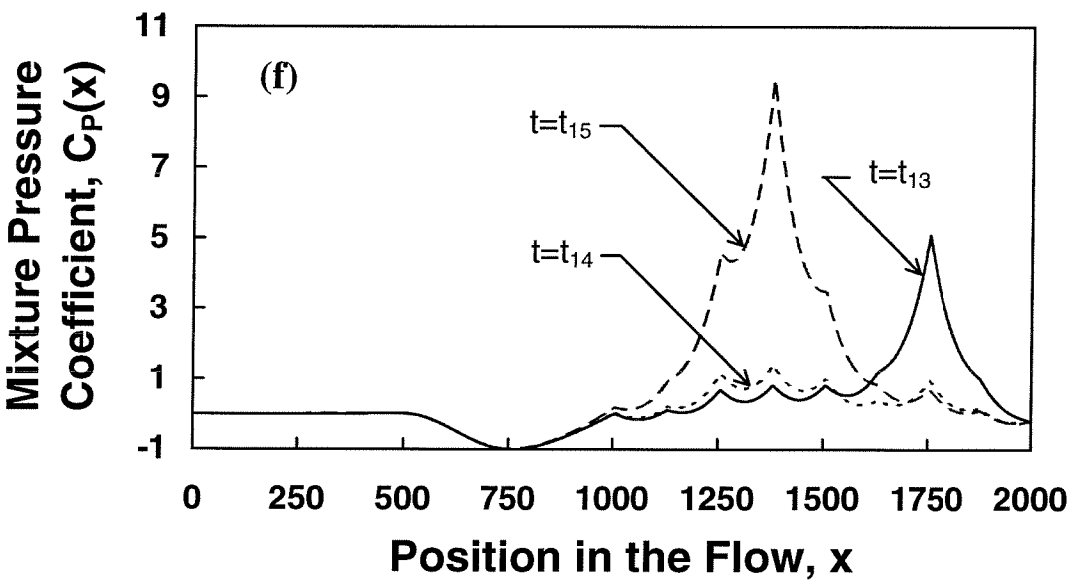
(f)
Mixture Pressure Coefficient, $C_P(x)$
11
9
7
5
3
1
-1
0
250
500
750
1000
1250
1500
1750
2000
Position in the Flow, x
$t=t_{15}$
$t=t_{13}$
$t=t_{14}$

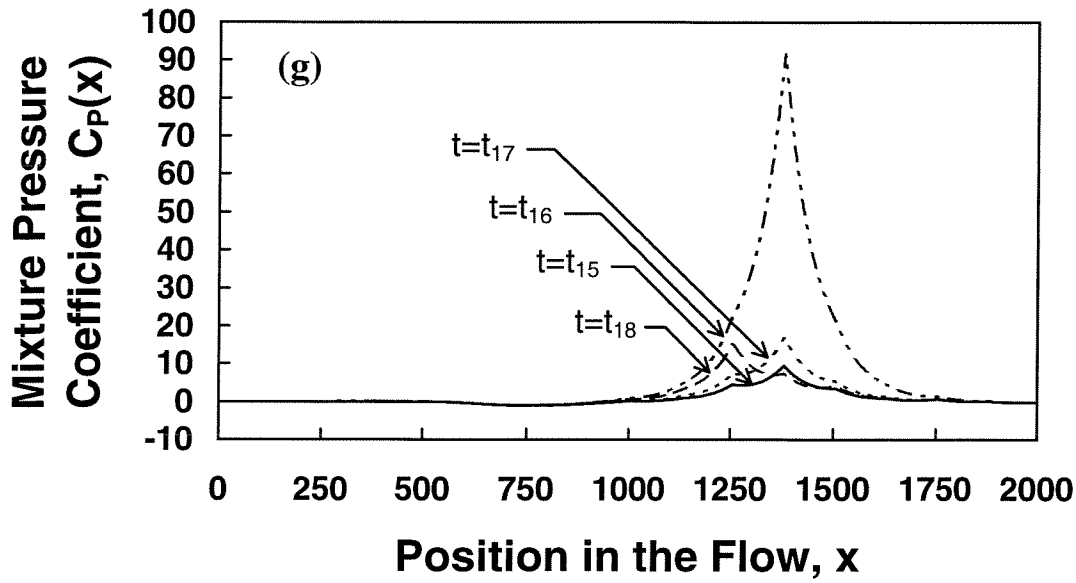
(g)
Mixture Pressure Coefficient, $C_P(x)$
100
90
80
70
60
50
40
30
20
10
0
-10
$t=t_{17}$
$t=t_{16}$
$t=t_{15}$
$t=t_{18}$
0
250
500
750
1000
1250
1500
1750
2000
Position in the Flow, x

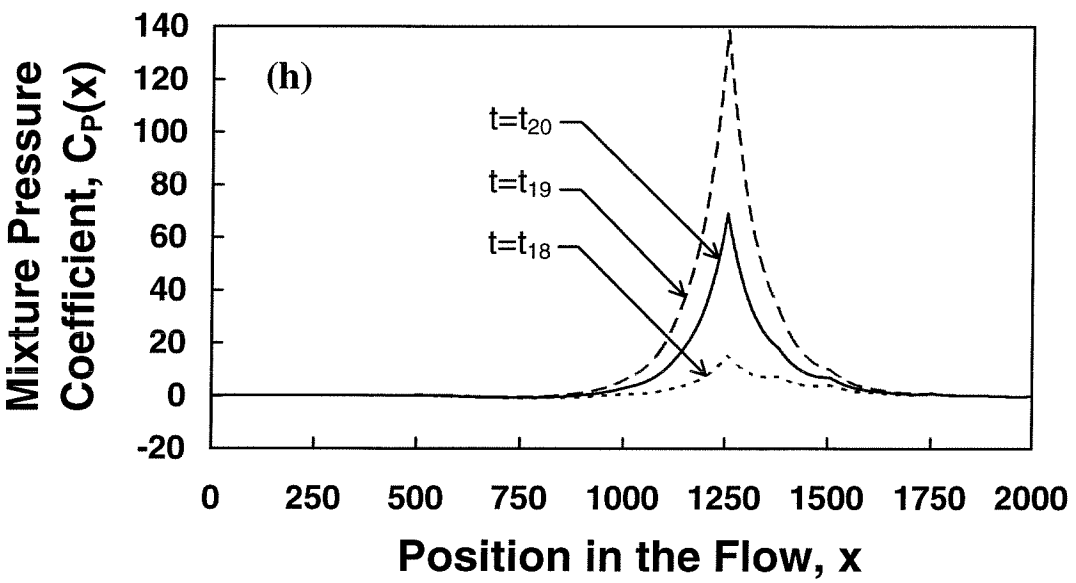
(h)
Mixture Pressure Coefficient, $C_P(x)$
140
120
100
80
60
40
20
0
-20
$t=t_{20}$
$t=t_{19}$
$t=t_{18}$
0
250
500
750
1000
1250
1500
1750
2000
Position in the Flow, x